

Near-Field Communications: A Comprehensive Survey

Yuanwei Liu, Chongjun Ouyang, Zhaolin Wang, Jiaqi Xu, Xidong Mu, and A. Lee Swindlehurst

Abstract—Multiple-antenna technologies are evolving towards large-scale aperture sizes, extremely high frequencies, and innovative antenna types. This evolution is giving rise to the emergence of *near-field communications (NFC)* in future wireless systems. Considerable attention has been directed towards this cutting-edge technology due to its potential to enhance the capacity of wireless networks by introducing increased spatial degrees of freedom (DoFs) in the range domain. Within this context, a comprehensive review of the state of the art on NFC is presented, with a specific focus on its i) fundamental operating principles, ii) channel modeling, iii) performance analysis, iv) signal processing, and v) integration with other emerging technologies. Specifically, i) the basic principles of NFC are characterized from both physics and communications perspectives, unveiling its unique properties in contrast to far-field communications. ii) Based on these principles, deterministic and stochastic near-field channel models are investigated for spatially-discrete (SPD) and continuous-aperture (CAP) antenna arrays. iii) Rooted in these models, existing contributions on near-field performance analysis are reviewed in terms of DoFs/effective DoFs (EDoFs), power scaling law, and transmission rate. iv) Existing signal processing techniques for NFC are systematically surveyed, encompassing channel estimation, beamforming design, and low-complexity beam training. v) Major issues and research opportunities associated with the integration of NFC and other emerging technologies are identified to facilitate NFC applications in next-generation networks. Promising directions are highlighted throughout the paper to inspire future research endeavors in the realm of NFC.

Index Terms—Beamforming, channel modeling, near-field communications, performance analysis.

I. INTRODUCTION

The advent of fifth-generation (5G) wireless networks has profoundly transformed various aspects of our daily lives and catalyzed significant advancements in industry. According to Qualcomm’s estimates, 5G is projected to contribute significantly to the global economy, reaching US\$ 13.2 trillion in global sales activity by 2035 [1]. Building on the success of 5G, both the academic and industrial sectors are now setting the stage for the development of next-generation 6G wireless networks. The envisioned applications of 6G, spanning metaverse, digital twin technology, ultra-high-definition

streaming, and extended reality (XR), necessitate achieving exceptionally high data rates, utilizing ultra-wide frequency bands, and facilitating massive connectivity [2], [3].

These ambitious objectives call for revolutionary wireless technologies to drive the evolution of 6G networks. A pivotal element in the next-generation wireless landscape is the adoption of extremely large aperture arrays (ELAAs) and higher frequencies [4]. The shift to ELAAs in high-frequency bands signifies more than just a quantitative increase in antenna size and carrier frequency. It represents a qualitative paradigm shift from traditional *far-field communications (FFC)* to *near-field communications (NFC)* [5].

A. From Plane Wave to Spherical Wave

The electromagnetic (EM) radiation field emitted by antennas is conventionally categorized into two distinct regions: the *far-field (Fraunhofer)* region and the *radiating near-field (Fresnel)* region [6]. This partition is defined by the *Fraunhofer distance (or Rayleigh distance)* $\frac{2A^2}{\lambda}$, where A represents the physical dimension of the antenna array and λ is the signal wavelength [6]. This boundary condition is illustrated in Fig. 1. In the far-field region extending beyond the Fraunhofer distance, EM waves exhibit propagation characteristics that significantly differ from those observed in the near-field region. Far-field EM propagation is effectively approximated using *plane waves*, while the near-field EM field demands precise modeling using *spherical waves*, as depicted in Fig. 2 [7].

Limited by the dimensions of current antenna arrays and the frequency bands in which they operate, the Fraunhofer distance in existing cellular systems typically covers only a few meters, rendering near-field effects negligible. Consequently, prevalent cellular communications heavily rely on theories and techniques from FFC. However, propelled by swift advancements in wireless technology, next-generation wireless communications are turning to ELAAs and higher frequencies to meet the escalating demand for communication services. The deployment of massive antenna arrays and the utilization of high-frequency bands enable NFC to be effective at distances of hundreds of meters, opening up novel opportunities for the development of NFC theories and techniques.

As an illustrative example, for an antenna array with a dimension of $A = 4$ m — a size plausible for future conformal arrays such as those deployed on building facades — the Fraunhofer distance is calculated as 373.3 m for signals at 3.5 GHz (frequency range 1 (FR1)) [8]. This distance increases to 2986.7 m at 28 GHz (frequency range 2 (FR2)). These

Yuanwei Liu, Zhaolin Wang, and Xidong Mu are with the School of Electronic Engineering and Computer Science, Queen Mary University of London, London E1 4NS, UK (email: {yuanwei.liu, zhaolin.wang, xidong.mu}@qmul.ac.uk).

Chongjun Ouyang is with the School of Electrical and Electronic Engineering, University College Dublin, Dublin, D04 V1W8, Ireland (e-mail: chongjun.ouyang@ucd.ie).

Jiaqi Xu and A. Lee Swindlehurst are with the Department of Electrical Engineering and Computer Science, University of California, Irvine, CA 92697, USA (email: {xu.jiaqi, swindle}@uci.edu)

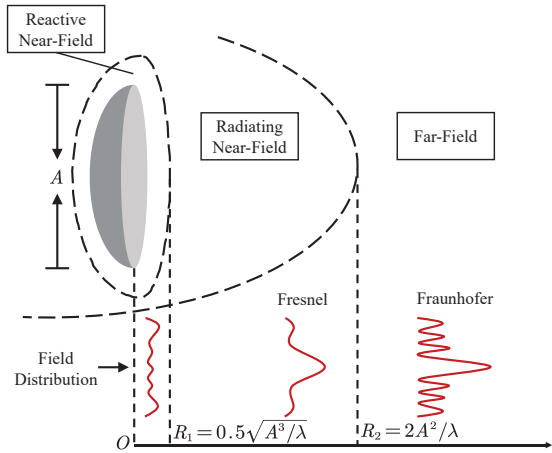
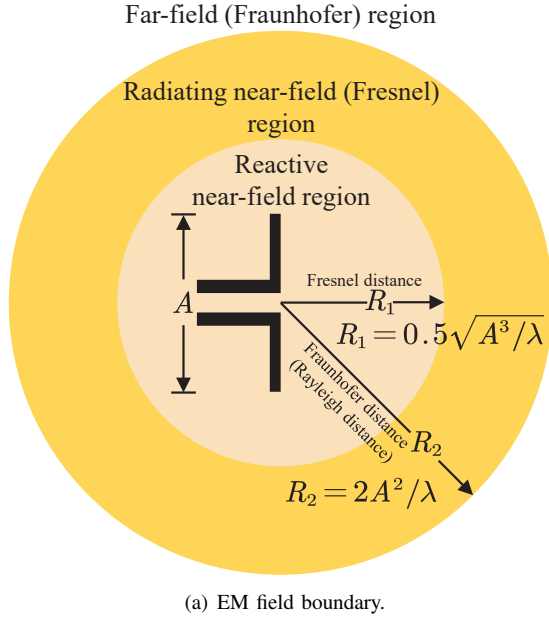


Fig. 1: EM field regions of an antenna, where A and λ denote the physical dimension of the antenna array and signal wavelength, respectively.

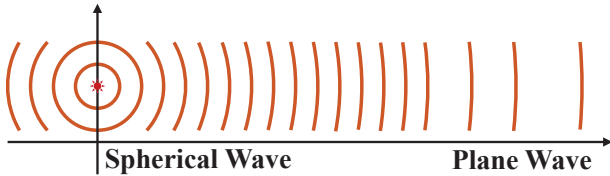


Fig. 2: The flattening of spherical waves with distance.

facts imply that the enlarged antenna aperture and shortened wavelength in ELAAs dramatically extend the near-field region, a facet previously overlooked in traditional wireless transmissions. In a nutshell, the exploration of NFC, which represents an exciting and relatively unexplored area, is of significant interest to next-generation 6G systems.

B. A Brief History of NFC

Before delving into further investigations, we provide a brief overview of the historical development of NFC. The history

of NFC is rooted in significant milestones that span several centuries. The journey begins with fundamental contributions to the understanding of wave propagation, specifically in the context of light waves, and evolves through the exploration of EM radio waves.

In 1678, the Dutch scientist Christiaan Huygens presented his “*Wave Theory of Light*” to the Académie des Sciences in Paris. This theory posits that each point along a moving wavefront can be represented by a point source emitting a spherical wave, a concept now known as *Huygens’ Principle*. Originally a preliminary chapter of his work “*Dioptrica*”, Huygens’s theory was officially published in 1690 under the title “*Traité de la Lumière*” (Treatise on Light) [9]. This treatise contains the first fully mathematized, mechanistic explanation of an unobservable physical phenomenon, specifically the propagation of light. The principle was initially deduced through mathematical inference and later experimentally supported by Thomas Young’s double-slit diffraction experiment in 1801 [10].

Huygens’ “*Wave Theory of Light*”, together with Young’s experiments, demonstrated the wave nature of light, challenging Isaac Newton’s “*Corpuscular Theory of Light*”. Subsequently, the wave theory of light gained widespread acceptance, and the study of diffraction patterns of light waves garnered significant research attention. In optics, the diffraction phenomenon can be categorized into two typical scenarios based on the distance between the diffracting object and the observed diffraction pattern. Specifically, when the diffraction pattern is created near the diffracting object, it is referred to as near-field diffraction, whereas if it is observed at a sufficiently long distance from the object, the term far-field diffraction is used.

In 1821, the German physicist Joseph von Fraunhofer constructed the first diffraction grating, consisting of 260 closely spaced parallel wires. Proficient in the mathematical wave theory of light, Fraunhofer utilized his diffraction grating to measure the wavelengths of specific colors and dark lines in the solar spectrum [11]. This notable achievement earned him personal nobility with the title “Ritter von”, signifying knighthood.

Concurrently, from 1815 to 1822, the French engineer and physicist Augustin-Jean Fresnel presented a series of memoirs to the French Academy of Sciences, elucidating his understanding of diffraction. By quantifying Huygens’s principle of secondary spherical waves and Young’s principle of diffraction, Fresnel provided the first satisfactory explanation of diffraction by straight edges, including the initial wave-based explanation of rectilinear propagation. Moreover, Fresnel formulated conditions to delineate the regions of far-field and near-field diffraction. Many crucial concepts were developed during this period, including the *Fresnel approximation*, *near-field region*, and *far-field region*.

In tribute to the distinguished contributions of Fraunhofer and Fresnel, the regions corresponding to the far field and radiating near field are designated as the *Fraunhofer* and *Fresnel* regions, respectively. The boundaries between the far field and radiating near field, as well as between the radiating near field and reactive near field, are called the *Fraunhofer*

distance and *Fresnel distance*, respectively. Additionally, the loose condition formulated by Fresnel to determine the diffraction region is referred to as the *Fraunhofer condition*.

Until 1891, the British scientist John William Strutt, also known as Baron Rayleigh or Lord Rayleigh, provided a characterization of the distance over which a diverging or converging beam of light remains approximately collimated. This distance, also considered to be the boundary between the near and far field, is calculated as $\frac{A^2}{2\lambda}$ for an antenna or array with aperture A operating at wavelength λ . It represents the axial distance from a radiating aperture to a point where the phase difference between the axial ray and an edge ray reaches $\frac{\pi}{2}$ [12]. This distance is referred to as the *Rayleigh distance* in honor of Baron Rayleigh, although the expression $\frac{A^2}{2\lambda}$ is not commonly used. Recently, the more commonly used expression for Rayleigh distance is $\frac{2A^2}{\lambda}$.

It is essential to highlight that the aforementioned contributions to wave propagation are primarily centered on light waves. However, in 1887, the German physicist Heinrich Hertz demonstrated the existence of radio waves using what is now recognized as a dipole antenna. Subsequently, significant research attention has been directed toward the near-field propagation of EM radio waves. In 1947, Cutler *et al.* [13] proposed to define the field boundary as the axial distance from a radiating aperture to a point where the phase difference between the axial ray and an edge ray is $\frac{\pi}{8}$, calculated as $\frac{2A^2}{\lambda}$. Then, in 1956, an exact expression for the Fresnel distance was derived by Polk [14].

In 1983, the first patent associated with NFC was granted, rooted in radio-frequency identification (RFID) technology. This innovation facilitated communications between two electronic devices over a short distance, typically on the order of several centimeters [15]. It is important to note that this technology primarily leveraged the reactive near-field region to support communications, which diverges from the focus of our paper¹.

The RFID-based NFC systems developed in 1983 predominantly utilized single-antenna transceivers. In 1984, Winters formulated the initial theory of multiple-input multiple-output (MIMO) communications [16]. Subsequently, in 1994, Paulraj and Kailath were granted a patent introducing the concept of employing MIMO arrays to increase the number of distinct spatial channels, thereby enhancing capacity or overall performance [17]. Shortly thereafter, in 1996, Foschini at Bell Labs laid down crucial theoretical foundations for MIMO [18].

Since 1996, considerable research efforts have been dedicated to practical measurements and testing of MIMO channels to validate their performance. Notably, in 1999, Driessen and Foschini [19] proposed using a spherical wave-based model to characterize line-of-sight (LoS) propagation in indoor MIMO systems. During this period, researchers observed that the capacity of short-range MIMO channels, reconstructed from measured path parameters, consistently fell short of directly measured capacities [20], [21]. In 2003, Jiang and Ingram

addressed this issue, attributing the discrepancy to incorrect modeling of the LoS path. They emphasized the necessity of employing a spherical wave-based model to reconstruct the channel response for accurate results [22]. Subsequently, in 2005, Jiang advocated the use of the spherical-wave model to characterize the propagation of short-range MIMO, a crucial aspect of NFC [23].

In 2010, Marzetta introduced the concept of massive MIMO, which proposes the use of a large number of antennas at both the base station and receivers, extending cell coverage and enabling beamforming [24]. Subsequent channel measurement results on massive MIMO indicated that large antenna arrays could significantly extend their near-field regions, necessitating the use of a spherical wave-based channel model for large aperture arrays [25].

Between 2016 and 2018, groundbreaking concepts such as holographic radio-frequency (RF) systems [26], [27], large intelligent surfaces [28], and ELAAs [29] were introduced. Each of these pioneering ideas revolves around the implementation of antenna arrays characterized by extraordinarily large dimensions, promoting a transition from FFC to NFC. These innovative approaches underscored the significance of spherical-wave propagations, capturing substantial research attention within our community. Fast forward to 2023, when Liu *et al.* [5] presented the first tutorial overview paper on NFC, aimed at providing a tutorial on NFC for researchers from diverse fields seeking an understanding of its evolving landscape.

For reference, the milestones of NFC are succinctly presented in the timeline illustrated in Table I. This timeline is derived from the historical survey of near-field propagations and spherical waves presented above. While NFC is not a recent development within our field, its resurgence in attention is attributed to its association with novel antenna forms and emerging applications, which will be elaborated on in Sections I-C and VI, respectively.

C. Recent Developments in Antenna Array Technology

Heinrich Hertz's epoch-making demonstration of the existence of radio waves using a simple dipole antenna in 1887 helped enable the development of techniques allowing the seamless flow of information across extensive distances. However, with the continuous evolution of wireless communication systems and their increasing demands for enhanced quality of service, the role and requirements placed on antennas and antenna arrays have undergone a profound transformation.

In response to these evolving needs, recent years have witnessed the emergence of various new forms of antennas that represent a paradigm shift, particularly in the context of challenging near-field environments. Antennas have transcended their traditional role as mere conduits for signals; instead, they have evolved into dynamic, adaptable, and intelligent components. Modern antennas actively shape, steer, and manage the flow of data to meet the intricate demands of contemporary wireless communication. Fig. 3 depicts four innovative antenna configurations: i) holographic MIMO [30]–[32], ii) reconfigurable intelligent surfaces (RISs) and simultaneously transmitting and reflecting (STAR)-RISs [33], [34], iii)

¹In our paper, the term “NFC” specifically pertains to wireless communications influenced by the near-field EM effects arising from the use of large aperture arrays and high-frequency bands.

TABLE I: Timeline of NFC Milestones

1678	Huygens presented his “Wave Theory of Light”.
1801	Young presented the double-slit diffraction experiment.
1815	Fresnel presented a series of memoirs about his understanding of diffraction.
1821	Fraunhofer constructed the first diffraction grating.
1887	Hertz demonstrated the existence of radio waves.
1891	Lord Rayleigh calculated the Rayleigh distance $\frac{A^2}{2\lambda}$.
1947	Cutler <i>et al.</i> reformulated the Rayleigh distance as $\frac{2A^2}{\lambda}$.
1956	Polk calculated the Fresnel distance.
1983	The first patent on RFID-based NFC was granted.
1984	Winters formulated the initial theory of MIMO.
1994	The first patent on MIMO was granted.
1996	Foschini laid down crucial theoretical foundations for MIMO.
1999	Driessen and Foschini utilized a spherical wave-based model to characterize LoS MIMO.
2003	Jiang <i>et al.</i> proposed to use spherical wave-based models to describe short-range MIMO.
2010	Marzetta proposed the concept of massive MIMO.
2015	Channel measurement results on massive MIMO necessitated the use of a spherical wave-based channel model.
2016	Prather proposed the concept of holographic MIMO.
2017	Hu <i>et al.</i> re-showed the potential of large intelligent surfaces in enhancing wireless transmissions.
2018	Amiri <i>et al.</i> proposed the concept of ELAA.
2023	Liu <i>et al.</i> presented the first tutorial review of NFC.

dynamic metasurface antennas (DMAs) [35], [36], and iv) fluid antennas [37], each of which can be advantageously designed to address specific challenges posed by the complexities of NFC.

These emerging antenna array technologies share common traits such as large aperture sizes and enhanced near-field beamforming capabilities. In this context, *extremely large MIMO (XL-MIMO)* [29], [38] is a related existing technology characterized by a substantial aperture size. XL-MIMO harnesses a massive number of antennas, often numbering in the hundreds or thousands, to concurrently serve multiple users with highly directional beams. In the near-field region, XL-MIMO can generate focused beams, enhancing both signal strength and spatial reuse, making it suitable for densely populated areas and indoor environments. In XL-MIMO systems, the antenna spacing is usually approximately half a wavelength. Implementation of XL-MIMO can be achieved through either a fully digital beamforming structure, where each antenna is equipped with an independent RF chain, or a hybrid beamforming structure utilizing a large-scale phased array [39]. Both of these structures entail high hardware costs [40]. Additionally, XL-MIMO systems may incur relatively elevated energy consumption, especially when numerous antennas are concurrently active for beamforming or signal processing [38].

In the subsequent sections, we provide a concise survey of the four antenna configurations shown in Fig. 3, and compare them with XL-MIMO.

1) **Holographic MIMO**: Holographic MIMO can be implemented using either a spatially-discrete (SPD) or a continuous-aperture (CAP) antenna array. An SPD antenna array deploys multiple antenna elements across a fixed aperture, and its performance improves as the number of antennas increases. Achieving this involves reducing the antenna spacing on the fixed aperture. As the antenna spacing approaches zero, the SPD array tends toward a CAP array. In contrast to SPD arrays, which consist of numerous discrete antennas with specific spacing, CAP arrays feature an infinite number of dimensionless antennas with infinitesimal spacing. However, in this limit, the “CAP array” essentially becomes a single antenna, representing a singular device rather than a collection of many small devices. Throughout the paper, we use “CAP array” and “CAP antenna array” interchangeably to refer to EM devices with a spatially-continuous aperture for clarity and consistency.

In both SOD and CAP implementations, holographic MIMO can generate programmable three-dimensional (3D) signal patterns by manipulating its radiated EM waves. Each pattern corresponds to a set of beams directed toward different directions, enabling precise control over signal direction and cov-

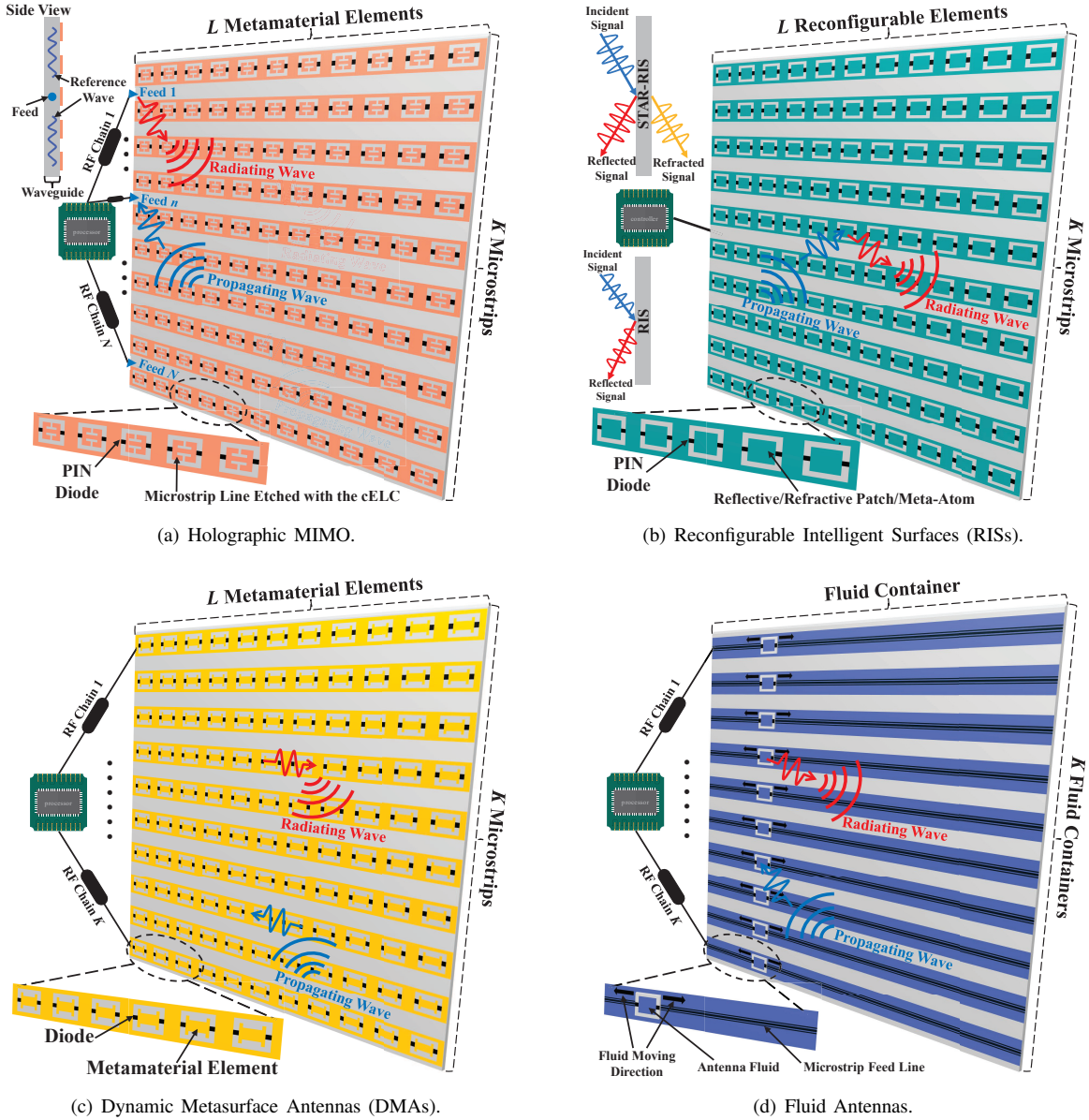


Fig. 3: New forms of antennas.

erage. This signal pattern can be likened to a “3D hologram” captured by a “holographic MIMO camera”, and this structural feature is the reason for its designation as holographic. Fig. 3(a) illustrates its SPD implementation, also known as a reconfigurable holographic surface (RHS). The RHS comprises densely packed sub-wavelength metamaterial elements, which realizes a novel hybrid beamforming structure with analog beamforming implemented through simple diode-based controllers. This structure has been experimentally proven to be much more energy-efficient than phased arrays [41], [42]. Regarding its CAP counterpart [31], it can be viewed as an active surface containing an infinite number of antennas with infinitesimal spacing, enabling a significantly higher channel capacity than XL-MIMO through appropriate beamforming design [43]. These findings suggest that holographic MIMO can be more energy-efficient than XL-MIMO, irrespective of

its spatial continuity. In the near-field, holographic MIMO dynamically shapes signal beams, optimizing connectivity for users and Internet-of-Things (IoT) devices, especially in complicated indoor scenarios.

2) *RISs and STAR-RISs*: RISs and STAR-RISs are planar surfaces equipped with a grid of closely spaced passive elements capable of reflecting, refracting, or absorbing EM waves [33], [34]. These surfaces can be dynamically adjusted to optimize signal strength and phase shifts, reshaping the wireless environment to mitigate interference and enhance signal coverage. The spatial density of the passive elements can be high, especially in applications requiring fine-grained control. RISs are highly energy-efficient since the individual reconfigurable elements do not require active power sources; they manipulate signals passively, consuming minimal energy [44]. In the near field, RISs can create localized high-

TABLE II: Comparing new forms of antenna technology with XL-MIMO.

	Spatial Continuity	Energy Consumption	Mobility	DoF	Spatial Resolution
XL-MIMO	Discrete	Very high	No	Very high	High
Holographic MIMO	Discrete/Continuous	Moderate	No	High	Moderate
RISs and STAR-RISs	Discrete/Continuous	Low	No	Moderate to high	Moderate to high
DMAs	Discrete/Continuous	Moderate to high	No	High	High
Fluid Antennas	Discrete	Low	Yes	Low	Moderate

intensity zones for efficient information or energy transfer.

3) **DMAs**: Metasurface antennas comprise sub-wavelength structured elements that manipulate the phase, amplitude, and polarization of incoming waves [35], [36]. DMA arrays can achieve very high spatial densities, and their energy consumption depends on their specific design and operation. In general, DMAs offer beam tailoring capabilities and enable the processing of transmitted and received signals in the analog domain with dynamic configurability using simplified transceiver hardware. In the near field, DMAs enable fine-tuning of signals, particularly valuable for applications like wireless power transfer. Additionally, DMA-based architectures require much less power and cost in comparison to conventional XL-MIMO antenna arrays [35].

4) **Fluid Antennas**: Fluid antennas employ electrically reconfigurable metamaterials to alter their shape and properties [37]. A fluid antenna system is designed to precisely adjust the antenna's position² within a specified aperture, typically allowing an enormous number of possible array configurations. The exceptional resolution in positioning the antenna not only facilitates interference mitigation in a novel manner [46] but also enables fluid antennas to achieve high effective transmit/receive spatial diversity through the use of reconfigurable liquids and dynamic changes in antenna positions [37]. The diversity gain provided by fluid antennas compensates for significant path losses in NFC. Furthermore, the mobility of a fluid antenna enables more energy-efficient radiation, rendering fluid antenna systems potentially more energy-efficient than XL-MIMO [47].

Taken together, the spatial density and energy consumption of these new antenna array technologies can vary widely based on their design, configuration, and application. Moreover, as antenna arrays become more densely populated and require more precise control, it is beneficial to describe them using spatially-continuous models, as will be detailed in Sections II and III. A summary of these novel antenna forms in terms of their spatial density, energy consumption, mobility, control mechanism, and spatial diversity can be found in Table II.

D. Prior Works

Several magazine papers [4], [7], [48]–[50], tutorials [5], [51]–[53], and surveys [54] have introduced NFC and its variants in the literature. However, their focus differs from our work. The works in [4], [7], [48] provided high-level

²The repositioning of a fluid antenna may not necessarily involve physical movement. In practice, this adjustment is more effectively achieved by switching on or off the units in an array of compact RF pixels. A fluid antenna that relies on physical movement is also referred to as a movable antenna [45].

concise introductions to the unique physical properties of NFC compared to FFC, identifying challenges and future research opportunities in implementing NFC-based wireless networks. The authors of [49] and [50] delved into Terahertz (THz) NFC and NFC degrees of freedom (DoFs), respectively, with a more one-sided focus.

The tutorial overview in [5] detailed deterministic channel modeling, hybrid beam focusing architectures, and performance analysis for NFC. This tutorial was extended in [51], placing additional emphasis on stochastic channel modeling, performance analysis, and practical design considerations. Two tutorials with a heightened focus on channel modeling and low-complexity signal processing schemes were presented in [52] and [53].

Recently, an overview of holographic MIMO was published, centering more on the roadmap and physical aspects of NFC supported by antenna arrays with a continuous aperture [54]. The work in [54] focuses primarily on holographic MIMO rather than NFC, since holographic MIMO can be employed to support both NFC and FFC applications.

E. Motivation and Contributions

While previous magazine articles, tutorials, and surveys have addressed general concepts or specific aspects of NFC, they lack an in-depth exploration of NFC's fundamental performance limits and its potential applications in wireless networks. Furthermore, there is a notable absence of comparative analysis of commonly employed mathematical tools for performance evaluations and optimizations in near-field wireless networks. The goal of this paper is to fill these gaps and provide a comprehensive review of principles governing near-field wireless networks. The key contributions of our work are outlined as follows.

- 1) **Fundamental Investigation of NFC Principles**: We conduct an in-depth exploration of NFC principles, spanning from EM theory in physics to information transmission theory in wireless communications. Categorizing near-field channel models into three fundamental types based on EM wave propagation, we further investigate the physical properties of the near-field region. This investigation transitions to communication-theoretic aspects, introducing several DoF-related metrics.
- 2) **Overview of Near-Field Channel Models**: We provide an overview of basic near-field channel models for both SPD and CAP antenna arrays. For both array types, we conduct a comprehensive survey of existing channel models, encompassing deterministic LoS and statistical

multipath propagation. Our focus lies in the spatial non-stationarity of near-field channels, a distinctive feature setting NFC apart from FFC.

- 3) **Performance Evaluation Techniques for NFC:** We develop performance evaluation techniques tailored to NFC, considering the reviewed near-field channel models. Incorporating three representative performance metrics — DoFs and effective DoFs (EDoFs), power scaling law, and transmission rate — we summarize current research contributions, outlining their advantages and limitations.
- 4) **Signal Processing Techniques for NFC:** We delve into signal processing techniques for NFC, with a particular emphasis on channel estimation, beamforming design, and low-complexity beam training. For each optimization objective, we consolidate protocols and approaches, accounting for the unique properties of the near-field region and novel antenna and array architectures dedicated to NFC.
- 5) **Identification of Research Opportunities:** We identify significant research opportunities linked to integrating NFC into other emerging technologies, including integrated sensing and communications (ISAC), RIS, non-orthogonal multiple access (NOMA), wireless power transfer (WPT), simultaneous wireless information and power transfer (SWIPT), and physical layer security (PLS). We discuss potential solutions and avenues for future exploration.

F. Organization

The remainder of this paper is structured as follows. Section II delves into the fundamental principles of NFC from the standpoint of physics and EM theory. Section III investigates near-field LoS and non-LoS (NLoS) channel models for both SPD and CAP antenna arrays. In Section IV, we provide a survey of associated contributions, focusing on the near-field performance analysis of DoFs/EDoFs, power scaling law, and transmission rate. Signal processing techniques for NFC, encompassing channel estimation, beamforming, and beam training, are summarized in Section V. Section VI investigates the integration of NFC with other emerging 6G wireless technologies. Finally, Section VII concludes the paper. Fig. 4 illustrates the organizational structure of the paper, and Table III presents key abbreviations used throughout this treatise.

II. FUNDAMENTALS OF NFC

In the realm of wireless communications, the profound synergy between physics and EM theory has played an indispensable role. Rooted in the foundational work of luminaries like Faraday and Maxwell, the discovery of EM induction gave birth to the wireless revolution, enabling information to be transmitted electrically through the air without the constraints of physical wires. Today, we are witnessing a historical moment in which the marriage of antenna development and EM theory continues to drive wireless technology to a higher level. Thus, the key is to understand NFC from physics to communication and information theory. In this section, we will first discuss three categories of near-field channel models from

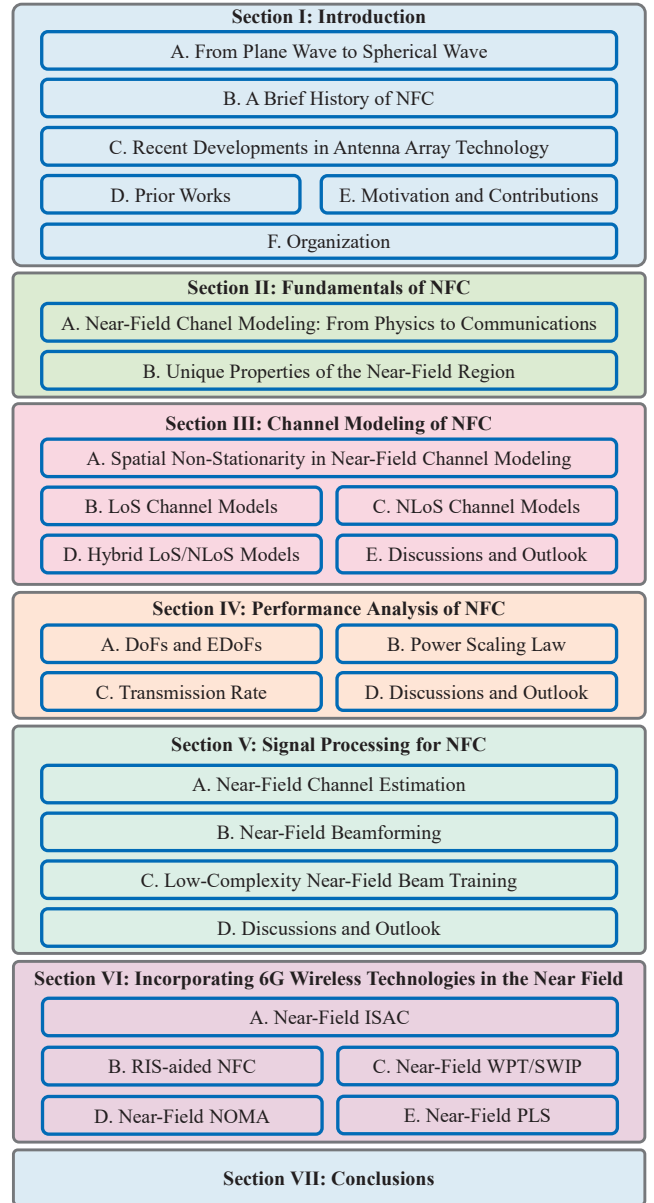


Fig. 4: Condensed overview of this survey on NFC.

the perspective of physics. Then, we will identify the unique physical properties of the near-field region, namely, different radiation patterns, different field regions/approximations, and different metrics. Moreover, we will discuss the number of DoFs available in near-field channels from the perspective of information theory.

A. Near-Field Channel Modeling: From Physics to Communications

From the perspective of physics, the wireless communication channel response is fully governed by the propagation of EM waves in given radio environments. Although the laws of EM radiation are elegantly revealed by Maxwell's equations [55], the complexity of communication channel modeling stems from the fact that the geometrical and physical properties of both transceivers and radio environments vary from case to case. As such, calculating the channel response

TABLE III: List of Acronyms

AoA	Angle of Arrival	PAS	Power Angular Spectrum
AoD	Angle of Departure	PL	Polarization Loss
ATR	Average Transmission Rate	PLOS	Power Location Spectrum
BBU	Baseband Unit	PLS	Physical Layer Security
CAP	Continuous-Aperture	PPBSM	Physical Propagation-Based Stochastic Model
CBSM	Correlation-Based Stochastic Model	PS	Phase Shifter
CCM	Clustered Channel Model	PSWF	Prolate Spheroidal Wave Function
CRB	Cramér-Rao Bound	RCS	Radar Cross-Section
CSI	Channel State Information	RF	Radio-Frequency
DAM	Delay Alignment Modulation	RFID	Radio-Frequency Identification
DMA	Dynamic Metasurface Antenna	RHS	Reconfigurable Holographic Surface
DoF	Degree of Freedom	RIS	Reconfigurable Intelligent Surface
EAL	Effective Aperture Loss	RoS	Rough Surface
ED	Eigen-Decomposition	RRS	Reconfigurable Refractive Surface
EDoF	Effective DoF	RZF	Regularized Zero-Forcing
EIT	Electromagnetic Information Theory	SBL	Sparse Bayesian Learning
ELAA	Extremely Large Aperture Array	SG	Stochastic Geometry
EM	Electromagnetic	SIC	Successive Interference Cancellation
EMI	Ergodic Mutual Information	SINR	Signal-to-Interference-Plus-Noise Ratio
ETPA	Equal Transmit Power Allocation	SISO	Single-Input Single-Output
ETR	Ergodic Transmission Rate	SNR	Signal-to-Noise Ratio
FDC	Finite-Dimensional Channel	SPD	Spatially-Discrete
FC	Far-Field Communications	SSFT	Split-Step Fourier Transform
FPBSM	Fourier Plane-Wave-Based Stochastic Model	STAR	Simultaneously Transmitting and Reflecting
FR1	Frequency Range 1	S-V	Saleh-Valenzuela
FR2	Frequency Range 2	SVD	Singular Value Decomposition
FSPL	Free-Space Path Loss	SWIPT	Simultaneous Wireless Information and Power Transfer
GHz	Gigahertz	THz	Terahertz
i.i.d.	Independent and Identically Distributed	TTD	True Time Delayer
i.n.i.d.	Independent but not Identically Distributed	UCA	Uniform Circular Array
IoT	Internet-of-Things	ULA	Uniform Linear Array
ISAC	Integrated Sensing and Communications	UPA	Uniform Planar Array
ISI	Inter-Symbol Interference	UPL	Unequal Path Loss
LMMSE	Linear Minimum Mean Square Error	USW	Uniform Spherical Wave
LoS	Line-of-Sight	VCR	Virtual Channel Representation
LS	Least-Squares	VR	Visibility Region
MIMO	Multiple-Input Multiple-Output	WDM	Wavenumber-Division Multiplexing
MISO	Multiple-Input Single-Output	WMMSE	Weighted Minimum Mean Square Error
MLA	Modular Linear Array	WPT	Wireless Power Transfer
MMSE	Minimum Mean Square Error	w.r.t.	With Respect To
mmWave	Millimeter-Wave	WSMS	Widely-Spaced Multi-Subarray
MRC	Maximum Ratio Combining	WSR	Weighted Sum Rate
MRDN	Multiple Residual Dense Network	XL-MIMO	Extremely Large MIMO
MRT	Maximum Ratio Transmission	XR	Extended Reality
NFC	Near-Field Communications	ZF	Zero-Forcing
NLoS	Non-Line-of-Sight	1D	One-Dimensional
NOMA	Non-orthogonal Multiple Access	2D	Two-Dimensional
NUSW	Non-Uniform Spherical Wave	3D	Three-Dimensional
OFDM	Orthogonal Frequency Division Multiplexing	4D	Four-Dimensional
OMP	Orthogonal Matching Pursuit	5G	Fifth-Generation
OTFS	Orthogonal Time Frequency Space	6G	Sixth-Generation

from a purely theoretical standpoint is almost impossible for any practical communication system. Facing this problem, pioneers in the field of wireless communication developed various techniques and models to approximate the physical channel [56]–[59]. For example, for the path loss of a wireless channel, Friis’ formula [56] gave a far-field approximation by considering an omni-directional transmit antenna, a receive antenna with a certain gain, and a free-space radio environment. In urban and indoor environments, a radio signal transmitted from a fixed source will encounter multiple objects. For these

scenarios, ray-tracing techniques [57], finite-state Markov models [58], and other simple wireless channel paradigms [59] were developed to approximate complex radio environments. In practical scenarios, blockages and multi-path propagation give rise to shadowing [60] and multi-path fading which can be modeled using Rayleigh [61] or Rician fading [62].

However, all the above techniques assume the far-field approximation which stems from Friis’ original. In contrast, other EM-based techniques do not rely on far-field approximations and apply to the near-field region. Generally speaking,

near-field channel models can be loosely classified into the following two categories: CAP models and SPD models. In most far-field communication scenarios, CAP models are not necessary because SPD models achieve reasonably good accuracy [5]. However, as the aperture size and spatial density of the transceive antennas increase, CAP models need to be considered for characterizing near-field communication channels. In the following, we elaborate on these channel models.

1) *CAP*: As introduced in Section I-C, new forms of antenna configurations such as DMAs, RISs, and fluid antennas can have very high spatial density. For these types of arrays, only CAP channel models are able to characterize their spatially-continuous array responses. CAP channel models are a category of physically-compliant models that are based on different physics principles. Two of the most commonly-used principles are the **EM wave equation** (which stems from Maxwell's equations) and the **Huygens–Fresnel principle** [9] (which originates from optics). Both principles describe the propagation of EM waves within a medium or vacuum. In wireless communication channel modeling, these two principles lead to two different approaches, namely Green's function-based approaches and integral equation approaches. On one hand, for a monochromatic field varying in time as $e^{-j\omega t}$, the EM wave equation reduces to the Helmholtz equation [63], and Green's function method is used to solve the Helmholtz equation. On the other hand, for EM waves propagating in homogeneous media, the Huygens–Fresnel principle states that every point on a wavefront is itself the source of spherical wavelets. Based on this principle, describing the propagation of EM waves can be transformed into an integration problem. In the following, we briefly summarize existing progress on these two approaches for CAP near-field channel models.

- **Green's Function-Based Approaches**: Green's function is a mathematical tool used in the field of communication channel modeling, particularly in electromagnetics. In this approach, Green's functions, also known as impulse response functions or fundamental solutions, are leveraged to describe the interaction between EM waves and the environment, such as obstacles, antennas, and propagation media [64]. As early as 1974, the Green's function method was already used for modeling EM wave propagation around edges and surfaces [65]. Later, a Green's function estimation approach was proposed in homogeneous and scattering media to establish the feasibility of time reversal signal processing [66]. Recently, in [67], a physics-based analytical model was described for characterizing the free-space path-loss of a wireless link when an RIS is present, using the vector generalization of Green's theorem. The model applies to two-dimensional metasurfaces operating in reflection or transmission mode and provides closed-form expressions for path loss in both far-field and near-field scenarios.
- **Integral Equation Approaches**: Integral equation approaches are a mathematical framework used in communication channel modeling, particularly in the study of EM wave propagation and scattering. These approaches

are based on the formulation of integral equations that describe EM fields, including the Huygens–Fresnel principle [9], the Rayleigh–Sommerfeld diffraction theory [63], and the Kirchhoff–Fresnel diffraction formula [68]. Exploiting integral equation approaches, [69] compared the volume and the surface electric field for indoor EM wave propagation. In [70], a rigorous and versatile mathematical model was proposed for the prediction and exploration of information transmission through complex diffuse multipath environments. In [34], near- and far-field channel models were proposed for STAR-RISs based on Kirchhoff–Fresnel diffraction.

2) *SPD*: SPD models are a category of models used in communication channel modeling to describe the behavior of antennas or antenna arrays that are physically separated from each other in space. In these scenarios, the volume or surface integrals arising from Green's functions can be reduced to summations over the antennas [34]. Ever since the proposal of multi-antenna communication systems more than two decades ago, the MIMO channel has been represented by a collection of SPD gains [71, Fig. 2].

As illustrated in Fig. 5, Green's function-based approaches generally require detailed information about the radiation source, i.e., the current distribution of the transmitter [72]. In contrast, the integral equation approaches and SPD models only require knowledge of the signal strength distribution on one given wavefront, or at each transmit antenna. These channel models reveal the unique properties of NFC. Later in this section, we will elaborate on the unique properties of the near-field region. In Section III, we further provide a comprehensive overview of near-field channel modeling.

B. Unique Properties of the Near-Field Region

The near field has unique properties compared to those for the far field. Most prominently, they yield different radiation patterns, different field regions, boundaries, and approximations, and different metrics. In the following, we elaborate on these differences and highlight the unique opportunities provided by near-field systems.

1) *Different Radiation Patterns*: One of the most fundamental differences that separate near- and far-field communications lies in the complex radiation patterns produced in each regime. Near-field patterns are complex and contain both the incident and scattered fields, resulting in non-uniform field distributions. EM wave behavior in this regime is described by the Kirchhoff–Fresnel diffraction formula [68]. Near-field patterns are highly sensitive to the distances between sources and observation points, making their behavior challenging to accurately predict [5]. For a multi-antenna transmitter with an arbitrary beamforming design, the angular distribution of its far-field channel gain is independent of distance. That is, the far-field radiation pattern of a transmitter is “fixed” and forms beam-like structures, as illustrated in Fig. 1(b). However, in the near field, the angular distribution of the channel gain varies with distance [73], and hence there exist no beam-like structures. As a result, the signal strength in NFC can vary significantly even within a small area due to the complex near-field radiation pattern. This high variability requires careful

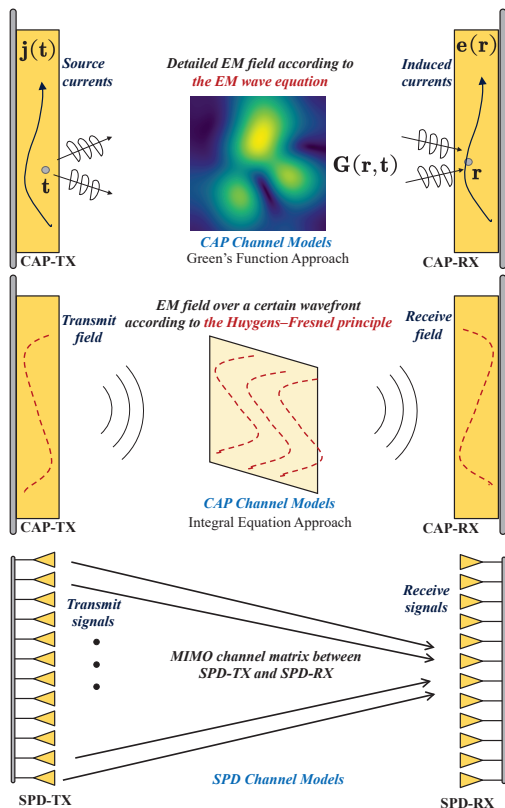


Fig. 5: Illustrating CAP and SPD channel models. From top to bottom: Green's function-based approach, integral equation approach, and SPD models.

signal management and also opens up the possibility of near-field beamfocusing in NFC systems.

2) *Different Field Regions, Boundaries, and Approximations*: The near-field region is characterized by its proximity to a transmit antenna (or array of antennas) and is defined by the area around the antenna where the behavior of the EM fields significantly deviates from that in the far field. In NFC, there are three different field regions, each with its own set of EM properties, as illustrated in Fig. 1.

The first near-field region is the reactive near field, which is the closest to the antenna [5]. In this region, EM fields are primarily dominated by reactive components, such as electric and magnetic fields, rather than propagating EM waves. The energy is stored in these fields, and there is limited propagation. The reactive near-field region extends only a fraction of a wavelength from the antenna, and its size depends on the operating frequency and the size of the antenna [6].

Beyond the reactive near-field region lies the radiating near-field region, also known as the Fresnel region. In this region, EM fields exhibit a mix of reactive and radiative characteristics. While there is still energy storage in the fields, some energy begins to radiate away as EM waves. The radiating near-field region extends farther from the antenna compared to the reactive near-field region, typically up to a few wavelengths from the antenna. In NFC, this region is essential for efficient energy transfer and communications.

The radiating field can also be classified into different regions based on the different approximations appropriate

within these regions, i.e., the Fresnel and Fraunhofer approximations. For free-space transmission of EM signals, the Fresnel-Kirchhoff formula provides the solution to the Helmholtz equation in the radiating field [68]. However, since the Fresnel-Kirchhoff formula includes the Euclidean distance between points on the transmit and receive apertures, the resulting integration is difficult to calculate. There are two major approximations and field regions:

- **Fresnel Field Region**: This is the region where the Fresnel approximation [74] is valid. In the Fresnel approximation, the Euclidean distance is expanded into a Taylor series, and only the first two terms are retained. As a result, for a transmitter with a large aperture, the Fresnel field region is equivalent to the paraxial region [75].
- **Fraunhofer Field Region**: This is the far-field region where the Fraunhofer approximation [63] is valid. This approximation further removes the quadratic terms corresponding to the position on the transmit aperture. Thus, compared with the Fresnel field region, the Fraunhofer field region is further away from the array aperture.

The boundaries separating the far field from the radiating near field, and the radiating near field from the reactive near field, are denoted as the Rayleigh distance (or Fraunhofer distance) and the Fresnel distance, respectively [76].

Recently, there has been a growing interest in the near-field region between two transceivers with large apertures. For instance, when considering a transmitter with an aperture of size A communicating with a receiver equipped with a single antenna, the Rayleigh and Fresnel distances are given by $\frac{2A^2}{\lambda}$ and $\frac{1}{2}\sqrt{\frac{A^3}{\lambda}}$, respectively [76], where λ is the wavelength of the signal. However, between two large apertures, the field boundaries may change significantly due to the path difference between different pairs of transmit and receive antennas. In [67], a near-/far-field boundary for the *electrically-small regime* of RISs was provided and compared with the Rayleigh distance. In [77], the near-/far-field boundary for a channel between a transmitter and a receiver with large apertures was studied, yielding the extended Rayleigh distance as $\sqrt{\frac{2\Delta x_{T,max}\Delta y_{T,max}}{\lambda}} \sqrt{\frac{2\Delta x_{R,max}\Delta y_{R,max}}{\lambda}}$, where $\Delta x_{T/R,max}$ and $\Delta y_{T/R,max}$ are the maximum dimensions of the transmit/receive arrays in the x and y directions, respectively. In [4], $\frac{2(A_1^2 + A_2^2)^2}{\lambda}$ was proposed as the near-/far-field boundary for two MIMO arrays with aperture sizes A_1 and A_2 . Following a similar approach to [4], the reactive/radiating near-field boundary for these two MIMO arrays can be determined as $\frac{1}{2}\sqrt{\frac{A_1^3 + A_2^3}{\lambda}}$ [52].

In Fig. 6, we illustrate the Rayleigh and Fresnel distances with respect to (w.r.t.) a transmitter equipped with a ULA. It can be observed that the Fresnel distance is much smaller than the Rayleigh distance, indicating the adequacy of the Fresnel approximation in the majority of the near-field region. The Rayleigh and Fresnel distances are determined based on phase discrepancies caused by spherical-wave propagation without considering amplitude/power differences [76]. However, the propagation distance affects both phase and amplitude. To address this, [78] introduced the concept of uniform-power distance that is numerically derived as the minimum distance

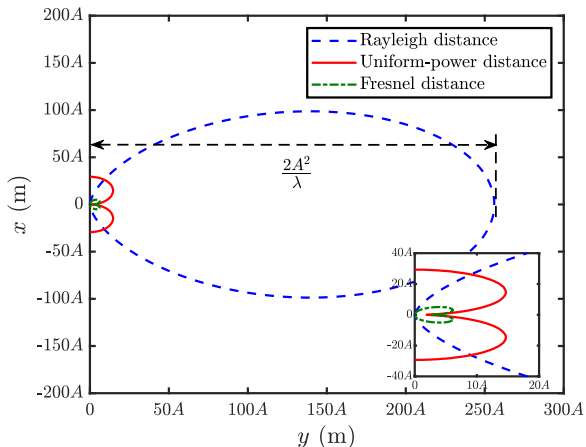


Fig. 6: Illustration of Rayleigh distance, uniform-power distance, and Fresnel distance, where the transmitter is equipped with a ULA comprised of $N = 257$ antennas and operates at 28 GHz. The antenna spacing is $d = \frac{\lambda}{2} = 0.54$ cm. The aperture of the ULA is $A = (N - 1)d = 1.37$ m.

where the power ratio between the weakest and strongest links exceeds a specific threshold. Fig. 6 presents the uniform-power distance for a threshold value of 0.95. Beyond the uniform-power distance, the channel gain disparity of each link becomes negligible. However, for distances less than the uniform-power distance, considering amplitude variation across the receive aperture is necessary when modeling the channel response. Fig. 6 emphasizes that the uniform-power distance does not consistently fall below the Rayleigh distance, as they are defined based on different criteria: channel gain variations and phase errors, respectively. We designate the radiating near-field regions within and beyond the uniform-power distance as the non-uniform spherical wave (NUSW) and uniform spherical wave (USW) regions, respectively. These concepts are applicable to both SPD and CAP arrays.

3) *EM Information Theory (EIT) and DoFs*: Recently, in order to characterize the unique features of near-field channels, EIT has been proposed as a fundamental analytical tool that integrates classical information theory with EM theory.

Existing models that are built on far-field and discretized assumptions encounter challenges when dealing with ultradense MIMO arrays or CAP arrays [79]. In the pioneering work of Migliore [80], the interdisciplinary concept of EIT is introduced to combine classical EM theory and information theory. This integration aims to investigate information transmission mechanisms in spatially continuous EM fields. EIT serves as a unifying framework that consolidates fundamental laws and methodologies. It provides a systematic approach for modeling systems and analyzing performance, seamlessly integrating EM propagation into the study of wireless information systems. Specifically, EIT employs *Green's function-based channel modeling approaches* to explore the capacity of near-field channels.

A significant application of EIT lies in the examination of DoFs and EDoFs in near-field channels. In essence, a DoF analysis offers insights into the number of independent signal dimensions available for conveying information in a wireless

channel. The fundamental capacities of near-field channels can be revealed by determining the number of available DoFs [81]. In a wireless channel, the number of DoFs is contingent upon various factors such as bandwidth, range, and aperture size. Broadly speaking, a wideband channel offers more DoFs compared to a narrowband channel, since a wireless system with an extremely narrow bandwidth can only support a single data stream, resulting in a single DoF. In terms of aperture size, a wireless system equipped with larger transceiver apertures can provide more DoFs than one with a smaller aperture. When the transmit aperture size is highly constrained, the EM waves generated from different transmit points become nearly identical and indistinguishable at the receiver, reducing the number of DoFs. In addition to bandwidth and aperture size, the transmission range, considering both far- and near-field propagation, also plays a pivotal role in determining the number of DoFs, which is the focus of our discussion. To streamline the DoF-related discussion, we assume: i) the EM signal is monochromatic, ii) the channel is narrowband, with the signal bandwidth lower than the coherence bandwidth, and iii) the transceivers possess relatively large apertures, allowing the EM waves from different antennas to be distinguishable. The following sections will introduce the definitions of DoF and EDoF by examining a single-user LoS MIMO channel supported by SPD and CAP arrays. Detailed analyses of DoFs and EDoFs for various near-field channels will be presented in Section IV.

- *SPD-MIMO*: In the context of SPD-MIMO, the comprehensive channel response in the narrowband case is represented as a matrix \mathbf{H} with dimensions $N_r \times N_t$, where N_r and N_t represent the numbers of receive and transmit antennas, respectively. Leveraging the singular value decomposition (SVD) of this channel matrix facilitates the effective decomposition of the SPD-MIMO channel into multiple independent single-input single-output (SISO) sub-channels. These sub-channels operate in parallel, free from mutual interference. Mathematically, the number of positive singular values or the rank of the correlation matrix $\mathbf{H}\mathbf{H}^H$ corresponds to the number of sub-channels with a non-zero signal-to-noise ratio (SNR). Each such sub-channel accommodates an independent communication mode within the MIMO channel. The aggregate number of communication modes represents the *spatial DoFs* of the channel, denoted as DoF. Furthermore, for a MIMO Gaussian channel, the rate of capacity growth can be expressed as $\text{DoF} \cdot \log_2(\text{SNR})$ at high SNR. Therefore, the number of DoFs is also referred to as the *high-SNR slope* or maximum *multiplexing gain* relative to a SISO channel [5].

In a far-field MIMO LoS channel, the presence of only a single incident angle at all points across the array corresponds to plane-wave propagation. In such cases, the channel has a rank of 1, corresponding to only a single DoF. In contrast, within the near-field region, spherical waves manifest nonlinearly varying phase shifts and power levels for each link. This inherent diversity increases the rank of the channel matrix, whose DoFs approach $\min\{N_r, N_t\}$. This implies that, by reducing the antenna spacing within a fixed aperture, the number of spatial DoFs can be significantly increased. However, it is essential to note that when two antennas are

in close proximity to each other, the waves they generate at the receiver become nearly indistinguishable. This limitation should be considered, as it could potentially restrict the achievable increase in channel capacity when incorporating a large number of transceive antennas within a fixed aperture.

We denote the ordered positive singular values of matrix \mathbf{H} as $\sigma_1 \geq \dots \geq \sigma_{\text{DoF}}$. Extensive simulations and measurements have consistently shown that, for small values of n , the σ_n values exhibit a slow decay until they reach a critical threshold, beyond which rapid decay occurs. This critical threshold is termed the “number of EDoFs”, denoted as EDoF_1 , and is illustrated in Fig. 7. This phenomenon becomes more pronounced as the number of transceive antennas increases. In scenarios where the transceivers are equipped with ELAAs, it is frequently observed that the dominant sub-channels possess nearly identical channel gains, i.e., $\sigma_1 \approx \dots \approx \sigma_{\text{EDoF}_1} \gg \sigma_{\text{EDoF}_1+1} > \dots > \sigma_{\text{DoF}}$. In such cases, EDoF_1 can be approximated as $\text{EDoF}_1 \approx \frac{(\sum_{i=1}^{\text{DoF}} \sigma_i)^2}{\sum_{i=1}^{\text{DoF}} \sigma_i^2} = (\text{tr}(\mathbf{H}\mathbf{H}^H) / \|\mathbf{H}\mathbf{H}^H\|_F)^2$. This approximation is used to indicate the number of EDoFs, and we denote it as EDoF_2 . EDoF_2 can be calculated for any arbitrary channel matrix, irrespective of whether the system operates in the near or far field and under either LoS or NLoS propagation. As an illustrative example, consider the LoS channel. In a far-field LoS MIMO channel with a single source, the channel matrix has a rank of 1, and hence $\text{EDoF}_2 = 1$. Conversely, for a single-user near-field LoS MIMO channel, EDoF_2 can fall between 1 and DoF, depending on the distance of the source to the array and the array aperture.

We note that the concept of EDoF_2 was originally introduced by Muharemovic *et al.* [82], extending Verdú’s previous work in [83] and approximating the MIMO channel capacity as $\text{EDoF}_2 \cdot [\log_2(\frac{E_b}{N_0}) - \log_2(\frac{E_b}{N_0}_{\min})]$ in the low-SNR regime, where $\frac{E_b}{N_0}$ represents the bit energy over noise power spectral density, and $\frac{E_b}{N_0}_{\min}$ is the minimum value required for reliable communications. Additionally, $\frac{E_b}{N_0}$ is determined by the product of the channel capacity and the SNR [83, Eqn. (14)]. It is important to emphasize that the original definition of EDoF_2 has a distinct physical interpretation when compared to EDoF_1 and DoF. In recent years, some researchers have identified applications of EDoF_2 in approximating the number of EDoFs of NFC [50].

- **CAP-MIMO:** Next, we consider the scenario where both transceivers are equipped with CAP arrays, denoted as CAP-MIMO. Unlike an SPD antenna array, which provides finite-dimensional signal vectors, the CAP array supports a continuous distribution of source currents within the transmit aperture. This configuration results in the generation of an electric radiation field at the receive aperture. The spatial channel impulse response between any two points on the transceive CAP arrays is described by Green’s function. This function connects the transmitter’s current distribution and the receiver’s electric field through a spatial integral. Green’s function accurately models the EM characteristics in free space and effectively captures the channel response between the transceivers.

Similar to the SPD-MIMO channel, the spatial CAP-MIMO channel can be decomposed into a series of parallel SISO

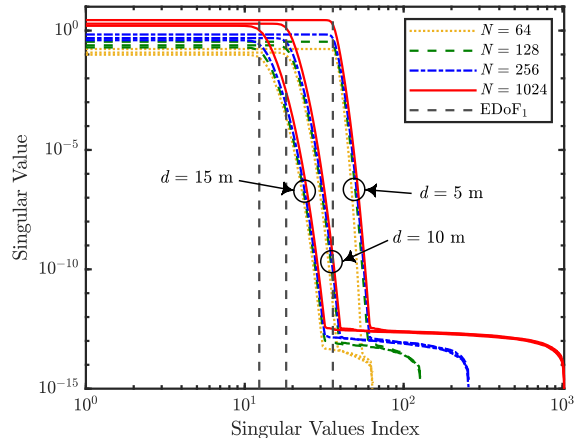


Fig. 7: Illustration of the singular values and EDoF_1 for various SPD-MIMO LoS channels, where both transmitter and receiver are equipped with N -element uniform linear arrays (ULAs), and the system operates at a frequency of 28 GHz (with a corresponding wavelength of 1 cm). The ULAs have an aperture of 1.37 m. The center of the transmit array is located at the origin of a three-dimensional space, while the center of the receive array is at $(0, d, 0)$ with d denoting the link distance. The ULAs face each other and are parallel to the z -axis.

sub-channels by determining the equivalent “SVD” of Green’s function [84, Eqn. (27)]. The resulting equivalent “left singular vectors” and “right singular vectors” form two complete sets of orthogonal basis functions, corresponding to the transmit and receive apertures, respectively. The resulting equivalent “singular values” represent the channel gains of the decomposed sub-channels. Alternatively, these “singular values” can be obtained through an eigenvalue decomposition of the Hermitian kernel of Green’s function, analogous to the correlation matrix $\mathbf{H}\mathbf{H}^H$ for SPD arrays; refer to [84, Eqn. (42)] and [5, Section II-C] for further details. The number of non-zero “singular values” of Green’s function, or equivalently, the non-zero eigenvalues of its kernel, is defined as the number of DoFs, denoted as DoF. DoF also represents the number of SISO sub-channels at a non-zero SNR, each supporting an independent communication mode.

Given that CAP-MIMO can be regarded as SPD-MIMO with infinitesimal antenna spacing and an infinite number of antennas, the number of DoFs of a near-field CAP-MIMO channel can theoretically approach infinity due to spherical wave propagation [84]. Consequently, the near-field effect significantly augments the spatial DoFs for CAP-MIMO. However, despite the potentially infinite number of positive singular values, the number of dominant singular values is rather limited. Notably, extensive research has demonstrated that the ordered singular values of near-field CAP-MIMO channels exhibit a step-like behavior, and the number of EDoFs, denoted as EDoF_1 , corresponds to the sharp knee in this curve [50]. Within the framework of EIT, various methods exist to compute the EDoFs in near-field CAP-MIMO, as elaborated in Section IV-A. One of the simplest methods among these involves using an EDoF_2 -based approximation.

In CAP-MIMO, EDoF2 is defined by replacing the channel matrix \mathbf{H} in $(\text{tr}(\mathbf{H}\mathbf{H}^H)/\|\mathbf{H}\mathbf{H}^H\|_F)^2$ with its Green's function-based counterpart [85].

III. CHANNEL MODELING OF NFC

Having discussed the fundamental physical properties of NFC, in this section, we focus our attention on NFC channel modeling. In particular, we highlight the spatial non-stationarity encountered in near-field channel modeling and then provide a comprehensive discussion of non-stationary near-field channel modeling in both LoS and NLoS scenarios.

A. Spatial Non-Stationarity in Near-Field Channel Modeling

In a conventional far-field MIMO system, the aperture of the antenna array is typically much smaller than the propagation distance between transceivers. Consequently, the entire array can be effectively treated as a single point, and signals transmitted from different locations of the array experience equal path loss and have common angles of departure/arrival (AoAs/AoDs) upon arrival at different locations within the receive array. Furthermore, the entire array is visible to users or scatterer clusters, and the radiated power is distributed evenly across the array, as depicted in Fig. 8(a). This phenomenon results in the entire channel exhibiting the characteristic of *spatial stationarity* in the far-field region.

However, as we enter the era of 6G networks marked by the widespread deployment of ELAAs, notable changes in channel behavior have come to the fore. Recent channel measurements have indicated that *non-stationary* channel characteristics become increasingly prominent as the array aperture grows significantly larger [86]–[88]. One aspect of spatial non-stationarity manifests itself as the appearance or disappearance of scatterers or users when transitioning from one antenna element's perspective to another. This implies that different antenna elements may observe distinct sets of scatterers or users and experience variations in parameters such as power and delay. This phenomenon is particularly pronounced in near-field channels [53], [89], [90], where two main issues related to non-stationarity emerge.

1) *Spherical Wavefront*: In NFC systems, the distance between the transceiver and scatterer may be less than the Rayleigh distance. Consequently, it is imperative to consider spherical instead of planar wavefronts.

2) *Visibility Region (VR)*: NFC communication systems often feature arrays with an exceptionally large aperture, and different segments of the array will have distinct perspectives of the propagation environment. Consequently, these segments observe the same channel paths but with varying power levels or even entirely different channel paths. This phenomenon is substantiated by recent empirical findings [91]–[95]. In this configuration, users or clusters of scatterers can only perceive a fraction of the antenna array due to the rapid signal attenuation and the substantial array size. The portion of the antenna array that remains visible to users or scatterers is referred to as the VR w.r.t. the array [96]. The VR reveals the uneven distribution of channel power across the array and arises from the following two primary factors [53], [96].

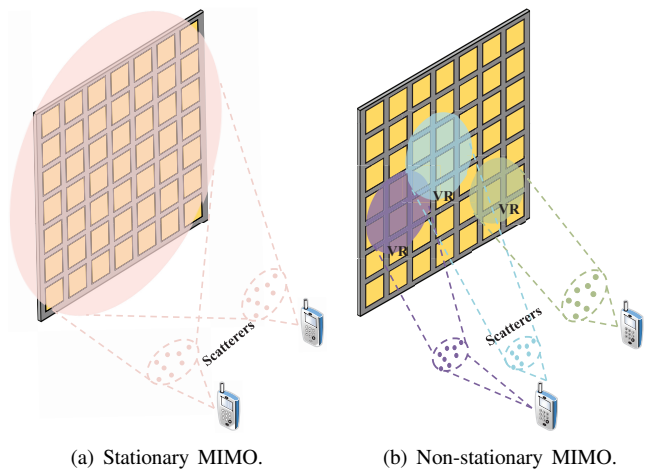


Fig. 8: VRs of stationary MIMO and non-stationary MIMO.

- i) *Unequal Path Loss (UPL)*: When the propagation distance is comparable to or smaller than the array aperture, the path loss experienced by transmitted signals becomes highly dependent on the precise distances between transmit and receive antenna elements. Since the path loss between the transmission point \mathbf{t} and the reception point \mathbf{r} is inversely proportional to the propagation distance $\|\mathbf{r} - \mathbf{t}\|$, a significant variation in path loss for different pairs of transmit and receive antennas occurs due to wide variety to distances between them. As depicted in Fig. 9(a), the channel power is primarily captured by a subset of antennas within the array aperture, with a concentration of power near the source. Conversely, antennas much farther from the source experience significantly weaker channels.
- ii) *Blockage due to Obstacles*: An ELAA, with its extensive aperture, may be deployed on the facade of a building in an urban environment. Urban settings are typically crowded, with users often in close proximity to the array. Urban elements such as trees, vehicles, and infrastructure can potentially obstruct the channel between the array and a particular user. In contrast to the far field, where the entire channel may be blocked, near-field scenarios can lead to the blockage of only a portion of the array. The blocked portion is determined by the geometric relationships among the array, user, and obstacles. Furthermore, the obstructed portion will often reflect the contours of the obstructing objects. As illustrated in Fig. 9(b), the blocked subarrays, depicted in dark colors, exhibit patterns similar to the obstacles that cause them. This uneven distribution of channel power due to blockage is independent of the variations caused by UPL.

Each user or scatterer possesses its own specific VR, and the locations of VRs for different users or scatterers can be separate, partially overlapping, or completely overlapping, contingent upon the surrounding environment and the relative positions of users or scatterers along the antenna array. Consequently, antenna elements in different areas of the array may fall within the VRs of different scatterers or users, leading to variations in signal power, angular power spectra, and power

delay profiles among antennas.

The aforementioned points collectively underline the *spatial non-stationarity* inherent in near-field channels, which is distinct from far-field channels. This property has been mathematically validated in [97] and confirmed empirically through measurements conducted in [98] and [99]. In the following, we will discuss non-stationary near-field channel models considering scenarios involving both LoS and NLoS propagation.

B. LoS Channel Models

As previously mentioned, the expansion of the near-field region predominantly occurs within the millimeter-wave (mmWave) and sub-THz frequency bands. Consequently, the resulting channels are characterized by a dominance of LoS propagation. Developing a LoS channel model that is both tractable and amenable to analysis holds significant importance in the context of NFC. Such a model is essential for gaining valuable insights into system design. In the following, we will delve into the revision of LoS models tailored for near-field channels supported by SPD and CAP arrays, respectively. In the interest of brevity, our emphasis is placed on narrowband channels.

1) *SPD-NFC*: The narrowband LoS channel coefficient between a pair of SPD antennas is typically characterized by a complex-valued channel response that links the transmit point \mathbf{t} and the receive point \mathbf{r} . The channel response comprises two foundational components: amplitude and phase. In the context of NFC, the phase component is conventionally expressed as $e^{-j\frac{2\pi}{\lambda}\|\mathbf{r}-\mathbf{t}\|}$, where λ represents the wavelength. In contrast, a diverse range of methods exists for modeling the amplitude component, offering flexibility to tailor the modeling approach according to the scenario under study. Broadly, when modeling the amplitude component in SPD-NFC, three essential properties merit consideration:

- i) *Free-Space Path Loss (FSPL)*: This pertains to the power loss incurred due to free-space radiation, and it is inherently a function of the propagation distance $\|\mathbf{r} - \mathbf{t}\|$ and the wavelength λ .
- ii) *Effective Aperture Loss (EAL)*: This aspect accounts for power loss resulting from the mismatch between the direction of the incident signals and the normal direction of the maximum effective aperture or area³ of the receive antenna. It reflects the deviation from optimal reception conditions [6], [100]–[102].
- iii) *Polarization Loss (PL)*: This term signifies the power loss due to polarization effects and is typically quantified

³Effective aperture or effective area characterizes the received power of an antenna [6], [100]–[102]. Assume that the incident wave has the same polarization as the receive antenna and is traveling towards the antenna in the antenna's direction of maximum radiation (the direction from which the most power would be received). Then, the effective aperture A_e describes how much power is captured from a given incident wave. Let p_0 be the power density of the incident wave in Watt/m². Then, the antenna's received power in Watts is given by $p_0 A_e$. An antenna's effective area or aperture is defined for reception. However, due to reciprocity, an antenna's directivity for reception and transmission are identical, so the power transmitted by an antenna in different directions is also proportional to the effective area [6], [100]–[102].

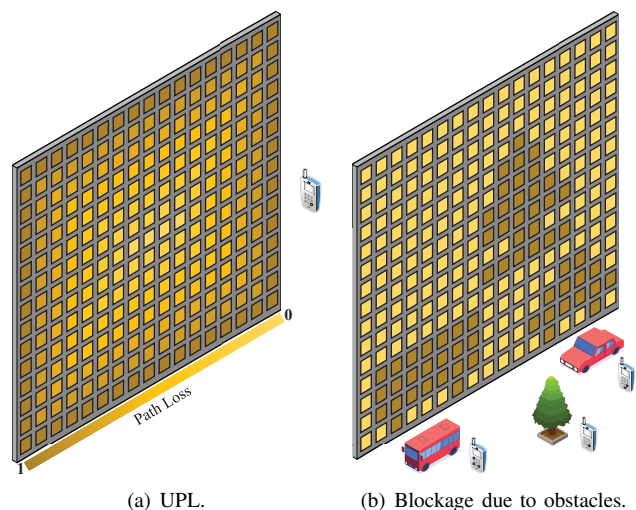


Fig. 9: Manifestations of the VR in NFC. In (a), light and dark squares represent antennas whose path losses are strong and weak, respectively. In (b), light and dark squares represent antennas whose channels are visible and blocked, respectively.

as the squared norm of the inner product between the polarization vector at the receive and transmit antennas [6], [101]. Polarization losses provide insight into the alignment or misalignment of signal polarizations.

Incorporating these considerations into the modeling of the amplitude component allows for a comprehensive understanding of near-field channel characteristics.

The deployment of ELAAs in NFC gives rise to a high-dimensional channel environment. Understanding this complicated channel involves considering the relationship between the array aperture and the distance between the transceivers. In this regard, the characterization of amplitude components for SPD antennas can be elucidated through two distinct models as follows.

- *USW Model*: This model applies when the array aperture is relatively smaller compared with the propagation distance, with the receiver situated within the *USW region* [5], [103]. In this scenario, the channel response exhibits a *uniform spherical wave* feature, where amplitude variation across the receive aperture can be safely disregarded. In other words, the amplitudes remain consistent for any pair of transmit and receive points at the transceivers. Additionally, with regard to EAL and PL, a small array aperture relative to the communication distance results in the receiver perceiving signals from various array elements at nearly the same angle. Consequently, signals from different transmit antennas encounter comparable EAL and PL.

In contrast to the amplitude component, the received signal phases depend precisely on the distances between the transmit and receive antennas. Specifically, the phase component between \mathbf{t} and \mathbf{r} is proportional to the propagation distance $\|\mathbf{r} - \mathbf{t}\|$, and this relationship manifests itself as a square root function w.r.t. the antenna index. In the USW region where the propagation distance is significantly greater than the dimensions of each SPD antenna, the “*Fresnel approximation*” effectively approximates the aforementioned square root term

as a quadratic term w.r.t. the antenna index using a Maclaurin series expansion [5], [104], [105]. In addition to the quadratic phase approximation, a piecewise-far-field channel characterized by piecewise-linear phase properties to approximate the near-field channel with high accuracy was introduced in [106, Fig. 3]. This approximation was considered as a piecewise linearization of the classical near-field channel model.

The above arguments suggest that spatial non-stationarity in the USW model primarily manifests itself in the phase component of each complex-valued channel response.

The USW model was originally proposed by Driessen and Foschini [19] to characterize non-fading LoS propagation in MIMO systems with widely spaced antennas. Subsequently, in 2006, the authors of [107] described the rank and singular values of the channel matrix in a 2×2 short-range MIMO setup, specifically addressing near-field MIMO channels. This foundational work was further expanded to encompass arbitrary near-field LoS MIMO channels employing uniform linear antenna arrays [108]. Due to its tractability and ease of analysis, the USW model has found widespread adoption in numerous research endeavors related to NFC. For instance, it has been extensively employed in the design of channel estimation [109]–[112] and beam training [113]–[115] algorithms for near-field MIMO channels. Furthermore, building upon this model, the authors of [116] demonstrated the asymptotic orthogonality of near-field beamforming vectors in the range domain, when the number of antennas approaches infinity. However, this conclusion is not entirely precise, as the USW model cannot be applied to an infinitely large array [117].

While the USW model has attracted significant research interest, the majority of investigations have primarily focused on the impact of FSPL, often overlooking the effects of EAL and PL when characterizing the amplitude component. Additionally, in the aforementioned works, the USW models considered the influence of the spherical wavefront but omitted the influence of the VR. The USW model inherently assumes equal path loss along the entire SPD array. As such, incorporating the effects of VR into the USW model necessitates accounting for blockages caused by obstacles between the user and the array. A significant step in this direction was taken by the authors of [53], who introduced the concept of VR in the USW model by introducing a zero-one VR mask that multiplies the array response vector, expanding the model's applicability and accuracy.

- *NUSW Model*: When the array aperture is comparable to the propagation distance, i.e., when the receiver is situated within the *NUSW region*, the channel response takes on a distinctive *non-uniform spherical wave* characteristic. In this context, both the amplitude and phase exhibit pronounced variations across the receive aperture [5]. Consequently, precise modeling of the phase component and accounting for FSPL within this region necessitate consideration of the exact propagation distance between the specific transmit and receive points [5]. Furthermore, owing to the closely matched array size and propagation distance, the receiver perceives signals from different array elements at varying angles [5]. This phenomenon results in dynamic fluctuations in EAL and PL across the array. Compared with the USW model, the NUSW model

offers a *more intricate yet inherently accurate* representation when the array aperture is similar in size to the propagation distance. It is important to note that *spatial non-stationarity in the NUSW model is manifest in both the phase and amplitude components of each complex-valued channel response.*

The application of the NUSW model has evolved over the years, with various milestones marking its progress. The first NUSW model-based MIMO channel response was proposed by Driessen and Foschini [19] based on ray tracing, and was used to describe LoS propagation in MIMO systems. In 2003, Jiang and Ingram [22] harnessed this model to find the previously unknown answer to the question of why the capacity of short-range MIMO channels reconstructed from the measured path parameters, such as the AoA and AoD, was always less than the capacity measured directly [20], [21]. In [22], the authors showed that a major reason for the discrepancy is incorrect modeling of the LoS path, and using the NUSW model to reconstruct the channel response, especially in terms of computing received signal phases based on the precise distances between transmit and receive antennas, is necessary to remove the discrepancy. Furthermore, these authors provided empirical results at 5.8 GHz, defining a threshold distance below which the spherical-wave model was essential for accurate performance estimation using ray tracing [23]. Since then, the NUSW model has found extensive application in short-range MIMO communications, including femtocells and IEEE 802.11 (WiFi) [118]–[122], among others.

The NUSW model made its debut in near-field LoS conditions in 2015, where the authors of [25] showed that spherical wavefronts were more effective than plane wavefronts in decorrelating the spatial channels. However, they only considered the FSPL by treating the array elements as dimensionless points, neglecting the effects of EAL and PL. As a further advancement, the authors of [123] incorporated the variation of the projected effective aperture into the signal amplitude model and used this model to analyze the power scaling law of near-field MISO channels. Importantly, this work focused on hypothetical isotropic antennas, where the directional gain pattern is constant and independent of the direction of signal incidence. Building on this, researchers from the same group [124] introduced a more generic directional gain pattern for each antenna element, as a function of the elevation and azimuth angles of the incident signal. On this basis, they proposed a more comprehensive NUSW model for LoS propagation in extremely large-scale IRS communications. However, the influence of PL was not considered in the works mentioned above. To address this gap, [125] extended prior research by accounting for both the EM polarization effect of the antenna elements and their signal amplitude variations in the NUSW model. This new NUSW model is specifically applicable when both the receiving-mode polarization vector of the receive antenna and the normalized electric current vector are along the same axis [125]. In [5], an improved NUSW model was proposed that applies to arbitrary polarization modes and current directions.

To incorporate the influence of the VR into the NUSW model, a binary VR mask vector can be introduced [53]. In the case of blockage, where part of the array is obstructed, the

mask covers only the unblocked array elements, represented by 1, while the obstructed elements are set to 0 [53]. However, in the absence of obstacles, the mask should select array elements that capture the majority of the power across the whole array [53]. In this scenario, an all-one mask vector can be used, aligning with the inherent assumption in the NUSW model that path loss varies unevenly across the entire SPD array. The NUSW models mentioned above have mainly used an all-ones mask when there is no blockage. Alternatively, a zero-one mask can be also used, resulting in an approximate channel model with reduced dimensionality. This can help simplify transceiver design, as demonstrated in previous works [126], [127].

In summary, the development and application of the NUSW model in the context of near-field LoS channel modeling have seen significant progress and have been accompanied by considerations of factors such as directional gain patterns, polarization effects, and the influence of the VR. The primary contributions in the realm of near-field LoS channel modeling for SPD antennas are summarized in Table IV.

2) *CAP-NFC*: We shift our attention to LoS channel models for NFC supported by CAP arrays. In contrast to SPD-NFC, which involves a large number of discrete antennas having specific spacing, CAP-NFC adopts a continuous array model composed of an infinite number of antennas separated by infinitesimal distances. This eliminates the need to specify *a priori* the number of antennas and their relative positions, and resembles the optical communication systems introduced by Gabor [128].

Compared to the SPD antenna array, which delivers finite-dimensional signal vectors, the CAP array supports a continuous distribution of source currents $\mathbf{j}(\mathbf{t}) \in \mathbb{C}^{3 \times 1}$ within the transmit aperture \mathcal{V}_T . This gives rise to the generation of an electric radiation field $\mathbf{e}(\mathbf{r}) \in \mathbb{C}^{3 \times 1}$ at the receive aperture \mathcal{V}_R , as depicted in Fig. 10. The spatial LoS channel impulse response between any two points (\mathbf{r}, \mathbf{t}) on the CAP transceiver arrays is described by the tensor *Green's function* $\mathbf{G}(\mathbf{r}, \mathbf{t}) \in \mathbb{C}^{3 \times 3}$ [129]. This function connects the transmitter's current distribution and the receiver's electric field via a spatial integral $\mathbf{e}(\mathbf{r}) = \int_{\mathcal{V}_T} \mathbf{G}(\mathbf{r}, \mathbf{t}) \mathbf{j}(\mathbf{t}) d\mathbf{t}$ [130]. Green's function accurately models the EM characteristics in free space and effectively represents the channel response between the transceivers, akin to the channel matrix for SPD-NFC. It is important to note that the tensor Green's function includes the triple polarization, where each element of $\mathbf{G}(\mathbf{r}, \mathbf{t})$ is the scalar Green's function between one certain polarization of the receive point and one polarization of the source point. The scalar Green's function is without polarization. Additionally, the influence of effective aperture [28], [131], [132], polarization mismatch [5], [133], and the VR can be incorporated into Green's function. Furthermore, when the receiver is situated in the USW region, the uniform channel power approximation can be employed to simplify Green's function.

As a first attempt, Miller [134] introduced the use of scalar Green's function to characterize LoS channel responses between two 3D CAP arrays. Significantly, this model is applicable in both the radiating near-field and far-field regions. Building on this foundation, subsequent authors [28],

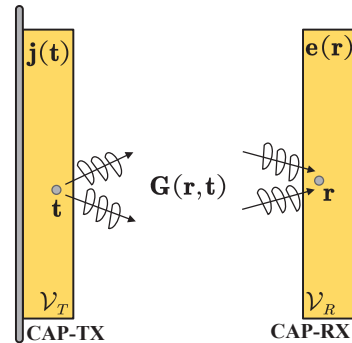


Fig. 10: Illustration of CAP-NFC in LoS propagations.

[131], [132] extended the model to account for the effects of the projected aperture. They focused on characterizing LoS propagation between a CAP array and a point in its radiating near field. Utilizing the Fresnel approximation, [84] further contributed by proposing a simplified scalar Green's function model tailored specifically to the near-field LoS scenario within the USW region. Additionally, this model has been utilized to describe near-field LoS propagation in STAR-RIS communications [77]. Subsequently, the authors of [135]–[137] expanded the scalar model in a tensor-based model to explore the DoFs of CAP-NFC.

By incorporating Fourier transforms, the authors of [138] expanded the tensor Green's function into a summation of three terms. The first term corresponds to radiating near and far fields, while the remaining two terms pertain to the reactive near field. Importantly, the power of these last two terms decayed much more rapidly than $\|\mathbf{r} - \mathbf{t}\|^{-2}$ and does not significantly contribute to EM radiation. By excluding these two terms, [139] derived a simplified tensor Green's function LoS model for communications between a pair of active intelligent surfaces. This model specifically addressed the radiating near-field and considered the influence of effective aperture and uni-polarization mismatch. Furthermore, this model has been adopted by the authors of [133] to characterize LoS propagation in applications with extremely large aperture passive reflecting surfaces. Additionally, the authors of [5] further extended this model by accounting for the impact of polarization mismatch for tri-polarized antennas. Remarkably, each antenna in SPD-NFC can be treated as a small CAP array, allowing their EM properties to be effectively characterized by Green's functions. Building upon this insight, the authors of [140] introduced a tensor Green's function LoS model tailored for SPD MU-MIMO channels, with a particular focus on its applicability within the USW region.

A summary of the primary contributions regarding near-field LoS channel modeling for CAP arrays can be found in Table V.

C. NLoS Channel Models

Given the expansive array apertures typical for NFC systems, the existence of a LoS propagation link between the transmitter and receiver is quite common. In such scenarios, the LoS propagation channel predominantly governs EM transmission. However, practical wireless propagation is often

TABLE IV: Contributions on LoS Channel Modeling for SPD-NFC

Category	Ref.	Array	Amplitude			VR		Characteristics
			FSPL	EAL	PL	UPL	Blockage	
Uniform	[108]	ULA	✓	✗	✗	✗	✗	The first application of the USW model to near-field MIMO
	[104]	ULA	✓	✗	✗	✗	✗	Fresnel approximation-based phase shifts
	[116]	UPA	✓	✗	✗	✗	✗	Fresnel approximation-based phase shifts
	[53]	ULA&UPA	✓	✗	✗	✗	✓	The generation of the VR comes from the blockages
Non-Uniform	[25]	ULA	✓	✗	✗	✓	✗	The first application of the NUSW model to near-field MIMO
	[126]	ULA	✓	✗	✗	✓	✓	The generation of the VR comes from both UPL and blockages
	[123]	UPA	✓	✓ (Isotropic)	✗	✓	✗	A clear model for effective aperture area of isotropic antennas
	[124]	UPA	✓	✓ (Arbitrary)	✗	✓	✗	An LoS model for extremely large-scale IRS communications
	[125]	UPA	✓	✓ (Isotropic)	✓ (Uni-polarized)	✓	✗	A clear model for polarization mismatch of uni-polarized antennas
	[5]	UPA	✓	✓ (Isotropic)	✓ (Tri-polarized)	✓	✗	A general model that considers FSPL, EAL, and arbitrary PL

TABLE V: Contributions on Green's Function-Based LoS Channel Modeling for CAP-NFC

Category	Ref.	Amplitude			Expansion Terms		Region of Application	Characteristics
		FSPL	EAL	PL	radiating	Reactive		
Scalar	[134]	✓	✗	✗	✓	✗	The radiating near-field region	The first application of scalar Green's function to near field
	[28], [131], [132]	✓	✓	✗	✓	✗	The radiating near-field region	The influence of EAL is considered
	[84]	✓	✗	✗	✓	✗	USW region	Fresnel approximation-based propagation distance
	[77]	✓	✗	✗	✓	✗	USW region	A near-field LoS model for STAR-RIS communications
Tensor	[135]–[137]	✓	✗	✗	✓	✓	The whole near-field region	A tensor Green's function-based model for all EM regions
	[139]	✓	✓	✓	✓	✗	The radiating near-field region	The influence of EAL and uni-polarization mismatch is considered
	[133]	✓	✓	✓	✓	✗	The radiating near-field region	An LoS model for extremely large-scale IRS communications
	[5]	✓	✓	✓	✓	✗	The radiating near-field region	A general model that considers FSPL, EAL, and arbitrary PL
	[140]	✓	✗	✗	✓	✓	USW region	A tensor Green's function-based LoS model for MU-MIMO

affected by scattering effects, introducing scenarios with NLoS conditions [5], [53], [89], [141]. In the upcoming sections, we explore stochastic NLoS channel models tailored for NFC in the absence of LoS rays.

1) *SPD-NFC*: We commence our discussion by examining NLoS channel models tailored for SPD-NFC. Several works have modeled the NLoS propagation channel in this context, and among these works, two primary NLoS propagation channel modeling approaches can be identified: *physical propagation-based stochastic models (PPBSMs)* and *correlation-based stochastic models (CBSMs)*.

PPBSMs characterize the propagation environment by considering double-directional EM wave propagation between the transmit and receive arrays. This modeling scheme incorporates key *physical propagation parameters* such as the directions of arrival/departure, multipath delay, scatterer distribution, radar cross-section (RCS) of the scatterers, system bandwidth, and antenna configurations including antenna types, mutual coupling, antenna pattern, polarization, and array geometry. These parameters collectively describe the near-field NLoS channels by accounting for the channel characteristics and the surrounding scattering environment [141]. Furthermore, PPBSMs allow for the statistical modeling of multipath component parameters, which collectively form the total impulse response of the channel. In contrast, CBSMs characterize the impulse response as a function of unstructured channel statistics that do not depend on the physical parameters of individual multipath rays, such as the AoA/AoD. While CBSMs are relatively straightforward to simulate, they may offer limited insights into the propagation characteristics of NLoS channels. Generally, PPBSMs find useful applications in the deployment or optimization of site-specific radio systems. They are also instrumental in channel evaluation during system design in crucial reference cases [141]. CBSMs find a wide range of useful applications in simulation environments, such as link- and system-level simulations, because they are easy

to generate and can be very useful in representing various channel responses [141].

- *PPBSM*: As previously mentioned, the pronounced expansion of the near-field region primarily arises from expanded antenna apertures and the reduction in wavelength at higher frequencies. The increased FSPL inherent to extremely high-frequency propagation results in limited spatial selectivity and scattering. Additionally, the close proximity of large antenna arrays contributes to increased antenna correlation. In addressing this amalgamation of factors, the extended Saleh-Valenzuela (S-V) model emerges as a promising candidate among PPBSMs for characterizing densely populated arrays operating in environments with sparse scattering characteristics. This model equips us with the necessary tools to accurately describe the complex mathematical structures inherent in SPD-NFC channels [142].

In 1987, Saleh and Valenzuela introduced an NLoS model during their tenure at Bell Laboratories [142]. This model aimed to capture the stochastic characteristics of indoor SISO multipath propagation, specifically by modeling the arrivals of multipath components in clusters. According to this clustered model, the wireless channel is assumed to consist of multiple scatterers grouped into clusters based on their respective time delays. The S-V model has served as the foundation for many clustering-based multipath channel models, as seen in [143], which extends [142] to multiple antenna systems employing spatial diversity. This extended model incorporates spatial information, such as AoAs/AoDs, into the channel response. In this extended model, scatterers are clustered based on their respective delays and AoAs/AoDs. Each cluster is then treated as a sub-channel, characterized by specific delay profiles and spatial signatures. The aggregation of these sub-channels results in a comprehensive representation of the overall channel response. Since then, this extended S-V model has been widely recognized as one of the most utilized NLoS channel models based on clusters, often referred to as the

clustered channel model (CCM) [144]. It typically involves describing the channel response in terms of three fundamental components: the *transmit array response*, the *receive array response*, and the *complex gain associated with each ray* in every scattering cluster, as illustrated in Fig. 11(a). The complex gain is often modeled as a complex Gaussian variate, which reflects the RCS of the corresponding scatterer. Here, the Gaussian assumption arises as a diffusion approximation of the scattering mechanism [145]. To adapt the CCM for SPD-NFC, the receive and transmit array response vectors can be replaced with the LoS channel vectors detailed in Table IV. For instance, in [146], a CCM-based NLoS channel model for near-field MIMO channels was proposed by incorporating the NUSW model and accounting for FSPL. In [53], another CCM-based NLoS channel model was introduced, incorporating the NUSW model and accounting for FSPL, EAL, PL, and VR.

While the CCM effectively captures the complexity of NLoS channels, it can impose significant computational demands. In response to this challenge, a streamlined variant of the extended S-V model was proposed, known as the finite-dimensional channel (FDC) model. In the FDC model, each cluster is simplified to contain only a single scatterer [147]. This model assumes that the channel's characteristics are primarily defined by a limited number of dominant paths, each characterized by its delay and AoA/AoD, as depicted in Fig. 11(b). The term “finite-dimensional” in the FDC model does not imply that the channel matrix itself is finite-dimensional, as every narrowband (flat fading) MIMO channel can be expressed as a finite-dimensional matrix. Instead, “finite-dimensional” is used to emphasize that the number of scatterers is finite, resulting in a channel response with a finite angular or polar spatial dimension [148]–[150]. The FDC model is distinguished by its simplicity and computational efficiency, rendering it a popular choice in the domain of SPD-NFC research, as evidenced in [5] and related literature. For instance, the authors of [111] and [151] leveraged the FDC model to depict NLoS conditions in SPD-NFC systems, within the contexts of MISO and MIMO channels, respectively. In these investigations, the USW model was employed to characterize the channel response between the SPD array and the scatterers. As a further advancement, the authors of [126] introduced a more versatile NUSW-based NLoS model tailored for near-field MISO channels.

The precise formulation of a PPBSM-based channel response is contingent upon various factors, including array geometry and the RCS pattern. Of particular significance is the realization that the RCS pattern is not solely contingent on the AoA or AoD, but also intricately linked to the distances of scatterer clusters from the antenna array. This comprehensive characterization is often referred to as the *power location spectrum (PLOS)* [97]. In the context of NFC operating in mmWave or THz bands, the S-V model is frequently employed to capture the sparse scattering phenomenon. This typically involves the use of a discrete PLOS function, accounting for a finite number of scatterers. However, some research endeavors opt for a continuous PLOS function to construct the PPBSM-based channel response, which necessitates a

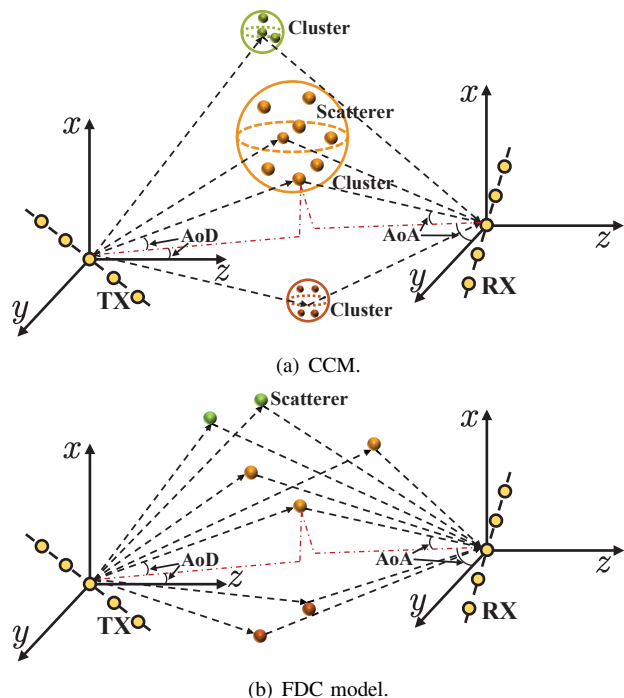


Fig. 11: Illustration of the extended S-V model.

continuous geometrical distribution of scatterers. For instance, the authors of [97] proposed a near-field NLoS PPBSM by adopting a one-ring scatterer distribution [152], [153]. In this model, scatterers are positioned on a ring according to the von-Mises distribution [154], with an arbitrarily located center. The one-ring model has garnered popularity and is commonly used in the context of MIMO systems. Beyond the one-ring model, alternative geometrical scatterer distribution models have been proposed, including the combined elliptical-ring model [155] and the one-disk model [156].

- **CBSM**: CBSM represents another prevalent channel modeling approach for near-field NLoS propagation. Unlike PPBSMs, CBSMs characterize the channel impulse response as a function of unstructured channel statistics that are independent of the physical parameters of individual multipath rays. Instead, CBSMs typically aim to characterize the correlation or covariance of the channels between different pairs of transmit and receive antennas [141]. In the realm of MIMO communications within multipath environments, spatial correlation assumes paramount importance for second-order statistical channel characterization. The characterization of spatial correlation plays a pivotal role in various aspects, including the formulation of the Kronecker channel model [157], [158] and the development of optimal transmission strategies reliant on statistical channel knowledge [159], [160]. CBSMs find widespread utility in simulation environments, such as link-level simulations, due to their ease of use and ability to represent diverse channel responses. Furthermore, CBSMs facilitate the analysis of essential performance indicators, including signal-to-interference-plus-noise ratio (SINR) [161] and ergodic capacity [162], contributing significantly to transceiver design.

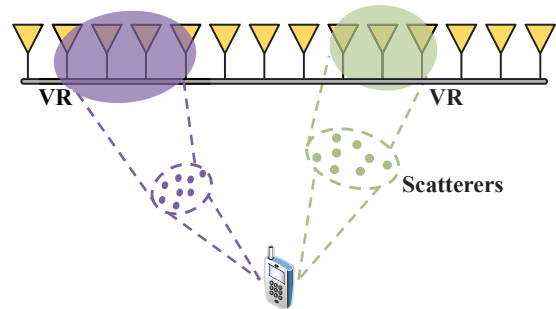
In the context of far-field NLoS channels, the precise nature

of spatial correlation often relies on the plane-wave assumption, contingent upon the *power angular spectrum (PAS)* [152]. Under this framework, the channel correlation coefficient for each pair of array elements depends on their relative position along the array [152]. Conversely, in NFC systems employing arrays with an expanded array aperture, spatial correlation between array elements hinges on their absolute positions along the array, not solely their relative distances [53], [97]. This reflects the *spatial non-stationarity* inherent to near-field NLoS channels.

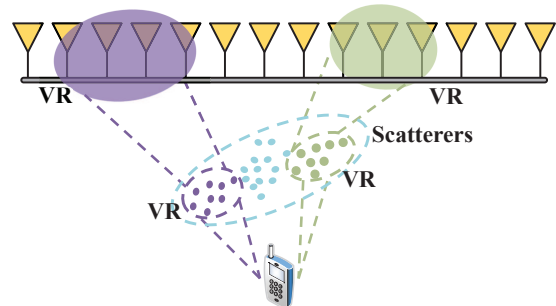
Most channel responses generated by the PPBSM, whether they use the CCM, FDC approach, or other geometrical scatterer distributions, exhibit characteristics of correlated Rayleigh fading due to the inherent Gaussian-distributed complex gain. In the case of MISO channels, the corresponding channel matrix follows a standard form denoted as $\mathbf{R}_n^{1/2} \mathbf{h}$, where \mathbf{R}_n represents the correlation matrix, and $\mathbf{h} \sim \mathcal{CN}(\mathbf{0}, \mathbf{I})$ accounts for the influence of small-scale fading. This is essentially a special case of the Kronecker model [163]. The precise calculation of the correlation matrix hinges on the PLOS including the array geometry and the RCS pattern, making it computationally intensive to compute from a given physical propagation scenario. In addition to leveraging the PLOS, some researchers have proposed constructing the near-field correlation matrix from its far-field counterpart, considering the spatial non-wide sense stationarity across the array aperture [96]. Specifically, the impact of the VR can be incorporated into the correlation matrix to account for the spatial non-stationarity.

The spatial correlation of a non-stationary channel can be established in two different ways, depending on whether scatterer clusters are considered, as depicted in Fig. 12. For the sake of clarity, we illustrate this with the example of a MISO channel. Let \mathbf{R}_f denote the spatial correlation matrix corresponding to a stationary channel, where the influence of scatterer clusters is not emphasized. In traditional multi-antenna systems, \mathbf{R}_f typically has non-zero diagonal entries. However, when introducing the concept of VR, only the diagonal entries related to the VR become non-zero, resulting in a block-sparse correlation matrix. To model the VR, we use a diagonal matrix \mathbf{D} , where \mathbf{D} has D non-zero diagonal entries if the user receives signals from only D antennas. This diagonal matrix \mathbf{D} serves as the VR mask. Consequently, the spatial correlation matrix of the non-stationary channel can be expressed as $\mathbf{R}_n = \mathbf{D}^{1/2} \mathbf{R}_f \mathbf{D}^{1/2}$ [161]. As before, the corresponding stochastic NLoS channel can be represented as $\mathbf{R}_n^{1/2} \mathbf{h}$. For a stationary channel, we have $\mathbf{D} = \mathbf{I}$, $\mathbf{R}_n = \mathbf{R}_f$. Thus, by determining the VR, the correlation matrix of a non-stationary near-field channel can be straightforwardly derived from existing far-field models. Common far-field correlation-based channel models include the independent and identically distributed (i.i.d.) model [164], independent but not identically distributed (i.n.i.d.) model, Kronecker model [163], Weichselberger model [165], virtual channel representation (VCR) model [147], and rough surface (RoS) model [166], among others.

Building on the framework introduced in [161], several spatially correlated channel models have emerged to incorporate



(a) The influence of scatterer clusters is not emphasized (single-scattering model).



(b) The influence of scatterer clusters is considered (double-scattering model).

Fig. 12: Illustration of spatial non-stationary correlation.

the VR. For example, using the framework from [161], the authors of [167] employed a binary VR mask to transform a stationary i.i.d. correlation model with $\mathbf{R}_f = \mathbf{I}$ into its non-stationary near-field counterpart. This model was developed for designing low-complexity message-passing detection algorithms for near-field uplink multiuser MISO channels. It has also found applications in works like [168] and [169], where it facilitates the design of iterative receivers and VR estimators for NFC. These studies, including [167]–[169], assumed an isotropic scattering environment with uniformly distributed independent multipath components. Taking a step further, the authors of [170] proposed an i.n.i.d. correlation model for near-field MISO channels. This model offers greater precision compared to previous works as it accounts for the influence of UPL from different antenna elements. However, the above-mentioned models assumed a diagonal correlation matrix \mathbf{R}_f to construct its near-field counterpart. This diagonal behavior results in statistical independence and fails to capture correlation effects. In environments with limited scatterers and small antenna spacing, as seen in most practical systems, spatial correlation becomes crucial. To address this, [171] proposed a correlated model for near-field uplink MISO channels employing the framework from [161] and the PAS-based correlation matrix established in [172]. This model accounts for Gaussian angular spread and was further used to design VR-aware user scheduling algorithms. It also found application in [173], where VRs were restricted to predivided subarrays, leading to a grant-based random access protocol for NFC. In contrast to these approaches, [174] and [175] used a one-ring model to calculate \mathbf{R}_f and \mathbf{R}_n . These studies adopted a binary VR mask \mathbf{D} to describe near-field spatial

correlation. As a more flexible alternative, [176] proposed an i.n.i.d. correlation model for near-field MISO channels, where the diagonal elements of the VR mask were not restricted to be 0 and 1. This comprehensive model considered UPL from different antenna arrays and assumed a rich scattering environment around the user, leading to optimizations in system energy efficiency. The same correlation model was also applied in [177] to enhance the spectral efficiency of near-field systems.

The presence of scatterer clusters can be viewed as forming a virtual antenna array [178], as depicted in Fig. 12(b). Taking the MISO channel as an example, in traditional multi-antenna systems, the covariance-matrix-based double-scattering channel model for S scatterers and N antennas can be expressed as $\mathbf{R}_{f,a}^{1/2} \mathbf{H}_a \mathbf{R}_{f,s}^{1/2} \mathbf{h}$ [179], where $\mathbf{H}_a \in \mathbb{C}^{N \times S}$ and $\mathbf{h} \in \mathbb{C}^{S \times 1}$ account for small-scale fading from the array to the scatterers and from the scatterers to the user, respectively, $\mathbf{R}_{f,a} \in \mathbb{C}^{N \times N}$ and $\mathbf{R}_{f,s} \in \mathbb{C}^{S \times S}$ represent the covariance matrices at the array and scatterer side, respectively. In near-field systems, where different scatterer clusters have varying VR representations, the channel response must be adapted. By concatenating the array-to-scatterer channel and the scatterer-to-user channel, the channel between the array and the user can be expressed as $\mathbf{D}_a \mathbf{R}_{f,a}^{1/2} \mathbf{H}_a \mathbf{R}_{f,s}^{1/2} \mathbf{D}_s \mathbf{h}$, where $\mathbf{D}_s \in \{0, 1\}^{S \times S}$ represents the VR mask that selects the scatterers visible to the user, $\mathbf{D}_a \in \{0, 1\}^{N \times N}$ is the VR mask selecting the antennas visible to the clusters, and $\mathbf{h} \sim \mathcal{CN}(\mathbf{0}, \mathbf{I})$ and $\text{vec}\{\mathbf{H}_a\} \sim \mathcal{CN}(\mathbf{0}, \mathbf{I})$ model the small-scale fading. This correlation-based double-scattering model was initially proposed in [162] to explore the impact of non-wide sense stationarity on the capacity of uplink multiuser MISO channels. Subsequently, it has been applied in [178] and [180] for ergodic channel capacity analysis and the design of low-complexity distributed receivers, respectively. In these studies, the spatial correlation matrix of the channel is influenced by the angular spread and antenna spacing [181].

Existing CBSMs for near-field NLoS channels primarily focus on MISO channels, although they can be straightforwardly extended to MIMO scenarios. When constructing correlation matrices, most previous research employs models such as i.i.d., i.n.i.d., and the Kronecker model. The CBSM correlation matrix governed by angular spread and antenna spacing is essentially a special case of the Kronecker model, as evidenced in prior studies [162], [171], [173]–[175], [178], [180]. In addition to these models, the Weichselberger, VCR, and RoS models can also be applied. A summary of the key contributions related to near-field NLoS channel modeling for SDP antenna arrays is provided in Table VI.

2) *CAP-NFC*: Next, we will direct our focus toward NLoS channel models applicable to NFC supported by CAP arrays. Numerous studies have been dedicated to modeling the NLoS propagation channel within this framework. Among these studies, two main approaches for NLoS propagation channel modeling stand out: *PPBSMs* and *Fourier plane-wave-based stochastic models (FPBSM)*.

- *PPBSM*: As previously discussed, PPBSMs serve to characterize the propagation environment by encompassing double-directional EM wave propagation, accounting for critical physical propagation parameters such as AoAs/AoDs and

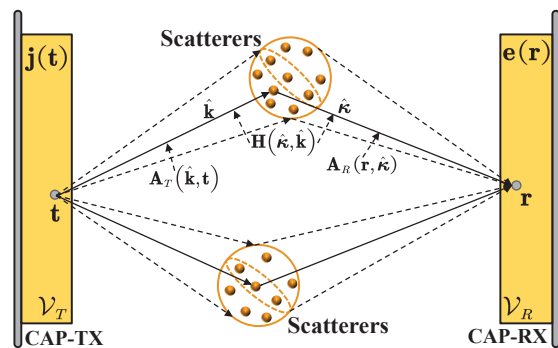


Fig. 13: Illustration of PPBSMs for CAP-NFC in NLoS propagations.

the scattering RCS pattern.

Within the PPBSM framework, the channel response can be expressed in terms of three fundamental components: the *transmit array response*, the *receive array response*, and the *complex gain* associated with each ray in each scattering cluster, akin to PPBSMs employed in SPD-NFC. The transmit array response, denoted as $\mathbf{A}_T(\hat{\mathbf{k}}, \mathbf{t})$, maps the excitation current distribution to the radiated field pattern. Similarly, the receive array response, denoted as $\mathbf{A}_R(\mathbf{r}, \hat{\mathbf{k}})$, maps the incident field pattern to the induced current distribution. The scattering response, represented as $\mathbf{H}(\hat{\mathbf{k}}, \hat{\mathbf{k}})$, provides the channel gain and polarization information between the transmit direction $\hat{\mathbf{k}}$ and receive direction $\hat{\mathbf{k}}$, as illustrated in Fig. 13. In contrast to the array responses in SPD-NFC, the array responses for CAP-NFC are characterized using scalar or tensor Green's functions. While the array response for the scalar Green's function is a complex number, the tensor Green's function results in a 3×3 complex integral kernel. The scattering response is sandwiched between the array responses and represents the attenuation and polarization of each ray, with the desirable property of being array-independent. We will now delve into modeling the scattering responses.

Recent measurements of non-stationary channels reveal that physical paths tend to cluster around the transmit and receive directions [146], as depicted in Fig. 13. Clustering can typically occur due to reflection from walls and ceilings, scattering from furniture, diffraction from doorway openings, and transmission through soft partitions. Clustering becomes prominent when the separation between the transmitter and receiver is comparable to the size of the scattering sources, a common occurrence in both indoor and urban environments. To accurately construct the scattering response, a comprehensive understanding of the PLOS of the scattering is required. For instance, the authors of [138] proposed a tensor Green's function-based NLoS model for communications between two CAP arrays beyond the uniform-power distance. In this model, the scattering response is calculated by following the ray-tracing model presented in [182] and grouping the paths into clusters, similar to the approach in [183]. The resulting NLoS model essentially represents a specific case of the CCM.

It is essential to note that the PPBSM entails the use of two Green's functions (i.e., $\mathbf{A}_R(\mathbf{r}, \hat{\mathbf{k}})$ and $\mathbf{A}_T(\hat{\mathbf{k}}, \mathbf{t})$), which can increase the computational complexity. Additionally, the presence of an arbitrary number of paths within each cluster

TABLE VI: Contributions on NLoS Channel Modeling for SPD-NFC

Category	Ref.	Approach	Channel	VR	Correlation	Characteristics
PPBSM	[146]	CCM	MIMO	✗	—	A 3-D non-stationary model accounting for the influence of FSPL
	[53]	CCM	MISO	✓	Kronecker model	A general model accounting for the influence of FSPL, EAL, and PL
	[111]	FDC	MISO	✗	Kronecker model	The USW model is employed to characterize the channel response
	[151]	FDC	MIMO	✗	—	The USW model is employed to characterize the channel response
	[126]	FDC	MISO	✓	Kronecker model	The NUSW model is employed to characterize the channel response
	[97]	PLOS	MISO	✗	One-ring model	The scatterers are located on a ring subject to von-Mises distribution
CBSM	[161]	$\mathbf{D}^{1/2}\mathbf{R}_t\mathbf{D}^{1/2}$	MISO	✓	Arbitrary	A framework to generate near-field correlation from the far-field one
	[167]–[169]	$\mathbf{D}^{1/2}\mathbf{R}_t\mathbf{D}^{1/2}$	MISO	✓	i.i.d. model	An isotropic environment with uniformly distributed independent scatterers
	[170]	$\mathbf{D}^{1/2}\mathbf{R}_t\mathbf{D}^{1/2}$	MISO	✓	i.n.i.d. model	The influence of UPL from different antenna elements is considered
	[171], [173]	$\mathbf{D}^{1/2}\mathbf{R}_t\mathbf{D}^{1/2}$	MISO	✓	Kronecker model	The PAS-based correlation matrix with Gaussian angular spread distribution
	[174], [175]	$\mathbf{D}^{1/2}\mathbf{R}_t\mathbf{D}^{1/2}$	MISO	✓	Kronecker model	A one-ring model is used to characterize the scattering environment
	[176], [177]	$\mathbf{D}^{1/2}\mathbf{R}_t\mathbf{D}^{1/2}$	MISO	✓	i.n.i.d. model	The diagonal elements of the VR mask matrix are not restricted to 0 and 1
	[162], [178], [180]	$\mathbf{D}_a\mathbf{R}_{f,a}^{1/2}\mathbf{H}_a\mathbf{R}_{f,s}^{1/2}\mathbf{D}_s\mathbf{h}$	MISO	✓	Kronecker model	The spatial correlation is influenced by angular spread and antenna spacing

further diminishes the analytical tractability of this model. Consequently, these factors have limited the adoption and simulation of PPBSM-based CAP-NFC models, despite their accuracy.

- *FPBSM*: As previously discussed, PPBSMs are known for their capacity to provide exceptionally accurate insights into signal propagation in specific environments [184]. However, their reliance on numerical EM solvers based on Green’s functions renders them highly site-specific. The intricate physical models they employ are often too complex for practical analysis. In light of these challenges, the introduction of a channel model based on a Fourier plane-wave series expansion offers a promising alternative for describing NLoS propagation in CAP-NFC.

The FPBSM hinges on the fundamental premise that *wave propagation can be universally expressed in terms of plane waves*, irrespective of the communication range, even in the near-field region, and across diverse propagation environments. This concept is grounded in Weyl’s decomposition of spherical waves into plane waves [185], [186] and scattering matrix theory [187]–[190].

In the FPBSM framework, the transmit field originating from a source \mathbf{t} is initially represented as a two-dimensional (2D) Fourier plane-wave spectrum, in line with Weyl’s identity [186]. This representation mathematically relates a spherical wave to an uncountably infinite number of plane waves, each propagating in different directions. The transmit field is mathematically described as a 2D integral, encompassing the product of the array response and the plane-wave spectrum across two horizontal wavenumber coordinates. The receive field, on the other hand, is generated by the interaction with scatterers and is measurable at any point \mathbf{r} . Importantly, the receive field does not necessitate external stimuli at the receiver, rendering it locally source-free. In the physical realm, the receive field must adhere to the homogeneous Helmholtz equation [185, Sec. 1.2.2], which can also be represented using a 2D Fourier plane-wave spectrum [191, Sec. 6.7]. The input spectrum is then transformed into the output spectrum of plane waves through a linear scattering kernel integral operator. This operator embodies the scattering mechanism, linking all incident plane waves with every received plane wave.

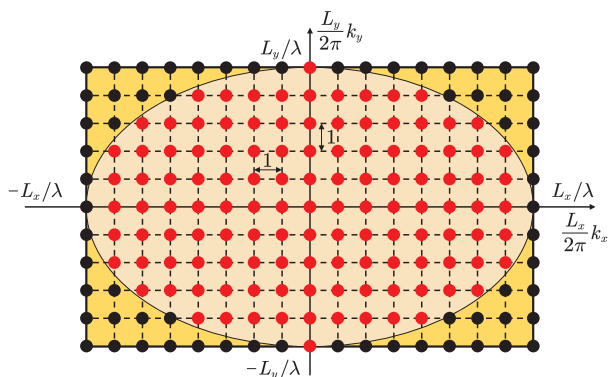
Consequently, the channel response modeling an arbitrary NLoS propagation environment from \mathbf{t} to \mathbf{r} is precisely represented as a four-dimensional (4D) Fourier plane-wave

spectrum, constructed from three key contributions [192]:

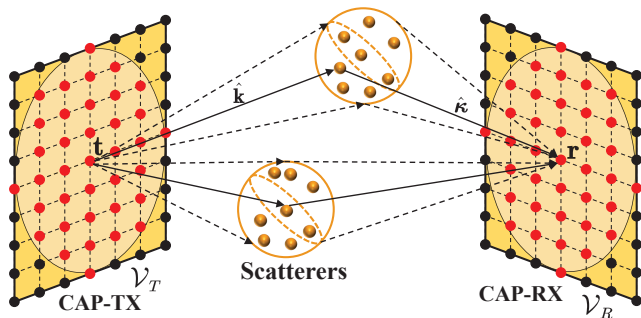
- The *transmit array response* maps the impulsive excitation current at point \mathbf{t} to every outgoing propagation direction $\hat{\mathbf{k}}$ of the transmit field, determined by the wavenumber of the transmit field and the coordinates of \mathbf{t} ;
- The *receive array response* maps every incoming propagation direction $\hat{\mathbf{k}}$ of the receive field to the induced current at point \mathbf{r} , determined by the wavenumber of the receive field and the coordinates of \mathbf{r} ;
- The *angular response* maps every source direction $\hat{\mathbf{k}}$ to every receive direction $\hat{\mathbf{k}}$. It illustrates the coupling between each transmit and the receive propagation direction, encompassing the 4D power spectral density, capturing the scattering propagation environment and the channel’s random characteristics.

This 4D Fourier plane-wave representation relies on two horizontal wavenumber coordinates at the source and receiver, each parameterizing the transmit and receive directions. In this representation, Fourier transforms at the transmit and receive apertures establish a connection between the spatial and wavenumber (or angular) domains. The comprehensive influence of the scattering environment is encapsulated within an angular kernel, characterizing the coupling between every pair of transmit and receive directions [192].

Moreover, by employing the theory of Fourier spectral series expansion, which involves partitioning the wavenumber domain into equally spaced discrete angular sets and applying the first mean-value theorem [193, Ch. 3] across these sets, the 4D Fourier plane-wave channel model can be discretized into a Fourier plane-wave series expansion. This discretization is akin to the transition from Fourier integrals to Fourier series for time-domain signals [194]. Leveraging the fact that the angular response is non-zero solely within specific wavenumber regions, the discretized plane waves are confined within lattice ellipses, as illustrated in Fig. 14. The discrete Fourier plane-wave series expansion is derived by sampling within the finite integration area. It is important to note that the approximation error diminishes as the array size becomes sufficiently large [194]. For illustrative purposes, we use a 2D planar array in Fig. 14, although the FPBSM is versatile and applicable to describe the channel response of 1D linear arrays as well as 3D volumetric arrays [194].

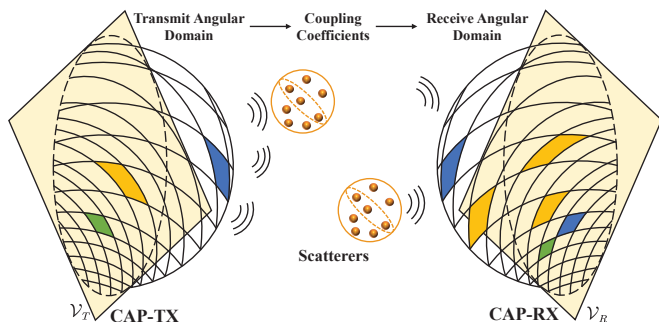


(a) The 2D lattice with elliptical wavenumber support. L_x and L_y are the aperture sizes along the x - and y -axes. k_x and k_y are integers.

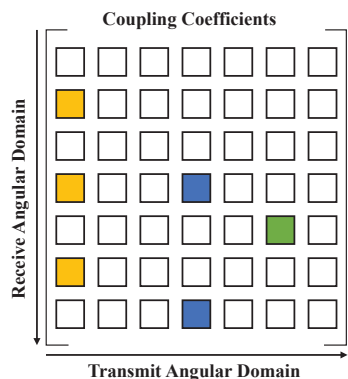


(b) Illustration of FPBSMs.

Fig. 14: Illustration of FPBSMs for CAP-NFC in NLoS propagations.



(a) Channel coupling between the transmit angular domain to the receive angular domain.



(b) Power transfer from the transmit angular domain to the receive angular domain.

Fig. 15: Illustration of the Fourier plane-wave series expansion-based model in the angular or wavenumber domain.

Subsequent to discretization, the continuous incident and received plane waves are replaced by their discretized counterparts. This transformation reveals that only a finite number of plane waves are necessary to convey the fundamental channel information between the two CAP arrays, emphasizing the lower-dimensional angular representation in EM channels. This results in a significant reduction in channel dimensions, which in turn significantly lowers the complexity involved in tasks such as channel estimation, optimal signaling, and coding [195]. Furthermore, the continuous angular response is replaced by a sequence, describing the channel coupling between each pair of transmit and receive angular sets designated by the aforementioned discretized plane waves, as depicted in Fig. 15(a). For instance, in Fig. 15(b), the coupling coefficients are arranged in matrix form. Three distinct angular sets, activated by the source (orange, blue, and green), transfer their radiated power to six angular sets at the receiver. The resulting random channel coupling coefficients are modeled as zero-mean circularly-symmetric complex-Gaussian random variables. Their variance represents the discrete angular power distribution of the channel, indicating the proportion of power transferred from the transmit angular domain to the receive angular domain. The strength of the coupling coefficients varies and depends on both array apertures and the scattering mechanism. Due to their inherent Gaussian-distributed complex gains, FPBSMs exhibit the characteristics of correlated Rayleigh fading [194], [195]. As summarized in [194], FPBSMs are more amenable to analysis compared to PPBSMs [194].

The application of plane-wave-based models in wireless research is predominantly confined to the far-field regime. A well-established example of this approach is demonstrated by the widely recognized VCR model, introduced in the seminal works [147], [196]. In these studies, an angular decomposition of a 2D MIMO channel is presented, featuring a fixed set of directions. This approach conceptualizes wave propagation occurring on a 2D plane rather than in the full three-dimensional space. A significant advancement in this field is attributed to the pioneering work of Marzetta in [197]. In this groundbreaking research, the proposal is made to employ a 2D Fourier plane-wave representation for modeling the receive field. On this basis, the authors of [192] proposed a 4D Fourier plane-wave representation to model NLoS propagation in CAP-NFC. This model incorporates both reactive and radiative propagation mechanisms to calculate the channel response. Building on this, the same group of researchers further developed a Fourier plane-wave series approximation [194], with a specific focus on isotropic propagation environments with scattering separability. In this case, the discrete angular power distribution of the channel is effectively separable into two independent terms, accounting for power transfer at the transmitter and receiver.

A noteworthy application of this approach is found in [195], [198], where an FPBSM-based NLoS model for near-field single-user MIMO systems is presented. This model characterizes the channel response between each pair of transmit and receive antennas using the Fourier plane-wave series expansion. The study includes several examples demonstrating

the discrete angular power distribution under non-isotropic conditions, where the power distribution is jointly determined by the array's spatial resolution and the scattering mechanism. The resulting model essentially represents a specific case of the Weichselberger model [165], in which the angular domain is represented by a random matrix with zero mean and non-separable covariance [199]. With the introduction of scattering separability, this model effectively degenerates into the well-known Kronecker model [163]. Expanding on this foundation, [200], [201] have extended this model to more practical scenarios, taking into account non-ideal factors introduced by mutual coupling at the transceivers, and encompassing phenomena such as antenna pattern distortion and antenna efficiency. In another development, [202] derives the discrete angular response for the single-user MIMO channel by assuming a wrapped Gaussian azimuth angle distribution and a truncated Laplacian elevation angle distribution. The resulting model is analyzed for its capacity.

The applicability of the Fourier model introduced in [195] to a multi-user scenario is presented in [203]. In this work, a lower bound for the system spectral efficiency is derived for maximum ratio transmission (MRT) and zero-forcing (ZF) precoding. This model has found applications in optimizing the energy efficiency of near-field downlink multi-user communication systems [204], and has been extended to cell-free scenarios featuring multiple ELAA-based access points connected to a central processing unit [205]. The same model is also used in formulating antenna selection algorithms [206] and power control strategies [207] for uplink cell-free systems. The aforementioned works [200]–[205] are based on the assumption of scattering separability. Advancing beyond this assumption, [208] considers a non-separable correlation structure, employing random matrix theory to analyze the channel capacity of a near-field single-user channel. These works primarily focus on scalar EM fields, which in general have a physical correspondence with acoustic propagation. A more comprehensive extension to tensor EM channels, without considering the randomness of the environment, is detailed in [43].

A summary of the primary contributions regarding near-field NLoS channel modeling for CAP arrays can be found in Table VII. “SU” and “MU” represent single-user and multiuser, respectively.

D. Hybrid LoS/NLoS Models

Channel modeling for both LoS and NLoS propagation has been extensively reviewed. However, in practical scenarios, hybrid propagation channels, which encompass both LoS and NLoS links, may be encountered.

1) *SPD-NFC*: In the context of SPD-NFC, generating hybrid LoS/NLoS channels is a straightforward process. This hybrid model can be constructed by simply adding the LoS component, typically modeled using the USW or NUSW approaches, to the NLoS component, often represented by PPBSM or CBSM; see [112] for an example. NLoS propagation typically exhibits Rayleigh fading, whereas hybrid propagation is described using Rician fading.

2) *CAP-NFC*: For CAP-NFC, there are two approaches to model hybrid LoS/NLoS propagation channels, depending on whether Green's functions are employed to describe the EM characteristics. When Green's functions are used, hybrid LoS/NLoS channels can be established by combining the LoS model presented in Section III-B2 with the PPBSM model detailed in Section III-C2.

An alternative modeling method is based on the Fourier plane-wave representation, which accommodates both LoS and NLoS propagation channels [192]. In this approach, the LoS propagation channel is initially derived based on the scalar Green's function. Subsequently, this scalar Green's function-based channel can be exactly represented by a Fourier plane-wave expansion employing Weyl's identity. Additionally, NLoS propagation can also be derived based on the Fourier plane-wave representation, as discussed in detail earlier. Consequently, the hybrid propagation channel is established by merging these two components. A practical example of the FPBSM-based hybrid model is outlined in [208].

E. Discussions and Outlook

In this section, we have provided an extensive examination of fundamental concepts related to channel modeling in NFC. Our discussions have emphasized the spatial non-stationarity that is prevalent in near-field channels. To facilitate easy reference, we have summarized the reviewed channel models in Table VIII. We trust that these summarized findings will offer insights into performance analysis and signal processing design for NFC, providing valuable guidance for future research endeavors. However, there are still numerous open research problems in this area. In the following, we elaborate on three major points.

- **Non-Stationary FPBSMs for CAP-NFC**: Existing contributions on FPBSMs are primarily rooted in modeling the radiating near field as a zero-mean, spatially-stationary, and correlated Gaussian scalar random field [194]. This model adeptly captures the EM characteristics of spherical wavefronts. However, it tends to overlook the impact of spatial non-stationarity stemming from the VR. Accounting for the influence of VR is crucial, particularly in modeling the angular power distribution, which necessitates the collection of angular channel measurements within a specified propagation scenario. At the time of this writing, a comprehensive analysis of the effects of non-stationarity and methods for integrating these effects into FPBSMs remains an open research issue.
- **Hybrid-Field Channel Modeling**: In practical communication scenarios, some scatterers are located within the near field, while others reside in the far field. Consequently, it is imperative to consider the practical channel characteristics of such hybrid-field propagation scenarios. Channel components contributed by near- and far-field scatterers should be modeled separately. Research on hybrid-field channel modeling is still in its infancy, with only a few recent works emerging in this area [110], [111], [210]. These works predominantly focus on FDC-based modeling schemes, and further efforts are required to develop other types of hybrid-field models.

TABLE VII: Contributions on NLoS Channel Modeling for CAP-NFC

Category	Ref.	Channel	Scattering Separability	Angular Response	Evanescence Waves	Characteristics
PPBSM	[138]	SU	—	CCM	✗	A tensor Green's function-based model for CAP-NFC within the USW region
FPBSM	[192], [197]	SU	Both	Arbitrary	✓	The first application of 4D Fourier plane-wave representation to CAP-NFC
	[194]	SU	Separable	Isotropic	✓	The first application of 4D Fourier plane-wave series expansion to CAP-NFC
	[195], [198]	SU-MIMO	Both	Isotropic/CCM/3D von Mises-Fisher [192]	✗	The resulting model is the Weichselberger model
	[200]	SU-MIMO	Separable	Isotropic	✗	The influence of scan impedance mismatch caused by coupling effect is introduced
	[201]	SU-MIMO	Separable	3D von Mises-Fisher	✗	The influence of antenna pattern distortion and efficiency decrease is introduced
	[202]	SU-MIMO	Separable	Wrapped Gaussian/truncated Laplacian	✗	Standard 3D MIMO channel models [209] are used to model the angle distribution
	[203]	MU-MIMO	Separable	Isotropic	✗	The first application of 4D Fourier plane-wave series expansion to MU-MIMO
	[204]	MU-MIMO	Separable	3D von Mises-Fisher	✗	The achievable ergodic rate is analyzed
	[205]–[207]	MU-MIMO	Separable	Isotropic	✗	The application of Fourier plane-wave series expansion to uplink cell-free systems
	[208]	MU-MIMO	Non-separable	Arbitrary	✗	The capacity is analyzed by considering the non-separable correlation structure
	[43]	MU-MIMO	—	—	✗	Tensor EM channels without randomness are considered

TABLE VIII: Summary of Channel Modeling Approaches for NFC

Antenna	Propagation	Section	Approach	Ref.	Characteristics
SPD	LoS	III-B1	USW	[108]	Amplitude variation across the receive aperture can be safely disregarded
			NUSW	[25]	Both the amplitude and phase exhibit pronounced variations across the receive aperture
	NLoS	III-C1	PPBSM	[111]	This model is based on the full knowledge of power location spectrum
			CBSM	[161]	The influence of the VR is taken into consideration
Hybrid	III-D1	LoS+NLoS	[112]	This model can be constructed by simply adding the LoS component to the NLoS component	
CAP	LoS	III-B2	Green's function	[134]	Scalar or Tensor Green's functions are used to characterize the EM characteristics
	NLoS	III-C2	PPBSM	[138]	Three components: the transmit/receive array response and the complex gain associated with each ray
			FPBSM	[192]	Rooted in the fact that wave propagation can be expressed in terms of plane waves
	Hybrid	III-D2	Green's function	[138]	The EM characteristics of LoS and NLoS components are both denoted by Green's functions
FPBSM			[208]	The LoS and NLoS components are both represented by Fourier-plane wave series expansion	

- **Spatial Models Tailored for NFC:** Stochastic geometry (SG) tools have demonstrated the ability to account for the spatial randomness of users, thus facilitating the derivation of computable or even closed-form expressions for key performance metrics. Various models including homogeneous Poisson point processes, Poisson cluster processes, binomial point processes, and hard core point processes are available for this purpose [211]. Nevertheless, these models are not specifically tailored to the near-field context. Integrating the unique physical properties of near-field scenarios into SG tools could lead to the development of new spatial and channel statistical models. This, in turn, may streamline the derivation of computable expressions for a wider range of critical performance metrics.

IV. PERFORMANCE ANALYSIS OF NFC

In this section, we present an extensive literature review concerning the performance analysis of NFC using the near-field channel models that we discussed in Section III. To systematically assess the current approaches for NFC, we will explore various performance metrics, including: i) DoFs and EDoFs, ii) power scaling law, and iii) sum-rate.

A. DoFs and EDoFs

In the realm of wireless communications, the concept of DoFs has emerged as a useful metric for comprehending the capabilities and potential of different communication systems [81]. In essence, the number of DoFs of a system provides valuable insights into the number of independent signal dimensions that can be harnessed for transmitting information over a given wireless channel. As highlighted earlier, NFC can offer increased DoFs compared to FFC. With a comprehensive understanding of the DoF characteristics intrinsic

to NFC systems, we can unveil their superior data capacity and transmission capabilities compared to FFC [50]. Given this context, our next endeavor is to review the current body of literature dedicated to the analysis of DoFs and EDoFs for NFC. This review encompasses scenarios involving both LoS and NLoS propagations. For the sake of brevity, we will primarily focus on single-user NFC systems.

1) *LoS Channels:* In the following, we will delve into the DoFs and EDoFs for near-field LoS channels supported by SPD and CAP arrays. As outlined in Section II-B3, we focus on the impact of transmission range on the DoFs/EDoFs and omit the influence of bandwidth and aperture size for the sake of brevity.

- **SPD-NFC:** In near-field SPD-MIMO, the overall channel response can be represented by a matrix \mathbf{H} with dimensions $N_r \times N_t$, where N_r corresponds to the number of receive antennas and N_t represents the number of transmit antennas. We apply the SVD to this channel matrix and decompose it into multiple independent SISO sub-channels, each operating in parallel without mutual interference. In this context, the number of spatial DoFs is equal to the number of positive singular values [81], [212]. In the near-field region, spherical waves exhibit non-linearly varying phase shifts and power levels for each link. This diversity can lead to a full-rank channel matrix whose DoFs approach $\min\{N_r, N_t\}$. This suggests that, by reducing the antenna spacing within a fixed aperture size, the number of spatial DoFs can be significantly increased.

However, it is important to note that DoFs are a performance metric relevant primarily in high-SNR scenarios. It quantifies the number of parallel SISO sub-channels without accounting for noise and interference. The singular values of the channel matrix represent the gains of these parallel sub-channels. Consequently, only those sub-channels with power levels sufficiently high w.r.t. the noise and interference can

reliably support wireless information transfer when the total transmit power is fixed. Moreover, extensive simulation and measurement results suggest that the rate of decrease in the ordered singular values can be divided into two stages, in which the singular values remain roughly constant in the first stage and then decay rapidly to zero, as illustrated in Fig. 7 [213]–[217]. The index corresponding to this knee singular value is often referred to as the number of EDoFs, denoted as EDoF_1 and defined in Section II-B3. This step-like behavior is not an isolated phenomenon; it has been frequently validated by measurements and is believed to hold true for various systems and environments [50], [218]–[220]. Exploiting this property, the EDoFs of near-field SPD-MIMO systems can be accurately approximated by $\text{EDoF}_2 = (\text{tr}(\mathbf{H}\mathbf{H}^H)/\|\mathbf{H}\mathbf{H}^H\|_F)^2$, as defined in Section II [50].

Expanding on the foundation laid out above, the authors of [221] conducted a numerical analysis of the EDoFs, here referred to as EM EDoFs, for a near-field SPD-MIMO channel described by free-space LoS propagation. In this study, the channel response between each transceiver pair is modeled using the tensor Green’s function, resulting in a MIMO channel matrix encompassing full polarizations, with dimension $3N_r \times 3N_t$. In this matrix, nine $N_r \times N_t$ matrices correspond to the nine scalar Green’s functions. Numerical findings in [221] indicate that the number of EDoFs exhibits an inverse relationship with the propagation distance, implying that near-field characteristics can augment the EDoFs of a MIMO channel. The EM channel model in [221] is developed for free-space conditions, but in the near field, free-space propagation does not accurately represent reality since EM waves can only propagate above the ground [222]. Accounting for this factor, an approach based on the Sommerfeld identity [185] is introduced to enable the computation of Green’s function in the resulting half-space. This enables the numerical measurement of the EDoFs for a near-field SPD-MIMO channel [223]. Results demonstrate that the difference between the number of EDoFs in the half-space and that in free space is considerable for NFC, emphasizing the significant influence exerted by the ground on channel capacity [223]. In addition to Green’s function, an alternative approach based on split-step Fourier transforms (SSFTs) and the parabolic equation method [224], [225] is employed to model EM wave propagation and assess the number of EDoFs [226]. This method offers reduced complexity compared to the tensor Green’s function approach [226]. It is noteworthy that the EDoFs in the aforementioned works are calculated numerically without closed-form expressions. As a step further, the authors of [85] have proposed a closed-form expression for the number of EDoFs using the NUSW model and the Fresnel approximation to simplify the channel matrix. Despite the varied approaches employed, the collective contributions on EDoFs for SPD-NFC under LoS channels have uncovered two common insights. First, *EDoFs can be enhanced by reducing the propagation distance or increasing the aperture size*. Second, *by reducing the antenna spacing within a fixed aperture size, the number of EDoFs eventually reaches a saturation point at some limit on the antenna spacing* [85], [221], [223], [226]. It is important to note that this limiting value serves as an upper bound for

the number of EDoFs for SPD-NFC, which coincidentally equals the EDoFs for CAP-NFC. This is not surprising, as the CAP array represents a special case of an SPD array with infinitesimal antenna spacing [5].

- *CAP-NFC*: Much like SPD-MIMO systems, the DoFs for CAP-MIMO hinge on the behavior of the singular values of Green’s function. In the context of CAP-NFC, the ordered singular values exhibit a step-like behavior, with the number of EDoFs corresponding to the sharp knee in this curve [50]. Several methods exist to compute the number of EDoFs for near-field CAP-MIMO, such as studying the eigenvalues of the Hermitian kernel of Green’s function, utilizing Landau’s eigenvalue theorem for multidimensional bandlimited signals (or fields), employing the Nyquist sampling theorem and Fourier theory, or applying an EDoF_2 -based approximation.

One of the most straightforward approaches to calculating the EDoFs for CAP-MIMO is using the EDoF_2 -based approximation, which yields tractable closed-form expressions. The authors of [223] extended the expression of EDoF_2 for SPD-MIMO, i.e., $\text{EDoF}_2 = (\text{tr}(\mathbf{H}\mathbf{H}^H)/\|\mathbf{H}\mathbf{H}^H\|_F)^2$, to the case of CAP-MIMO. Using this new formula, they conducted a numerical investigation of the EDoFs between two continuous-aperture linear arrays situated in a half-space. Furthermore, in a subsequent development, the authors of [85] derived a closed-form expression for EDoF_2 that leverages the Fresnel approximation. Beyond these methods, there exist various other rigorous techniques for calculating the number of EDoFs in the context of CAP-NFC.

In a pioneering work, Piestun and Miller [136] introduced a comprehensive framework for determining the singular values of the Green’s operator and the corresponding eigenfunctions, analogous to the “left singular vectors” and “right singular vectors” of SPD-MIMO. These eigenfunctions constitute two complete sets of orthogonal basis functions, one associated with the transmit aperture and the other with the receive aperture. The framework of [136] relies on the tensor Green’s function, making it applicable to CAP-MIMO LoS channels. However, this method necessitates the exact eigen-decomposition (ED) of the Hermitian kernel of Green’s function, a computationally intensive process that does not yield closed-form solutions. As a result, despite its broad applicability, this framework has predominantly been employed in special cases where closed-form solutions for both the EDoFs and the optimal basis functions are available.

For instance, Miller [84] concentrated on a scalar version of this framework in a paraxial setup⁴ and assumed that the transmit and receive CAP arrays are parallel to each other. This configuration occurs beyond the uniform-power distance, where the array aperture is significantly smaller than the propagation distance, enabling the use of the Fresnel

⁴In our paper, the term “paraxial setup” denotes a scenario in which the midpoints of the transmitter and receiver are perfectly aligned along the same line, although they are not necessarily parallel to each other [227]. An example featuring 2D planar arrays is illustrated in Fig. 16(a). We assume that the transmit array is positioned on the x - z plane, centered at the origin. The receive array is allowed arbitrary tilt (denoted by the angle β) w.r.t. the z -axis and arbitrary rotation (denoted by the angle α) on the x - z plane w.r.t. the x -axis. The definition of the “paraxial setup” can also be extended to 1D linear arrays [228] and 3D volumetric arrays [84].

approximation to simplify the spherical wavefront. Miller employed the theory of compact and self-adjoint operators over Hilbert spaces to achieve the ED of Green's operator. This analysis demonstrated that the optimal basis functions are related to the prolate spheroidal wave functions (PSWFs) [229], and the number of EDoFs was immediately deduced from the energy concentration property of the PSWFs. A similar approach was adopted in [228] to derive a closed-form expression for the EDoFs associated with the optimal basis functions in NFC between two continuous linear arrays, also in a paraxial setting but with different orientations. The findings revealed that the number of EDoFs is maximized when the two arrays are parallel to each other. In the more general non-paraxial setting, as shown in Fig. 16(b), solving the ED problem of the Green's operator has proven to be a formidable task, with recent breakthroughs for specific deployments [230]. The authors of [230] considered CAP-NFC between two non-paraxial 2D CAP arrays within the USW region, where the misalignment between the transceivers' centers is assumed to be much larger than the array apertures. Using a quartic approximation for the spherical wavefront, the authors derived the PSWF-related optimal basis functions for certain special non-paraxial scenarios, as illustrated in [230, Fig. 2]. These scenarios include cases where the transmit array is mounted on a wall, and the receive array is affixed to the ceiling within the same room, as well as cases where the transmit array is placed on a wall, and the receive array is attached to a perpendicular wall.

Apart from exact eigenfunction calculations, Miller [84] also proposed a heuristic approach to approximate the eigenfunctions. This approach is rooted in Gabor's diffraction theory [231], which divides a continuous 3D volumetric array into smaller non-overlapping volumes. In this context, [84] obtained simplified approximate eigenfunctions that are constant within a given small volume and zero outside it. The EDoFs were approximated as the number of these small volumes contained within the entire volumetric array. This simplified approach was found to work particularly well when the volumetric array has a uniform thickness. Inspired by this, the approach was also employed to analyze the EDoFs of STAR-RIS-based NFC in a paraxial setup [77]. Additionally, the authors of [232] leveraged diffraction theory and the energy-focusing property of near-field beam focusing to iteratively construct approximate basis functions for NFC between two non-paraxial continuous linear arrays. An approximate expression for the number of EDoFs was derived in [232] when one of the arrays is much smaller than the propagation distance.

Another commonly employed method to determine the EDoFs of near-field CAP-MIMO systems leverages Landau's eigenvalue theorem [233], [234]. Originally developed to characterize the eigenvalues of a specific integral equation known as Landau's operator, this theorem arose from the problem of simultaneously concentrating a function and its Fourier transform. It posits that the eigenvalues undergo a sharp transition from values close to one to values close to zero, with the scale of this transition characterizing the asymptotic dimension of the space of bandlimited functions [235]. It is notable that this asymptotic behavior closely resembles the

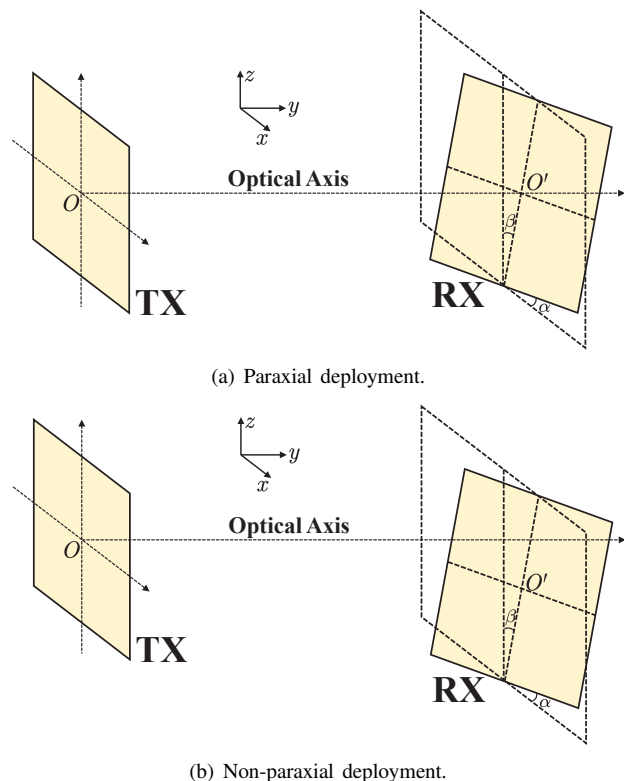


Fig. 16: Illustration of paraxial and non-paraxial deployments of planar arrays. The points O and O' denote the centers of the transmit array and receive array, respectively. Moreover, α and β denote a rotation and a tilt w.r.t. the x -axis and z -axis, respectively.

step-like behavior observed in the singular values of Green's function. Applying the Fresnel approximation in a paraxial scenario, the authors of [236] demonstrated that the scalar Green's function in a near-field CAP-MIMO system conforms to Landau's operator. The eigenproblem for the Green's function aligns with Landau's eigenvalue problem. Consequently, the EDoFs can be assessed using Landau's eigenvalue theorem, yielding a closed-form solution akin to that derived in [84]. This approach is also used to compute the number of EDoFs for NFCs involving continuous linear arrays [237] and RIS-aided continuous planar arrays [238]. Notably, these two works solely rely on the Fresnel approximation, eliminating the need for paraxial arrangements. Moreover, the authors of [230] harnessed Landau's eigenvalue theorem to determine the EDoFs of a near-field channel between two non-paraxial continuous planar arrays. Diverging from the approaches in [236]–[238], the work in [230] also derived closed-form expressions for the optimal basis eigenfunctions. This study further provided a general upper bound for the EDoFs when the array aperture is comparable to the propagation distance.

The motivation behind employing Landau's eigenvalue theorem to elucidate the EDoFs of Green's function stems from the fact that this function is inherently spatially bandlimited. This phenomenon resonates with the well-established idea that bandlimited signals can be accurately described by an orthonormal series expansion that involves a finite number of coefficients. The cardinality of these coefficients essentially corresponds to

the dimensionality of the space and, by extension, delineates the available EDoFs. This concept can be likened to the scenario in the time domain, where the bandwidth constraint denoted by B and the transmission interval denoted by T establish a fundamental limit of $2BT$ on the number of EDoFs.

Much like time-domain waveforms with finite bandwidth, EM channels can be construed as spatially bandlimited due to the analogous low-pass filtering that occurs during signal propagation, as noted by Bucci and Franceschetti in [218]. In this parallel, time is replaced by space, and frequency is replaced by spatial-frequency (or wavenumber), following the insights of Pizzo *et al.* [239]. Using the Nyquist sampling theorem and Fourier theory, it is well-established that a bandlimited signal can be represented by a sampled series. The coefficients of this series correspond to the values of the field sampled at the Nyquist rate, and the number of required samples aligns precisely with the number of EDoFs of the field [219]. Building on this foundation, researchers have proposed an approximate approach to compute the number of EDoFs between two CAP arrays. This method treats EDoFs as the number of Nyquist-rate samples required to represent a 2D bandlimited signal [139]. A closed-form expression for the number of EDoFs is derived for the case where the aperture of one CAP array is significantly smaller than the propagation distance. Furthermore, additional studies have furnished closed-form expressions for the number of EDoFs in near-field CAP-MIMO channels involving continuous linear apertures. These derivations are grounded in the ‘‘cut-set integral’’ approach, a technique that leverages the summation of a series of carefully designed bandlimited basis functions to approximate Green’s function. The EDoFs of Green’s function are consequently established by identifying the minimum number of basis functions necessary to faithfully represent the signal with arbitrary precision. It is important to note that this method is applicable only to one-dimensional (1D) CAP arrays.

Considering the above discussions, it becomes evident that the EDoF_2 -based approximation is the simplest way to estimate the number of EDoFs. However, this approach lacks the capability to offer insights into the optimal orthogonal basis eigenfunctions. Regardless of the diverse approaches utilized, the collective research contributions on EDoFs for CAP-NFC under LoS channels have consistently indicated that the *EDoFs are directly proportional to the product of the apertures of the CAP arrays and inversely proportional to the square of the product of the wavelength and the transmission distance*. A summary of the primary contributions regarding the analysis of EDoFs for near-field LoS channels can be found in Table IX.

2) *NLoS Channels*: We next turn our attention to the DoFs of NLoS channels by taking into account the influence of scattering.

- *SPD-NFC*: The singular values of SPD-MIMO channels in a rich scattering environment exhibit a phenomenon known as the ‘‘two-slope property’’ in which the rate of decay in the singular values can be effectively divided into two distinct stages [213], [214]. Both of these stages exhibit exponential decay, although the second stage decays at a significantly

faster rate compared to the first. When these singular values are plotted on a logarithmic scale, they appear as two linear sections, each characterized by a unique slope, which is the reason for the term ‘‘two-slope property’’. The slope of the first section is referred to as the primary slope, while the other is the secondary slope [213], [214], and the index corresponding to the transition point is taken to be the number of EDoFs of the system, denoted as EDoF_1 .

In cases where the antenna arrays are electrically small, the distinction between these two slopes is usually perceptible but not particularly pronounced. However, as the array apertures expand, a subtle knee in the singular value curve becomes discernible. For SPD-NFC, this two-slope property becomes a distinct step. In this scenario, the singular values remain approximately constant up to a certain point, beyond which they rapidly diminish to zero. The primary slope in this context is essentially zero, with nearly constant singular values rather than the exponential decay observed in other scenarios [213], [214]. This characteristic becomes more pronounced in isotropic scattering environments.

This two-slope property has led researchers to use $\text{EDoF}_2 = (\text{tr}(\mathbf{H}\mathbf{H}^H)/\|\mathbf{H}\mathbf{H}^H\|_F)^2$ as an approximation for EDoF_1 . For example, the authors of [241] used EDoF_2 to estimate the number of EDoFs of a near-field SPD-MIMO channel, encompassing both a direct and reflected path. In this study, the tensor Green’s function was employed to construct a full-polarization channel matrix containing comprehensive information about the EM environment. Similarly, this approach was used to assess the number of EDoFs of SPD-NFC in three representative 2D inhomogeneous environments characterized by keyholes, cylindrical scatterers, and cavities. These environments featured inhomogeneous permittivity profiles determined by the scatterers’ positions [242], [243]. While these NLoS contributions took into account the influence of multipath components, they treated the entire channel as deterministic, disregarding the channel’s inherent randomness. When considering this randomness, the number of EDoFs can be determined from the correlation matrix of the stochastic channel. In this context, some researchers have proposed a new formula for EDoF_2 that replaces $\mathbf{H}\mathbf{H}^H$ with its expectation $\mathbb{E}\{\mathbf{H}\mathbf{H}^H\}$, representing the spatial correlation at the receiver side [244]. However, this formula has two limitations. First, it only applies to channels with no spatial correlation at the transmitter, and second, it only applies to MIMO channels with more transmit than receive antennas. In pursuit of further improvements, the authors of [245] proposed the use of the spatial correlation matrix of the entire MIMO channel to calculate EDoF_2 , replacing $\mathbf{H}\mathbf{H}^H$ with $\mathbf{\Phi} = \mathbb{E}\{\text{vec}\{\mathbf{H}\}\text{vec}\{\mathbf{H}\}^H\}$. However, this formula comes with even more limitations, as it cannot approximate the number of EDoFs of the MIMO channel \mathbf{H} . For example, assume that \mathbf{H} consists of $N_r N_t$ i.i.d. standard complex Gaussian random variables, representing an uncorrelated Rayleigh fading channel. In this case, the number of EDoFs for \mathbf{H} is given by $\min\{N_r, N_t\}$. However, the correlation matrix $\mathbf{\Phi} = \mathbb{E}\{\text{vec}\{\mathbf{H}\}\text{vec}\{\mathbf{H}\}^H\}$ is an $N_r N_t \times N_r N_t$ identity matrix, and thus the number of EDoFs approximated by the new formula $\text{EDoF}_2 = (\text{tr}(\mathbf{\Phi})/\|\mathbf{\Phi}\|_F)^2$ is $N_r N_t$, which is larger than the true value $\min\{N_r, N_t\}$.

TABLE IX: Contributions on EDoF Analysis for LoS Channels

Antenna	Ref.	Tx	Rx	Paraxial Deployment	Fresnel Approximation	Eigenfunctions	Characteristics
SPD	[221]	Arbitrary	Arbitrary	Arbitrary	✗	SVD	The EDoF ₂ -based approximation is applied to a tensor Green's function-based channel in the free space.
	[223]	Linear	Linear	Arbitrary	✗	SVD	The EDoF ₂ -based approximation is applied to a scalar Green's function-based channel in the half-space.
	[226]	Arbitrary	Arbitrary	Arbitrary	✗	SVD	The EDoF ₂ -based approximation is applied to a PE-based EM channel.
	[85]	Linear	Linear	Paraxial	✓	SVD	A closed-form expression for EDoF ₂ is derived.
CAP	[223]	Linear	Linear	Arbitrary	✗	✗	A calculation formula for EDoF ₂ in CAP-MIMO is derived.
	[85]	Linear	Linear	Paraxial	✓	✗	A closed-form expression for EDoF ₂ is derived.
	[136]	Arbitrary	Arbitrary	Arbitrary	✗	✗	A general yet computationally intensive framework is provided for tensor Green's function. A standard definition of the eigenproblem is provided.
	[84]	Planar	Planar	Paraxial	✓	PSWF-related	The eigenproblem of Green's operator is explicitly solved in a closed form.
	[228]	Linear	Linear	Paraxial	✓	PSWF-related	The eigenproblem of Green's operator is explicitly solved in a closed form for continuous linear arrays with different orientations.
	[230]	Planar	Planar	Arbitrary	✗	PSWF-related	Landau's theorem is used to estimate the number of EDoFs, and optimal orthogonal basis eigenfunctions are provided.
	[77]	Planar	Planar	Paraxial	✓	Small volume-based	A small volume-based method is used to discuss the EDoFs of STAR-RIS.
	[232]	Linear	Linear	Arbitrary	✓	Beamfocusing-based	A diffraction theory and beamfocusing-based method is used to approximate the number of EDoFs and eigenfunctions.
	[236]	Planar	Planar	Paraxial	✓	✗	The first application of Landau's theorem to estimate the number of EDoFs of near-field CAP-MIMO channels is presented.
	[237]	Linear	Linear	Arbitrary	✓	✗	Landau's theorem is applied to estimate the number of EDoFs of near-field CAP-MIMO channels between two continuous linear arrays.
	[238]	Planar	Planar	Arbitrary	✓	✗	Landau's theorem is applied to estimate the number of EDoFs of RIS-assisted near-field CAP-MIMO channels.
	[139]	Planar	Planar	Paraxial	✓	✗	2D sampling theory is applied to estimate the number of EDoFs of CAP-NFC between a large-scale CAP array and a much smaller CAP array.
	[240]	Linear	Linear	Arbitrary	✗	✗	A sampling theory-based "cut-set integral" is used to approximate the number of DoFs, which applies only to 1D CAP arrays.

An enhancement of these previous works is presented in [195], which focuses on using FPBSM to analyze the EDoFs of an SPD-MIMO channel in the presence of small-scale fading. Within the FPBSM framework, a spherical wave can be effectively decomposed into an infinite spectrum of plane waves. This decomposition essentially represents a Fourier transformation from the near field (spatial domain) to the far field (angular domain or wavenumber domain). Additionally, by leveraging the theory of Fourier spectral series expansion, the continuous angular responses at the transceivers can be approximated by two sequences containing the angular spectra associated with lattice points falling within the 2D inner elliptical lattice, as illustrated in Fig. 14. Most of the angular domain channel information can be adequately captured by the coupling coefficients between each pair of transmit and receive angular sets centered around these inner lattice points, as depicted in Fig. 15. This approximation is asymptotically lossless when the aperture size of the transceivers approaches infinity, essentially resembling ELAAs. These arguments suggest that the EDoFs of the SPD-MIMO channel can be approximated by the EDoFs of the angular domain channel matrix formed by these coupling coefficients, simplistically referred to as the "coupling matrix" [195]. For isotropic fading scenarios, the EDoFs are calculated using $\min\{n_R, n_T\}$, where n_R and n_T represent the numbers of inner lattice points at the receiver and transmitter, respectively [195]. In cases of non-isotropic fading, the EDoFs of the coupling matrix depend on the angular power distribution. Nevertheless, $\min\{n_R, n_T\}$ serves as a general bound for the actual number of EDoFs [195]. These results primarily apply to the radiating near-field region. Additionally, in a further development, [246] extends this analysis to consider the influence of evanescent waves. These findings are also applicable to the reactive near-field region. In this study, the EDoFs of the spatial SPD-MIMO channel are similarly approximated by the coupling matrix. However,

when accounting for evanescent waves, the coupling matrix models not only the radiating region (lattice points within the 2D inner ellipse, as depicted in Fig. 14(a)) but also the reactive region (lattice points outside this ellipse). Taking into account that the amplitude of evanescent waves attenuates considerably faster with distance compared to radiated waves [138], a heuristic method is proposed to estimate the outer boundary of the lattice points outside the 2D inner lattice ellipse, which is a function of the propagation distance. Building on this, a heuristic formula is presented to approximate the number of EDoFs of SPD-MIMO systems operating in isotropic environments [246]. This study demonstrates that evanescent waves can enhance the EDoFs and subsequently improve the NFC channel capacity.

In addition to the aforementioned works that derived the number of EDoFs by examining the singular values of the channel matrix, other researchers have put forward a different approach, suggesting to use the number of significant singular values of either the correlation matrix at the transmitter or receiver side [247]–[250]. These approaches differ from those presented in [244], [245] which still require knowledge of the channel statistics, whereas [247]–[250] exclusively focus on the correlation matrices at only one side. The rationale for concentrating solely on the receiver or transmitter side is rooted in the notion that the transmitter and receiver can be treated symmetrically, and the overall number of spatial EDoFs is determined by the minimum of the two sides, similar to classical MIMO systems [212].

In [247], the EDoF analysis centers on the receiver correlation matrix. The analysis utilizes FPBSM to depict the receiver's EM field in the context of isotropic scattering. By incorporating the space-wavenumber relationship and drawing from the theory of Fourier spectral series expansion, the information of the receive field is effectively captured by the sampling points located within the inner elliptical lattice of

the receiver's angular domain, as illustrated in Fig. 14(a). The cardinality of this lattice ultimately determines the number of EDoFs. Building on this foundation, the study explores the EDoFs of various array geometries, including 1D linear arrays, 2D planar arrays, and 3D volumetric arrays. The findings indicate that the EDoFs are directly proportional to the product of the apertures of the transceivers. It is noteworthy that the FPBSM employed in [247] differs slightly from the one used in [195]. In the former, randomness is directly associated with the plane wave spectrum in the receiver's angular domain. In contrast, the latter attributes randomness to the coupling coefficients linking the transmit angular domain to that of the receiver.

The results obtained in [247] serve as a foundation for analyzing the number of EDoFs or significant singular values in the correlation matrix of a communication system aided by RIS [248]. As previously mentioned, the Fourier spectral series expansion is asymptotically lossless when the array apertures tend toward infinity. In practical systems with finite array apertures, the expressions derived in [247], [248] are approximate. To address this limitation, [249] proposed a heuristic formula for approximating the number of EDoFs of an RIS-assisted communication system. The mathematical structure of this formula is based on a heuristic hypothesis without rigorous mathematical proof, and its parameters are determined through numerical fitting. The study demonstrates that for a fixed array aperture, reducing the antenna spacing or increasing the number of antennas can sometimes lead to a decrease in the EDoFs, eventually reaching a constant value equivalent to the number of EDoFs of a conventional CAP-MIMO channel [249]. This observation is further elucidated by the subsequent work in [250], which revealed that the correlation matrix examined in [247]–[249] exhibits a symmetric Toeplitz block structure in isotropic scattering conditions. Consequently, the singular values of the correlation matrix have asymptotic behavior similar to the spectral sampling points of this matrix. Simulation results in [250] demonstrate that a larger antenna spacing results in more pronounced spectrum aliasing. This, in turn, magnifies certain spectral values around the periphery of the spectrum, which can be resolved by the antenna array. This magnification effect is primarily attributed to the presence of evanescent waves generated by the array. Additionally, the study delves into the impact of mutual coupling between antennas on the EDoFs, offering a comprehensive exploration of these phenomena [250].

- *CAP-NFC*: Having explored the EDoFs for SPD-NFC under NLoS scenarios, we now shift our focus to understanding the EDoFs in the context of CAP-NFC under NLoS conditions.

In accordance with the principles outlined in [84], a comprehensive approach involves the use of two pre-defined complete sets of orthogonal basis functions, designed for transmission and reception. Applying these basis functions allows a channel response based on Green's function to be effectively transformed into an infinitely large matrix. Each element of this matrix corresponds to a coupling coefficient, establishing the connection between a transmission mode within the CAP transmit array and a reception mode within the CAP receive array. This coupling coefficient can also be interpreted as a form

of transadmittance, associating the amplitude of a wave in one array with the source amplitude in the other. By performing an SVD on a suitably truncated version of this channel matrix, it becomes possible to approximate the number of EDoFs of the LoS channel. The accuracy of this approximation is contingent on the precision of the truncation. This method has been extended to analyze multipath channels, as demonstrated in [251] where the EDoFs of a near-field CAP-MIMO channel were investigated. In this context, a scatterer is assumed to act as a purely reflective plane, signifying the absence of EM field penetration [252]. This simplification disregards the potential specular effects that can occur when waves traverse clouds of small scattering particles. However, it is important to note that modeling scatterers as pure reflectors aligns with the more precise description as long as the total path length is considerably larger than the signal wavelength [253].

In situations where a single scatterer is involved, it is feasible to mirror-image either the transmitter or receiver relative to the scatterer. This process generates a virtual body and an equivalent free-space LoS transmission path. Consequently, the number of EDoFs can be straightforwardly determined [251]. In scenarios featuring multiple scatterers along the path, the aforementioned mirror imaging procedure can be repeated for each scattering point. By doing so, a virtual path is constructed that effectively amalgamates the reflections and losses incurred from each scattering body, accounting for their cumulative impact. In cases with multiple paths, a similar method can be employed to generate the coupling matrix for each individual path. Subsequently, these matrices can be projected back onto the same basis eigenfunctions [251]. This approach enables the formation of the coupling matrix for the entire multipath channel, incorporating the effects of each scattering body. The EDoFs can be determined by examining the eigenfunctions and singular values of this matrix [84].

The previously discussed research provides a comprehensive framework for determining the EDoFs for CAP-NFC NLoS channels. Nevertheless, ensuring the numerical accuracy of these computations necessitates the use of a coupling matrix with substantial dimensions, which can be computationally demanding. Consequently, this approach has seen limited adoption due to its computational complexity. To address this challenge, the EM field can be conceptualized as a bandlimited spatial signal, accurately represented through a set of finite, non-redundant sampling points in the wavenumber or angular domain. The EDoFs are then assigned a value slightly larger than the corresponding Nyquist number [218], [254]. Leveraging these principles, researchers have employed the Nyquist sampling theorem and Fourier theory to determine the EDoFs in CAP-MIMO NLoS channels.

For example, the authors of [138] investigated the EDoFs of a CBSM-based CAP-NFC channel, taking into account the tensor Green's function. This work calculated the number of EDoFs of the entire channel as the minimum of the EDoFs of two sub-channels: the transmitter-to-scatterers sub-channel and the scatterers-to-receiver sub-channel, as illustrated in Fig. 13. In each sub-channel, the EDoFs were calculated based on the space-wavenumber relationship. The EM response of the sub-channels for three typical uni-polarized arrays including linear,

circular, and spherical arrays, was approximated through an orthonormal expansion over polar and spherical spatial Fourier bases [138]. This approach provided analytical results for the EDoFs in terms of the product of the wavenumber and array aperture. Notably, similar results were also replicated in the work presented in [236], which employed Landau’s eigenvalue theorem. This research introduced a more versatile formula for calculating the number of EDoFs that is across diverse scattering environments. The extension of these findings to encompass non-monochromatic (wideband) environments and apertures with arbitrary geometries is presented in [235].

The aforementioned contributions have predominantly focused on the impact of scattering while overlooking the inherent randomness introduced by scatterers within the channel. When considering the channel’s intrinsic randomness, the determination of the number of EDoFs for NLoS CAP-MIMO channels can be accomplished by following the methodologies outlined in [195] and [247], notably by setting the antenna spacing to zero.

The cumulative body of research dedicated to EDoFs in NLoS CAP-NFC channels consistently underscores a *direct proportionality between the number of EDoFs and the product of the apertures of the CAP arrays*. It is essential to highlight that the existing findings *do not establish a clear relationship between the number of EDoFs and the propagation distance between the transceivers or the propagation distance between the scatterers*, unlike observations made for LoS channels. Two main factors contribute to this distinction. First, many existing studies primarily address the NLoS component introduced by scatterers while neglecting the LoS component, which is intricately linked to propagation distance. Second, when modeling scatterers, most work tends to consider spherical wavefronts but disregards other effects of spatial non-stationarity of scatterers in the near field, including both FSPL and EAL, as exemplified by [138] and [195]. When more spatial non-stationary effects are taken into account, the derived number of EDoFs should theoretically exhibit a relationship with propagation distance.

Indeed, as mentioned earlier, the authors of [238] harnessed Landau’s eigenvalue theorem to analyze the EDoFs in LoS communications involving an RIS positioned between two spatially-continuous planar apertures. Their analysis demonstrated an inverse proportionality between the EDoFs and the transmission distance to the RIS. Furthermore, if the scatterers are assumed to be clustered in a purely reflective plane as in [251], it can be established that the number of EDoFs is inversely proportional to the propagation distance, particularly for non-stationary scatterers.

To provide a concise overview of the primary contributions concerning EDoF analysis in near-field NLoS channels, Table X is presented above.

B. Power Scaling Law

We now turn our attention to another frequently used performance metric in NFC—the “*power scaling law*”. One of the fundamental advantages of employing large aperture arrays lies in the fact that the SNR exhibits growth as the number of

antennas N increases. Traditional research on massive MIMO has demonstrated that SNR scales proportionally with N when optimal beamforming techniques are applied. This implies that the received SNR increases at a rate of $\mathcal{O}(N)$, or alternatively, the transmit power required to achieve a target SNR during data transmission decreases as $\mathcal{O}(1/N)$. This phenomenon is often referred to as the “*power scaling law*” [255]. Recent findings have shown that when optimally configured, the SNR can grow at a rate of $\mathcal{O}(N^2)$ when employing an RIS with N elements. This opens up the possibility for an even more aggressive power scaling law, where the transmit power can be reduced as $\mathcal{O}(1/N^2)$ [256], [257]. However, it is essential to note that these derived results are not entirely rigorous. They were obtained under the far-field assumption and do not account for spatial non-stationarity, which may become relevant when the antenna array is large. To be more specific, if the received SNR were to grow unbounded at rates of $\mathcal{O}(N)$ or $\mathcal{O}(N^2)$, it could lead to a situation where the received power surpasses the transmit power. *This situation would violate the fundamental law of energy conservation* [5]. Motivated by these considerations, many researchers have made significant contributions to the understanding of the power scaling law in NFC systems.

1) *CAP-NFC*: One of the earliest contributions to the power scaling law for CAP-NFC was presented in [28]. In this pioneering work, the authors derived a closed-form expression for the received SNR in an uplink NFC channel between a single-antenna user and a large aperture CAP array deployed in a paraxial scenario. The analysis accounted for the effects of spatial non-stationarity, including both FSPL and EAL. As the array aperture tends towards infinity, the received SNR converges to $\frac{P}{2\sigma^2}$, where P and σ^2 denote the transmission and noise power, respectively. This result aligns with the intuitive notion that half of the isotropically transmitted power from the user reaches the CAP array, while the other half propagates away from it [132]. Importantly, this result adheres to the fundamental principle of energy conservation. The findings of [28] were further extended to analyze the received SNR in an uplink NFC channel between a single-antenna user and a large SPD array in [258]. The analysis assumed edge-to-edge deployment of antenna elements to maximize the total aperture area used for receiving, and it demonstrated that the asymptotic SNR also converges to the constant $\frac{P}{2\sigma^2}$. Note that the edge-to-edge deployment makes the SPD array equivalent to a CAP array. The same study also examined the SNR of a SISO channel aided by a CAP-RIS, but only under the far-field assumption, leading to results that violated the law of energy conservation. Concurrently, Dardari explored the received SNR in CAP-NFC between a small aperture CAP array and a larger CAP array for a paraxial scenario in [139]. This work introduced the NUSW model and considered the influence of FSPL, EAL, and PL. It was discovered that the received SNR converged to a constant $\frac{P}{3\sigma^2}$ rather than $\frac{P}{2\sigma^2}$ as the aperture size of the larger CAP array tended towards infinity [139]. Subsequently, the authors of [133] adopted the same approach to analyze the received SNR in near-field uplink MISO channels based on SPD arrays, half-duplex relay-aided SISO channels, and the SNR upper bound of a

TABLE X: Contributions on EDoF Analysis for NLoS Channels

Antenna	Ref.	Tx	Rx	Scattering	Randomness due to Scatterers	Eigenfunctions	Characteristics
SPD	[241]	Planar	Planar	FDC	✗	SVD	The EDoF ₂ -based approximation is applied to a tensor Green's function-based channel with a direct link and a reflection link.
	[242], [243]	Arbitrary	Arbitrary	Isotropic	✗	SVD	The EDoF ₂ -based approximation is applied to a tensor Green's function-based channel with inhomogeneous permittivity profiles influenced by scatterer positions.
	[244]	Volumetric	Volumetric	Arbitrary	✓	SVD	The EDoF ₂ -based approximation is applied by replacing $\mathbf{H}\mathbf{H}^H$ with $\mathbf{E}\{\mathbf{H}\mathbf{H}^H\}$. However, this formula only applies to channels with single-side correlation.
	[245]	Linear	Linear	Arbitrary	✓	SVD	The EDoF ₂ -based approximation is applied by replacing $\mathbf{H}\mathbf{H}^H$ with $\Phi = \mathbf{E}\{\text{vec}\{\mathbf{H}\}\text{vec}\{\mathbf{H}\}^H\}$. However, this formula cannot approximate the EDoF.
	[195]	Planar	Planar	FPBSM	✓	SVD or Fourier plane wave decomposition	The space-wavenumber relation and Fourier transform are applied to approximate the spatial EM channel. The number of EDoFs equals the number of inner lattice points.
	[246]	Planar	Planar	Isotropic	✓	SVD or Fourier plane wave decomposition	The space-wavenumber relation and Fourier transform are applied to approximate the spatial EM channel. The influence of evanescent waves is considered.
	[247]	✗	Arbitrary	Isotropic	✓	SVD or Fourier plane wave decomposition	The space-wavenumber relation and Fourier transform are used to estimate the number of EDoFs (the number of significant singular values of the correlation matrix).
	[248]	✗	Planar	Isotropic	✓	SVD or Fourier plane wave decomposition	The space-wavenumber relation is applied to approximate the number of EDoFs (the number of significant singular values of the correlation matrix of the RIS).
	[249]	✗	Planar	Isotropic	✓	SVD or Fourier plane wave decomposition	A heuristic formula based on the space-wavenumber relation is applied to approximate the number of EDoFs of the correlation matrix of the RIS.
	[250]	✗	Planar	Isotropic	✓	SVD or Fourier plane wave decomposition	A block-Toeplitz with Toeplitz block structure-based power spectrum method is applied to approximate the number of EDoFs of the correlation matrix of the RIS.
CAP	[251]	Arbitrary	Arbitrary	FDC	✗	SVD of the truncated coupling matrix	A general yet computationally intensive framework is provided by solving the eigenproblem via the SVD of the truncated coupling matrix.
	[138]	Uni-polarized	Uni-polarized	CCM	✗	PSWF-related	The space-wavenumber relation and Fourier transform are applied to approximate the number of EDoFs of the channel between the scatterers and the transmitter/receiver.
	[236]	Planar	Planar	Arbitrary	✗	✗	Landau's theorem is applied to estimate the number of EDoFs of CAP-NFC between two CAP planar arrays.
	[235]	Arbitrary	Arbitrary	Arbitrary	✗	✗	Landau's theorem is applied to estimate the number of EDoFs of CAP-NFC between two CAP arrays in wideband environments.

near-field RIS-aided SISO channel. It was established that the received SNR for all these scenarios converged to a constant value as the array aperture grew infinitely large. An intuitive explanation for this finite limit, despite the array's infinite size, is that each new receive antenna is deployed further from the transmitter, leading to a gradual reduction in the effective receive area perpendicular to the direction of propagation. Additionally, PL increases as the array expands [133]. These results were derived under the assumption of zero antenna spacing in the SPD array, effectively corresponding to a CAP array.

2) *SPD-NFC*: In a further development, the analysis of the received SNR was extended to encompass an uplink near-field channel between a single-antenna device and a linear SPD array. This investigation, conducted in [78], takes into account the influence of FSPL in a non-paraxial scenario. Unlike previous studies, this work does not assume zero element spacing, and it establishes that the asymptotic SNR is intricately related to several factors, including the AoA, antenna spacing, and the propagation distance between the user and the center of the linear array. The analysis is further extended to explore NFC in the context of a single-antenna device communicating with a planar SPD array [123]. In this scenario, the impact of EAL is considered as well. The findings from this research suggest that the asymptotic received SNR can be expressed as $\frac{P}{2\sigma^2}\epsilon$, where ϵ represents the array occupation ratio. When the array occupation ratio equals one ($\epsilon = 1$), the SPD array effectively becomes a CAP array, and the derived result aligns with the outcome presented in [28]. Additionally, the numerical results obtained in [123] indicate that the USW model does not yield a reasonable power scaling law in the asymptotic limit of large aperture sizes. In particular, *the results derived from the USW model are shown to be in contradiction with the law of energy conservation*. These findings echo the research presented in [259], which also analyzed the SNR of a near-field MISO channel taking into consideration both FSPL and EAL. This subsequent study shows that *the NUSW model, which*

solely considers the variable FSPL, also results in a power scaling law that contravenes the law of energy conservation. This corroborates the earlier observations presented in [133]. Moreover, the methodology applied in [78] and [123] is extended to derive the SNR for a near-field MISO channel that relies on a modular linear ELAA. Unlike the commonly assumed collocated configuration, modular arrays feature an arrangement of elements into modules comprising a moderate number of array elements, with the regularly spaced modules separated by a distance much larger than the signal wavelength [260]. This design caters to practical antenna array mounts and offers enhanced deployment flexibility for covering specific areas. In this context, a variable FSPL is considered, and the derived asymptotic SNR is inversely proportional to the module separation [260].

As previously mentioned, [133] derived an upper bound for the received SNR in a near-field RIS-aided SISO channel. This upper bound was based on the Cauchy-Buniakowsky-Schwarz inequality, which is generally known to be loose. To improve upon this, the authors of [261] introduced a tighter bound for the SNR, taking into account the influence of variable FSPL and EAL. The research revealed that the asymptotic SNR converges to a constant that is related to the propagation distances between the RIS and the transceivers. While previous works examining the variation of the projected effective aperture focused on hypothetical isotropic antennas with a constant directional gain pattern independent of the direction of signal incidence, the researchers in [262] introduced a more versatile directional gain pattern for each antenna element, determined by the elevation and azimuth angles of the incident signal. Building on this enhancement, they analyzed the SNR in SPD-NFC supported by extremely large-scale reconfigurable refractive surfaces (RRSs) [262]. While the numerical results in [262] observed the convergence of the received SNR to a constant, it did not provide a closed-form expression for the SNR. Advancing this line of research, the authors of [124] derived closed-form lower and upper

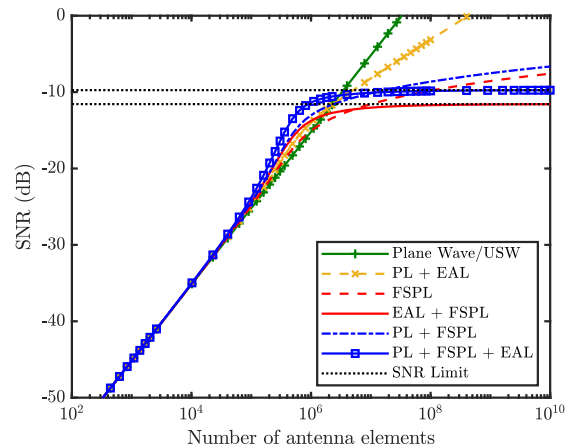
bounds for the received SNR in extremely large-scale RIS-aided near-field SISO channels. In this work, the influence of FSPL and a generic directional gain pattern was considered, and the tightness of the derived bounds was confirmed through numerical simulations. However, the influence of PL was not accounted for in these aforementioned works.

To address this knowledge gap, the authors of [125] extended prior research in [78], [123], [124], [259]–[262] by incorporating the EM polarization effect of the antenna elements and variations in signal amplitude in the NUSW model. Leveraging this model, a closed-form expression for the SNR was derived for NFC between a single-antenna device and a planar SPD array. As the array aperture approaches infinity, the SNR was shown to converge to $\frac{P}{3\sigma^2}\epsilon$, with ϵ representing the array occupation ratio. This outcome is similar to the result derived in [133]. This new NUSW model is specifically applicable when the polarization vector of the receive antenna and the normalized electric current vector are aligned along the same axis [125]. To provide a broader scope, the authors of [5] introduced an improved NUSW model that applies to arbitrary polarization modes and current directions. Based on this general model, a power scaling law for both SPD-NFC and CAP-NFC was derived. Furthermore, the study theoretically demonstrated that the USW model could yield a logarithmic power scaling law of $\mathcal{O}(\log N)$, which raises concerns about its compliance with the law of energy conservation.

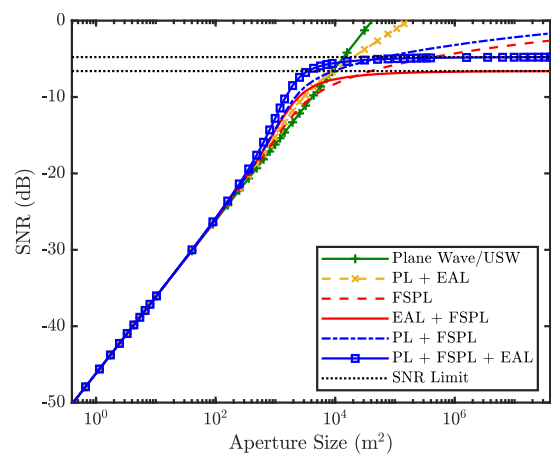
Based on the preceding discussion, it is evident that a precise characterization of the power scaling law in NFC necessitates consideration of three fundamental properties that distinguish it from far-field scenarios:

- i) FSPL: In NFC, the distance to the array elements varies across the array.
- ii) EAL: The effective antenna area varies as the array is observed from different directions.
- iii) PL: The loss from polarization mismatch varies with signals received from different directions.

To ensure that the derived scaling law adheres to the law of energy conservation, it is essential to account for the influence of FSPL in the case of linear arrays and both FSPL and EAL for planar arrays. However, there exists an exception for planar arrays, as demonstrated in [263]. In this study, the authors examined the SNR of a near-field downlink MISO channel supported by extremely large aperture RRSs. In their derivation, only the influence of FSPL was considered to model the spatial non-stationarity. Nevertheless, numerical results suggested that the received SNR also converges to a constant as the array aperture approaches infinity. This phenomenon can be attributed to the RRS's ability to generate distinct directional gain patterns, often referred to as holographic patterns, for each antenna element. Although the impact of EAL was not explicitly incorporated into the channel model, its influence was indirectly considered through the variable holographic patterns. Consequently, the resulting SNR exhibited an increase with larger array apertures, eventually reaching a constant value. This observation underscores again the necessity of considering the influence of FSPL and EAL for planar arrays to derive a scaling law that aligns with the



(a) SPD array.



(b) CAP array.

Fig. 17: Illustration of the received SNRs by considering different properties (FSPL, EAL, and PL) versus the number of antennas or aperture size for a downlink MISO channel. The transmitter is equipped with a squared planar array, and the system wavelength is 0.1256 m. The center of the transmit array is located at the origin of a three-dimensional space, while the receiver is positioned at coordinates (6.25 m, 10.82 m, 12.5 m). The other simulation parameters are the same as those used in generating [5, Figs. 23–24].

principle of energy conservation. To further emphasize the importance of considering all three properties in the study of near-field power scaling laws, Fig. 17(a) and Fig. 17(b) show the received SNR in a downlink SPD-MISO and CAP-MISO channel, respectively. The multiple-antenna transmitter is equipped with a planar array. As shown in Fig. 17, to obtain a scaling law that obeys the law of energy conservation, it is necessary to consider the influences of both FSPL and EAL.

In summary, a comprehensive overview of the primary contributions pertaining to the analysis of the power scaling law for near-field channels can be found in Table XI. Current research efforts aimed at unraveling the power scaling law in NFC have predominantly centered on single-user channels operating in LoS propagation scenarios. However, for a

TABLE XI: Contributions on Power Scaling Law Analysis for NFC

Antenna	Ref.	Spatial Non-Stationarity			Array	Paraxial Deployment	Characteristics
		FSPL	EAL	PL			
CAP	[28]	✓	✓	✗	Planar	Paraxial	One of the earliest contributions to the power scaling law in NFC is presented.
	[258]	✓	✓	✗	Planar	Paraxial	The power scaling law is derived for NFC between a single-antenna user and an SPD array with zero antenna spacing, i.e., CAP array.
	[139]	✓	✓	✓	Planar	Paraxial	The power scaling law is derived for NFC between a small CAP aperture array and a larger CAP array.
	[133]	✓	✓	✓	Planar	Paraxial	The power scaling law is derived for near-field uplink MISO channels, half-duplex relay-aided SISO channels, and RIS-aided SISO channels.
SPD	[78]	✓	✗	✗	Linear	Arbitrary	The asymptotic SNR is related to the AoA, antenna spacing, and the propagation between the user and the center of the linear array.
	[123]	✓	✓	✗	Planar	Arbitrary	The asymptotic received SNR can be expressed as $\frac{P}{\Delta\sigma^2}\epsilon$, where ϵ represents the array occupation ratio concerning the entire planar array.
	[259]	✓	✓	✗	Planar	Arbitrary	It is shown that the NUSW model, which solely considers the variant FSPL, also results in a power scaling law that contradicts the energy conservation law.
	[260]	✓	✗	✗	Linear	Arbitrary	The power scaling law is derived for a near-field MISO channel that relies on a modular linear ELAA between the user and the center of the linear array.
	[261]	✓	✓	✗	Planar	Arbitrary	Tight bounds are derived for the received SNR in a near-field RIS-aided SISO channel, which is related to the propagation distances between the RIS and the transceivers.
	[262]	✓	✓	✗	Planar	Arbitrary	A generic directional gain pattern is considered for each antenna element, based on which the power scaling law is derived for an RRS-aided NFC channel.
	[124]	✓	✓	✗	Planar	Arbitrary	A generic directional gain pattern is considered for each antenna element, based on which the power scaling law is derived for an RIS-aided near-field SISO channel.
	[125]	✓	✓	✓	Planar	Arbitrary	The asymptotic received SNR can be expressed as $\frac{P}{\Delta\sigma^2}\epsilon$, where ϵ represents the array occupation ratio concerning the entire planar array.
	[5]	✓	✓	✓	Planar	Arbitrary	General expressions are provided for SNRs in both SPD-NFC and CAP NFC by considering a NUSW model that applies to arbitrary polarization modes and current directions.
	[263]	✓	✗	✗	Planar	Arbitrary	The impact of EAL is not explicitly incorporated into the channel model but is indirectly considered through the variant holographic patterns.

more comprehensive understanding of this phenomenon, these established insights should be extended to encompass multiuser channels and NLoS propagation environments. Although power scaling laws for traditional multiuser massive MIMO fading channels have been well-documented in the literature, as exemplified in seminal works like [255] and [264], these studies are rooted in the far-field assumption. In this paradigm, the influence of spatial non-stationarity is often disregarded, consequently leading to derived results that deviate from the fundamental principle of energy conservation. While there seems to be no evident reason to doubt that the asymptotic trends given in Table XI would extend to NLoS propagation conditions—where the SNR or SINR appears to stabilize at a constant value with an increase in the array aperture—research in this domain remains both open and laden with nontrivial challenges.

C. Transmission Rate

After discussing research contributions related to the power scaling law in NFC, our focus now turns to another critical performance metric: the transmission rate, which is a key determinant of the system's throughput and spectral efficiency. The maximum achievable error-free transmission rate is often referred to as the channel capacity, which can only be achieved using specific channel coding/decoding and precoding/equalizing designs. However, identifying capacity-achieving channel codes and precoders/equalizers poses significant challenges. Consequently, research efforts are typically directed toward determining achievable transmission rates.

The analysis of transmission rates is closely intertwined with the system channel model. With this in mind, our next objective is to provide an overview of the existing literature that investigates transmission rates within both LoS and NLoS models.

1) *LoS Channels*: We now turn our attention to the analysis of transmission rates in near-field LoS channels supported by SPD and CAP arrays.

- *SPD-NFC*: The study conducted in [116] delved into the sum-rate analysis of a near-field downlink multiuser MISO channel, employing ZF precoding in conjunction with the USW model. The authors derived a closed-form approximation for the downlink sum-rate using Bessel-integral functions. Their theoretical analysis suggests that the channel correlation between different users diminishes as the number of antennas at the SPD array increases indefinitely. However, it is essential to acknowledge that this result lacks absolute precision due to the limitations of the USW model as the antenna count approaches infinity, as previously discussed in [117]. As elucidated in Section IV-A1, the singular values of near-field SPD-MIMO channels exhibit a step-like behavior. Leveraging this inherent property, the authors of [85] introduced EDoF₂ as an approximation for the EDoFs. This approach provides closed-form solutions using the dominant singular values, enabling the derivation of a closed-form expression for the capacity of a near-field single-user MIMO channel with isotropic inputs and uniform power allocation. Both the works in [116] and [85] assume a fixed orientation and antenna spacing for the SPD array. In contrast, the authors of [265] analyzed the channel capacity of a near-field single-user MIMO channel obtained with reconfigurable uniform linear arrays. Initially, they established a general upper bound for the information-theoretic capacity, considering arbitrary array orientation and antenna spacing, along with the associated conditions for achieving this capacity bound. Their findings highlight the significant influence of array orientation and antenna spacing on the realization of the capacity. Building on this, they proposed a method for finding the optimal array configuration, together with a low-complexity implementation. Additionally,

[238] extended their analysis to explore the channel capacity of an RIS-assisted near-field single-user MIMO channel. In this work, they provided a general upper bound for the channel capacity expressed as a function of the singular values of the transmitter-to-RIS and RIS-to-receiver channel matrices.

The works conducted by [85], [116], [238], [265] all build on the USW model as their foundation. In contrast, extensions to the NUSW model are explored in [25], [266], [267]. The study in [25] examined the sum-rate performance of a two-user near-field uplink MISO system employing a minimum mean squared error equalizer with successive interference cancellation (MMSE-SIC) for optimal reception. This work was subsequently expanded in [266], where parallel maximum ratio combining (MRC) and MMSE equalization schemes were considered. The numerical results in both studies indicated that the sum-rate reaches a saturation point as the number of receive antennas increases. However, while the MMSE scheme rapidly converges to the interference-free scenario, MRC yields a substantial performance gap. An extension to a more general multiuser scenario incorporating ZF decoding is presented in [267]. In these three contributions, the NUSW model was adopted to represent near-field propagation. The resulting sum-rate was found to be intricately related to the channel correlation between different users, and deriving a closed-form expression or approximation for this channel correlation proves to be a highly challenging task when operating under the NUSW model. As a pragmatic compromise, these works provide numerical results, demonstrating that *the channel correlation between distinct near-field users diminishes as the number of antennas in the SPD array increases.*

The aforementioned contributions rely on the assumption that the LoS channel between a pair of SPD antennas is described by a complex-valued coefficient, which can be regarded as a result derived from the scalar Green's function. The authors of [140] investigated the sum-rate of a near-field downlink multiuser MIMO channel using the tensor Green's function to characterize the LoS propagation between SPD antennas. Unlike the scalar model, the tensor model introduces two primary sources of interference: one arising from cross-polarization and the other from inter-user interference. To mitigate these interference sources, the authors derived a ZF-based dual-layer precoding design. The first layer focuses on addressing cross-polarization components, while the second layer manages the interference emanating from other users in the co-polarized channels. The work in [140] is based on the assumption of parallel arrays, which limits the ability to capture channel responses for arbitrary array placements. In an effort to overcome this limitation, the capacity of a near-field single-user tri-polarized MIMO channel with isotropic inputs and equal transmit power allocation (ETPA) under non-paraxial and non-parallel deployments was analyzed in [268]. This work leveraged the Fresnel approximation to simplify the channel matrix and derived a capacity upper bound, which serves as a performance limit for the system.

- *CAP-NFC*: Next, we will shift our attention to CAP-NFC, whose transmission rate acts as an upper bound for that of SPD-NFC.

In the pioneering work on large intelligent surfaces by Hu

et al. [132], an analysis of the channel capacity for a near-field uplink multiuser MISO channel was conducted, where uniformly distributed terminals communicate with a CAP array. A paraxial setup was considered, where user terminals are arranged in a uniform grid parallel to the CAP array. To facilitate analytical tractability, a spatio-temporal MRC-based equalizer was applied to each transmit signal, effectively approximating the uplink channel as a sinc-function-like inter-symbol interference (ISI) channel. Building on this approximation, the authors derived closed-form expressions for the channel capacity averaged over the number of terminals. This analytical work was rooted in their previous findings related to ISI channels [269], [270]. Furthermore, they extended their analysis to explore the limit of the channel capacity averaged over the grid area where the users are located (referred to as space-normalized capacity) as the number of users approaches infinity. Within this framework, they identified the optimal user spacing that maximizes the channel capacity. While the derivations presented in [132] were mathematically rigorous, they might not be readily accessible to all readers. To address this, the authors of [85] introduced a simplified EDoF₂-based approximation for calculating the dominant singular values and channel capacity between two linear continuous arrays. This approach resulted in a more straightforward closed-form expression for the channel capacity that takes into account the geometrical randomness of the CAP transmit array. A similar method was employed in [238], where Landau's theorem was used to estimate the number of EDoFs for an RIS-aided near-field CAP-MIMO channel. Building on these findings and leveraging the step-like characteristics of the channel's singular values, they derived a closed-form expression for the capacity upper bound.

The expressions obtained in the aforementioned three studies involve various approximations and simplifications, which somewhat constrain their generality. To address these limitations, a notable advancement was made in [137], which derived an exact expression for the channel capacity of a near-field CAP-MIMO channel between two continuous linear arrays. In this work, they utilized the tensor Green's function to model near-field LoS propagation, which provided additional precision to their analysis. By characterizing the two continuous regions as random fields, they employed mathematical tools such as the Mercer expansion [271] and Fredholm determinant [272] to derive comprehensive expressions for the channel capacity, initially considering the white-noise scenario and subsequently extending their findings to the colored-noise case. Building on this comprehensive framework, the research in [273] incorporated the influence of mutual coupling, enhancing the realism of the model and accounting for more complex interactions in practical scenarios. Theoretical analyses in [273] revealed an intriguing insight: as the antenna density increases without mutual coupling, the disparity between the channel capacity of CAP-MIMO and SPD-MIMO systems progressively diminishes, eventually converging to zero. This observation underscores the convergence of SPD-MIMO to the CAP-MIMO case under certain conditions, shedding light on the behavior of NFC systems with large antenna densities.

The expressions for channel capacity derived in [137] and [273] are predicated on the assumption of uniform transmit power allocation. As is well-established, achieving channel capacity hinges on acquiring the SVD of the channel response and applying an appropriate power allocation algorithm. However, as previously discussed in Section IV-A1, the computational complexity of decomposing the Green's operator is quite substantial.

To address this challenge, Sanguinetti and colleagues introduced a wavenumber-division multiplexing (WDM) scheme in [274], in which the spatially-continuous transmitted currents and received electric fields are represented using Fourier basis functions. This representation facilitates the derivation of a transmission rate expression based on the resulting wavenumber-domain channel response. These spatial Fourier basis functions tend to become asymptotically orthogonal in the wavenumber domain as the size of the array aperture approaches infinity. This characteristic bears resemblance to the principles of orthogonal-frequency division-multiplexing (OFDM). However, due to the non-finite spatial support of the EM channel, WDM does not inherently provide non-interfering communication modes or a diagonal wavenumber-domain channel response. As a result, linear equalizers based on SVD, MMSE, and MRC are instrumental in further eliminating interference [274]. While [274] assumed a paraxial and parallel deployment scenario, the results were extended to non-parallel deployment configurations in [275].

For easy reference, we have summarized the key contributions pertaining to the analysis of transmission rates in near-field LoS channels in Table XII. "SU", "TU", and "MU" represent single-user, two-user, and multiuser, respectively. "DL" and "UL" represent downlink and uplink, respectively.

2) *NLoS Channels*: We now refocus our attention on the transmission rate in NLoS channels while taking into account the influence of scattering. In NLoS scenarios, our primary objective is to determine the mean of the transmission rate, considering the stochastic nature of small-scale fading. This is commonly referred to as the average transmission rate (ATR) or ergodic transmission rate (ETR). As previously mentioned, the rate analysis is contingent upon the specific channel model employed. In the following sections, we will review existing analyses of ATR or ETR, with a particular emphasis on both *PPBSMs* (*physical propagation-based stochastic models*) and *CBSMs* (*correlation-based stochastic models*).

- *PPBSM*: Expanding on the discussion in Section III-C, we recall that the statistical characteristics of PPBSMs primarily stem from the inherent randomness and spatial distribution of the scatterers' reflection coefficients. In the study conducted by Liu *et al.* [5], closed-form expressions were provided for the ATR in a near-field downlink single-user MISO channel. This analysis encompassed both FDC (finite-dimensional channel) models and CCMs (clustered channel models). To model the array response between the transmit array and the scatterers, the NUSW model was adopted. While analyzing the ATR in CCM or FDC-based near-field MISO channels is relatively straightforward, extending this analysis to the MIMO scenario poses significant challenges. To date, the derivation of closed-form expressions for ATR in the MIMO scenario

remains an elusive goal, with only some bounds being established through the application of Jensen's inequality [276]. The inherently complex nature of PPBSMs presents analytical challenges for ATR analysis, which is why most research efforts have been directed toward ATR analysis under CBSMs.

- *CBSM*: In contrast to PPBSMs, CBSMs offer a more analytically tractable approach, as they directly model the mean and covariance of the channel.

Taking into account the non-stationarity of near-field channels due to blockages that affect the VR, [161] studied the ATR for a near-field downlink multiuser MISO channel. This analysis was based on the near-field channel correlation constructed from the single-scattering model depicted in Fig. 12(a), where the correlation matrix is formulated as $\mathbf{D}^{1/2}\mathbf{R}_f\mathbf{D}^{1/2}$, \mathbf{D} represents a binary VR mask, and \mathbf{R}_f is the correlation matrix based on the far-field model. Employing high-dimensional random matrix theory, the researchers derived deterministic expressions for the SINR achieved with ZF and MRT precoders, leading to closed-form expressions for the corresponding average sum-rates. Notably, the authors' findings concluded that, under optimal conditions where the VRs of different users do not overlap, thus reducing inter-user interference, the SINR achieved with both MRT and ZF can surpass that of a stationary channel [161]. These results were further expanded in [176], which proposed an energy-efficient antenna selection strategy. Employing the same channel model as [161] and [176], the authors of [277] studied the average sum-rate achievable using regularized ZF (RZF) precoding, and also provided a low-complexity algorithm for the design of the regularization.

While the work discussed above considered the downlink case, [171] investigated the uplink sum-rate of a near-field multiuser MISO channel, building on the correlation model $\mathbf{D}^{1/2}\mathbf{R}_f\mathbf{D}^{1/2}$. For the case of MRC equalization, an approximate expression for the average sum-rate was derived by applying Mullen's inequality [278] and Jensen's inequality. For linear MMSE (LMMSE) equalization, closed-form expressions for the average sum-rate were derived, accounting for scenarios where the VRs of different users either completely or partially overlap. These results are contingent on the assumption that perfect knowledge regarding the VRs of various users is available. In contrast, the authors of [169] introduced a novel VR estimation algorithm and proceeded to analyze a deterministic equivalent of the resulting average sum-rate for a near-field downlink multiuser MISO channel incorporating MRT precoding.

In addition to the single-scattering model presented in Fig. 12(a), an alternative approach using CBSM is based on the double-scattering model depicted in Fig. 12(b). In this context, Li *et al.* [162] conducted an analysis of the average sum-rate in a near-field uplink multiuser MISO channel employing MMSE-SIC equalization. The authors harnessed the principal minor determinant expansion theorem for the characteristic polynomial of a matrix [279] and the Binet-Cauchy formula for the determinant of a matrix product [280] to derive a closed-form expression for the upper bound for the average sum-rate. In the same scattering model, the authors of [178] evaluated the average sum-rate of a near-field uplink multiuser

TABLE XII: Contributions on Transmission Rate Analysis for LoS Channels

Antenna	Ref.	Scenarios	Array	Paraxial Deployment	Precoding	Equalization	Characteristics
SPD	[116]	MU-DL-MISO	Linear&Planar	Arbitrary	ZF	—	A closed-form expression for the sum-rate is derived under the USW model, which shows that the channel correlation decreases with the antenna number.
	[85]	SU-MIMO	Linear	Paraxial	Isotropic (ETPA)	MMSE-SIC	An EDoF ₂ -based scheme is used to approximate the EDoF, the dominant singular values, and thus, the channel capacity under the USW model.
	[265]	SU-MIMO	Linear	Paraxial&Reconfigurable	SVD	SVD	A general upper bound for the information-theoretic capacity is derived for NFC between two reconfigurable ULAs under the USW model.
	[238]	SU-MIMO	Planar	Paraxial	SVD	SVD	A general upper bound for the information-theoretic capacity is derived for the RIS-aided MIMO channel under the USW model.
	[25]	TU-UL-MISO	Linear	Arbitrary	ETPA	MMSE-SIC	The sum-rate performance of a near-field channel is numerically evaluated under a NUSW model.
	[266]	TU-UL-MISO	Planar	Arbitrary	ETPA	MRC&MMSE	The sum-rate performance under a NUSW model is shown to be related with the channel correlation.
	[267]	MU-UL-MISO	Planar	Arbitrary	ETPA	ZF&MRC&MMSE	The sum-rate performance under a NUSW model-based MU-MISO is shown to be related to the channel correlation.
	[140]	MU-DL-MIMO	Planar	Arbitrary&Parallel	Dual-Layer ZF	—	The tensor Green's function is used to characterize the LoS propagation, and a ZF-based dual-layer precoder is used to eliminate the interference.
	[268]	SU-MIMO	Planar	Arbitrary	SVD&ETPA	SVD	A capacity upper bound is derived for a near-field tri-polarized CAP-MIMO channel, which defines the system performance upper limit.
CAP	[132]	MU-DL-MISO	Planar	Paraxial	ETPA	MRC	The channel is approximated as a sinc-function-like ISI channel, based on which several expressions for the channel capacity are derived.
	[85]	SU-MIMO	Linear	Paraxial	ETPA	MMSE-SIC	An EDoF ₂ -based approximation scheme is used to evaluate the EDoF, the dominant singular values, and thus, the channel capacity.
	[238]	SU-MIMO	Planar	Arbitrary	SVD	SVD	Landau's theorem is utilized to estimate the EDoF of an RIS-aided MIMO channel, which yields a capacity upper bound.
	[137]	SU-MIMO	Linear	Paraxial&Parallel	SVD&ETPA	SVD	An exact expression for the channel capacity of a CAP-MIMO channel is derived using Mercer expansion and Fredholm determinant.
	[273]	SU-MIMO	Linear	Paraxial&Parallel	SVD&ETPA	SVD	An exact expression for the channel capacity of a CAP-MIMO channel is derived by considering the influence of mutual coupling.
	[274]	SU-MIMO	Linear	Paraxial&Parallel	WDM	SVD&MRC&MMSE	The transmission rate achieved by WDM is analyzed, where the transmitted currents and received electric fields using Fourier basis functions.
	[275]	SU-MIMO	Linear	Arbitrary	WDM	SVD&MRC&MMSE	The transmission rate achieved by WDM is analyzed, where the continuous linear arrays can be arbitrarily placed.

MISO channel employing MRC, ZF, and MMSE equalizers.

Besides the two VR-based models discussed earlier, an alternative approach for modeling near-field multipath fading is the *FPBSM*. Initially proposed for CAP arrays, this model can also be applied to SPD arrays to characterize the small-scale fading between pairs of antennas. The SPD-MIMO channel essentially resembles a Weichselberger fading channel [165], a more general model that encompasses the commonly used Kronecker model [163] as a special case. Leveraging this insight, researchers have employed random matrix theory to analyze the channel capacity of a near-field single-user MIMO system with isotropic inputs and MMSE-SIC equalization, resulting in an analytically tractable expression for the ATR [195]. This analytical framework can be straightforwardly extended to analyze the near-field multiple access channel by building on the findings in [281].

The outcomes from [195] were further extended in [202], where a non-uniform transmit power allocation is considered, and the channel capacity of a near-field single-user MIMO system is numerically analyzed. This analysis incorporates a wrapped Gaussian azimuth angle distribution and a truncated Laplacian elevation angle distribution for the scatterers. These two contributions were then applied to the downlink multi-user MIMO scenario in [203], where closed-form expressions were derived to approximate the average sum-rate achieved by ZF and MRT precoding. In this work, users are assumed to have perfect channel information, a challenging assumption to achieve in practice. Recognizing this challenge, the authors of [204] analyzed the achievable average sum-rate of a downlink multi-user MIMO system where each user only knows the channel mean. These two works on ATR in near-field multi-

user MIMO settings were further extended to the cell-free case in [205], where the achievable uplink ATR was numerically evaluated. The work mentioned above primarily focuses on the mean of the transmission rate. In a step further, the authors of [208] also studied the second-order statistics of the transmission rate of a near-field single-user MIMO channel under FPBSM. Using the central limit theorem, this work demonstrated that the transmission rate approaches a Gaussian distribution as the number of antennas tends to infinity.

We have compiled the key contributions regarding the analysis of transmission rates in near-field NLoS channels in Table XIII.

D. Discussions and Outlook

In this section, we have conducted a comprehensive review of mainstream contributions to the performance analysis of NFC. Our primary focus has been on three widely used performance metrics: DoFs, power scaling law, and transmission rate. We believe that the insights gained from our review can offer a foundational understanding of the fundamental performance limits of NFC. Additionally, we hope this synthesis will serve as an initial guide for researchers intending to contribute to this evolving field. Nevertheless, there exist numerous open research problems within this domain, some of which are outlined below.

- **Performance Analysis for Fading Channels:** Despite the numerous contributions discussed above, the majority of results explicitly distinguishing near-field from far-field performance are based primarily on LoS channels. This observation is more pronounced for work related to EDoFs, as current results on near-field channels exhibit

TABLE XIII: Contributions on Transmission Rate Analysis for NLoS Channels

Category	Ref.	Scenarios	Array	Correlation	Precoding	Equalization	Characteristics
PPBSM	[5]	SU-DL-MISO	Planar	Kronecker	MRT	—	A closed-form expression for the ATR is derived for a downlink single-user MISO channel.
	[276]	SU-MIMO	Linear	FDC	Isotropic (ETPA)	MMSE-SIC	Closed-form expressions are derived for the upper bounds of the near-field ATR, which can be trivially extended to the near-field case.
CBSM	[161]	MU-DL-MISO	Arbitrary	Single-Scattering (Kronecker)	ZF&MRT	—	Deterministic equivalents of SINRs achieved with ZF and MRT precoders are derived, leading to closed-form expressions for the average sum-rates.
	[176]	MU-DL-MISO	Linear	Single-Scattering (Kronecker)	ZF&MRT	—	Deterministic equivalents of SINRs are derived, based on which an antenna selection strategy is proposed to improve energy efficiency.
	[277]	MU-DL-MISO	Arbitrary	Single-Scattering (Kronecker)	RZF	—	The average sum-rate achievable through RZF precoding is discussed, associated with a low-complexity design of the regularizer.
	[171]	MU-UL-MISO	Linear	Single-Scattering (Kronecker)	ETPA	MRC&LMMSE	Closed-form approximations and expressions are derived for the MRC and LMMSE equalization schemes, respectively.
	[169]	MU-DL-MISO	Arbitrary	Single-Scattering (Kronecker)	MRT	—	A novel VR estimation algorithm is proposed, and the deterministic equivalent of the ensuing sum-rate is analyzed.
	[162]	MU-UL-MISO	Linear	Double-Scattering	ETPA	MMSE-SIC	A closed-form expression for the upper bound of the average channel capacity is derived using random matrix theory.
	[178]	MU-UL-MISO	Linear&Planar	Double-Scattering	ETPA	MRC&ZF&MMSE	The average sum-rate is numerically analyzed by considering the MRC, ZF, and MMSE equalization schemes, respectively.
	[195]	SU-MIMO	Planar	FPBSM (Weichselberger)	ETPA	MMSE-SIC	An analytically tractable expression for the ATR is derived using random matrix theory.
	[202]	SU-MIMO	Planar	FPBSM (Weichselberger)	SVD	SVD	The channel capacity is discussed by considering non-uniform transmit power allocation and two non-isotropic scattering models.
	[203]	MU-DL-MIMO	Planar	FPBSM (Weichselberger)	ZF&MRT	—	Closed-form expressions are derived to approximate the average sum-rate achieved by ZF and MRT precoding.
	[204]	MU-DL-MIMO	Planar	FPBSM (Weichselberger)	MRT	—	The achievable average sum-rate of a downlink multiuser MIMO system is analyzed, where each user only knows the expectation of the channel.
	[205]	MU-UL-MIMO	Planar	FPBSM (Weichselberger)	ETPA	Arbitrary	The average sum-rate of a near-field cell-free uplink multiuser MIMO channel is discussed under arbitrary precoding and equalization schemes.
	[208]	SU-MIMO	Planar	FPBSM (Weichselberger)	ETPA	MMSE-SIC	The second-order statistics of the transmission rate are discussed, which approaches a Gaussian distribution as the antenna number tends to infinity.

limited differentiation from their far-field counterparts. Furthermore, there is a scarcity of results concerning the transmission rate of CAP arrays and power scaling laws for near-field fading channels. The reason for the above research gaps lies in the fact that modeling a near-field multipath fading channel poses additional challenges compared to the LoS case. Striking a balance between tractability and precision in fading channel models remains a multidisciplinary challenge, necessitating collaborative efforts from both the channel modeling and performance analysis domains.

- **Information-Theoretic Performance Analysis:** A profound understanding of the information-theoretic aspects of NFC is imperative for its practical implementation. Given the distinctions in channel and signal models between NFC and FFC, further exploration into the information-theoretic limits of NFC is necessary. Among the key metrics in information theory, DoFs stand out. However, current contributions on DoFs predominantly focus on single-user MIMO scenarios. Future efforts should extend the discussion to encompass near-field broadcast channels, multiple access channels, multicast channels, interference channels, and wiretap channels. Moreover, beyond DoFs, other information-theoretic metrics such as coding rate, capacity/rate region, diversity–multiplexing tradeoff, and more remain relatively unexplored and merit thorough investigation.
- **Network-Level Performance Analysis:** The practical deployment of NFC is anticipated to take place within a multi-cell environment. However, the performance of multi-cell or network-level NFC remains largely unexplored. Critical factors in the analysis of multi-cell NFC include interference management, hybrid near-/far-field channel modeling, and the consideration of user

mobility. As wireless network density increases, inter-cell interference emerges as a significant challenge, underscoring the need for a comprehensive analysis of NFC performance at the network level. Additionally, the intricate propagation environments in multi-cell settings may lead to overlapping near fields for different BSs, introducing complexities in the corresponding analytical framework. Lastly, the consideration of user mobility will likely require tools from SG, which may contribute to new insights into spatial statistics. The incorporation of these nuanced issues into the performance analysis of NFC represents an ongoing and substantial research endeavor.

V. SIGNAL PROCESSING FOR NFC

As detailed in the preceding section, when contrasting NFC with FFC, fundamental disparities emerge in their EM characteristics and channel models. As a result, the signal processing techniques employed in NFC diverge significantly from those applied in FFC. In this section, we will provide an overview of pertinent research endeavors from three distinct vantage points: channel estimation, beamforming design, and low-complexity beam training.

A. Near-Field Channel Estimation

Numerous wireless applications crucially rely on channel state information (CSI) to mitigate the impact of factors such as fading, noise, and interference during data transmission. Given the stochastic nature of wireless channels, channel estimation is typically carried out prior to transmission to acquire the necessary CSI. Traditional channel estimation techniques, including the least-squares (LS) and the LMMSE methods, have been employed for unstructured channels [282]. However,

as the number of antennas has substantially increased, the LS and LMMSE methods often incur significant computational overhead. Moreover, these methods fail to identify the positions of scatterers within the channel, limiting the potential for advanced transceiver design. These challenges motivate the consideration of channel estimation for structured channels. Structured channels are usually encountered in high-frequency bands like mmWave and THz, where sparse scattering leads to a reduced number of channel parameters. Leveraging the structure of far-field channels, many low-overhead channel estimation methods have been proposed for FFC, making use of approaches such as compressive sensing [283]–[285] and parametric estimation [286]–[288]. However, for NFC, the spherical-wave propagation results in channel structures distinct from those encountered in FFC. Consequently, existing structured far-field channel estimation methods are no longer suitable for NFC.

1) *Compressive Sensing*: Compressive sensing leverages the sparsity of the channel in a particular domain to enhance channel estimation. In FFC, angular-domain sparsity is typically exploited, based on which the classical orthogonal matching pursuit (OMP) algorithm can be used to recover the angular-domain far-field channel [285]. In NFC, the assumption of angular-domain sparsity no longer applies due to spherical-wave propagation, as illustrated in Fig. 18. Specifically, the far-field channel exhibits discernible peaks in the angular domain, whereas the near-field channel is spread across a wider angular region due to the variation in angle-of-arrival across the array. To address this challenge, the authors of [109] refined the far-field OMP method by directly replacing the far-field array response vector with one for the near-field. To reduce the complexity, a sequential method was further proposed in which the conventional far-field OMP is adopted for angle estimation, followed by a refined OMP for range estimation. The authors of [126] further refined the far-field OMP method by taking the non-stationary property of the near-field channel into account, developing subarray-wise and scatterer-wise near-field channel estimation methods. A more detailed theoretical analysis of near-field compressive sensing in [111] unveiled an alternative form of sparsity in the polar domain, which encompasses joint range and angle information. Based on polar-domain sparsity, [111] introduced a novel polar-domain OMP to recover the near-field channel. In [289], the authors explored near-field channel estimation for a planar antenna array based on 3D compressive sensing, considering the elevation-azimuth angles and range. To tackle this complex problem, they proposed a triple parametric decomposition approach that effectively partitions the 3D compressive sensing task into multiple 1D subproblems. Another range-parameterized angular-domain representation of the near-field channel was conceived in [290] that addresses the storage burden and high column coherence of the polar-domain representation. By exploiting this new representation, a dictionary-learning OMP channel estimation method was developed. As a further advance, [291] proposed a sparse Bayesian learning (SBL) method for near-field channel estimation based on compressive sensing that requires a lower pilot overhead and computational burden

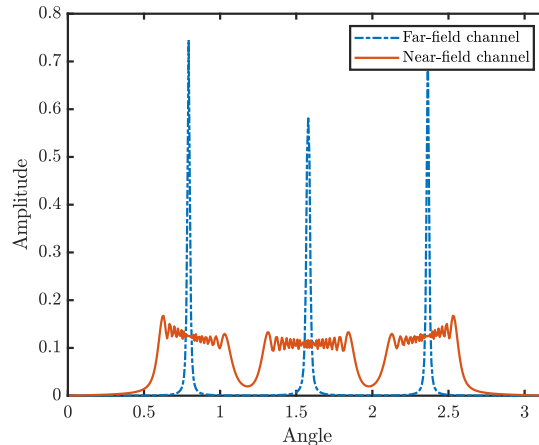


Fig. 18: Angular-domain representations of far-field and near-field channels, where the BS is equipped with $N = 400$ antenna ULA and operates at 28 GHz. There are three scatterers for the far-field (100 m) and near-field (5 m) channels.

than conventional compressive sensing. Inspired by classical OMP, [292] proposed a bilinear pattern detection approach for the near-field wideband channel estimation, where the spatial-wideband effect was effectively solved. Another near-field wideband OMP approach was devised in [293], which is based on a beam-squint-aware dictionary.

Considering the practical scenario where both users and scatterers within a communication channel can reside in either the near- or far-field regions, some research efforts have been dedicated to addressing the challenges of hybrid-field channel estimation. In particular, a hybrid-field OMP channel estimation method was proposed in [110] that demonstrated reduced estimation errors compared to both far-field and near-field OMP methods. In an effort to mitigate estimation complexity, the authors of [210] introduced an approach that combines support detection and OMP, and enables the successive estimation of far-field and near-field paths. However, these methods typically require prior knowledge of the proportion of far-field and near-field paths. To address this challenge, an enhanced hybrid-field OMP method was introduced in [294] that starts with a coarse estimation based on far-field OMP and subsequently refines the estimate by adjusting the proportion of far-field and near-field paths. Hybrid-field channel estimation for the MIMO scenario was studied in [295], and a reduced dictionary method was developed to first determine which model is appropriate for each user.

2) *Parametric Estimation*: Parametric estimation is based on the assumption that the communication channel can be characterized by a relatively small set of parameters, such as angles of departure and arrival [303]. By estimating these parameters, the communication channels can be reconstructed. The pros and cons of parametric estimation method compared to compressive sensing are summarized below. For compressive sensing, channel estimation involves building a channel codebook in a selected domain and applying a sparse recovery algorithm such as OMP. The codebook contains the samples of channels in this selected domain, which are also referred to as on-grid points. The estimation accuracy is limited by the

TABLE XIV: Summary to Approaches for Near-Field Channel Estimation

Approaches	Advantages	Disadvantages	Ref.
Compressive sensing	Low complexity	Complex codebook design; limited resolution	[109]–[111], [126], [210], [289]–[295]
Parametric estimation	High accuracy	High complexity; require the number of sources to be known	[111], [112], [296]–[298]
Machine learning	Require no structural information	Weak theoretical guarantees; Require large dataset	[293], [299]–[302]

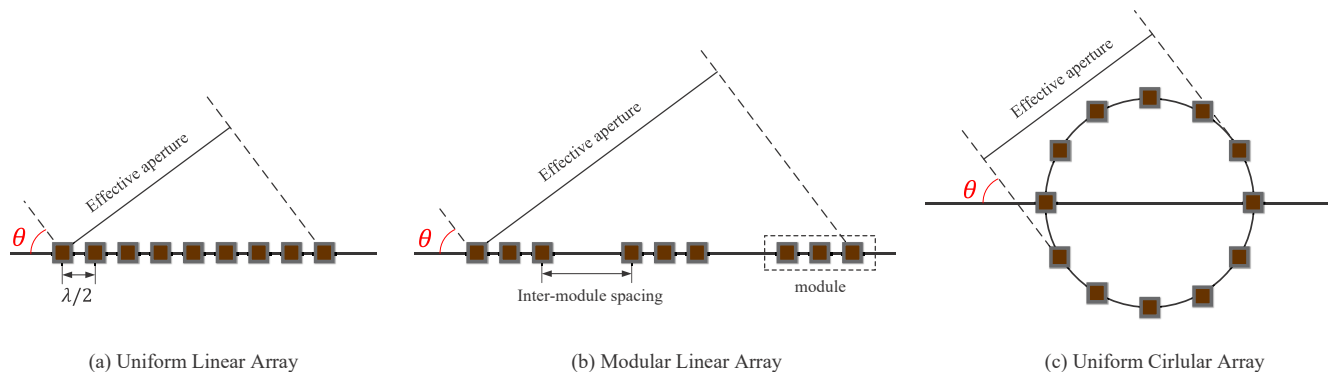


Fig. 19: Illustration of array geometries for NFC.

resolution of these on-grid points. In contrast to compressive sensing, parametric estimation methods typically estimate the channel parameters using a search over the continuous parameter space. Thus, parametric estimation approaches can be regarded as “off-grid” methods exhibiting higher accuracy, but typically at the cost of higher complexity. Compared to FFC, the key challenge of parametric estimation in NFC is related to the estimation of the range information. The authors of [111] proposed an iterative joint range and angle estimation algorithm for all paths in a near-field MISO channel based on the maximum likelihood principle, which demonstrated a better performance than compressive sensing. In [296], an approach based on cumulant matrices was introduced for the sequential estimation of angle and range for NLoS scatterers in the near-field MIMO channel. For LoS-dominated near-field MIMO channels, [297] divided a large array into several tiles such that the far-field assumption holds at each tile, and then applied parametric far-field channel estimation methods to each tile. Considering both LoS and NLoS paths, [112] devised a two-stage channel estimation method. In the first stage, the angle and range information for the LoS path was estimated and iteratively refined. Subsequently, in the second stage, the NLoS path parameters were estimated using near-field compressive sensing. Finally, a sub-array-based channel estimation algorithm was developed in [298] for near-field MIMO communications. In particular, the antenna arrays at both the transmitter and receiver were partitioned into multiple sub-arrays, with the channel between each sub-array approximated as a far-field channel. Subsequently, the estimates from each pair of subarrays are combined to determine the overall channel.

3) *Machine Learning*: Machine learning provides a promising set of tools to facilitate low-complexity near-field channel estimation, and has attracted significant attention. For example, the authors of [299] proposed a multiple residual dense network (MRDN) to estimate the near-field channels by

exploiting polar-domain sparsity. Then, they adopted atrous spatial pyramid pooling to enhance the performance of the MRDN by capturing the multi-scale information of the input. In [300], a model-based deep learning approach was introduced in which the near-field channel estimation was first formulated as a compressive sensing problem and then solved by the learning iterative shrinkage and threshold algorithm. The authors of [301] adopted a hybrid spherical- and plane-wave model, where the antenna array is divided into multiple subarrays whose channel parameters are first estimated using a deep convolutional neural network and used to recover the overall near-field channel. Federated learning was employed in [293] to facilitate OMP-based near-field channel estimation in wideband systems. To address the hybrid-field channel estimation problem, [302] conceived a general deep-learning-based framework exploiting iterative channel estimators. A fixed point network was proposed for implementing each iteration, consisting of a closed-form linear estimator and a deep-learning-based non-linear estimator.

B. Near-Field Beamforming

Transmit beamforming employs an antenna array to direct a signal towards a specific receiver, rather than broadcasting it in all directions. It can be achieved by adjusting the weights and phases of the antenna elements to create constructive and destructive interference patterns in the desired directions or locations. Beamforming can improve the quality, capacity, and reliability of wireless communication by enhancing the desired signal and reducing interference. As discussed in previous sections, in contrast to FFC, an antenna array in NFC can resolve not only the direction of the signal but also the distance over which it has propagated. As a result, near-field beamforming can be designed in both the angle and range domains and has greater flexibility than far-field beamforming. In the following, we first review array geometries and control

techniques for near-field beamforming, followed by a review of existing near-field beamforming designs.

1) *Array Geometries and Control Techniques*: Array geometries play a pivotal role in shaping the spatial distribution of the beamformer radiation pattern in terms of beamwidth and grating lobes. Furthermore, different control techniques in the analog and digital domains can be employed to realize beamforming, contingent upon the specific demands of the system and the physical limitations.

- *Array Geometries*: Recall that compared to the far-field case, near-field beamforming introduces an additional dimension related to distance. This additional dimension plays a crucial role in enhancing communication performance, as we will detail in upcoming sections. As a result, a key goal in designing the array geometry in NFC is to expand the near-field region w.r.t. the antenna array, which enables a larger number of communication users to reap the advantages of near-field beamforming. According to the expression for Rayleigh distance, $2A^2/\lambda$, the array aperture is the key factor in determining the size of the near-field region. To avoid grating lobes, ULAs and uniform planar arrays (UPAs) are typically designed to satisfy the Nyquist sampling criterion in the spatial domain [304], [305], i.e., the antenna spacing should be no larger than half of the wavelength, $\lambda/2$, as depicted in Fig. 19(a). However, for NFC, such a constraint may limit the aperture of the antenna array, thus confining the near-field region. As a remedy, a modular array [260], which is also referred to as a widely-spaced multi-subarray (WSMS) [306], [307], has been proposed. For the example illustrated in Fig. 19(b), the linear array is divided into multiple modules, and is referred to as modular linear array (MLA). Within each module, the antenna spacing satisfies the half-wavelength criteria, while the inter-module spacing is typically much larger than the signal wavelength. Therefore, compared to a conventional collocated array, a modular array exhibits a larger near-field region, but may incur grating lobes due to the wide spacing between subarrays. The concept of the modular array was first introduced in [306] and [307] for mmWave and THz communications, respectively, where the authors posited plane wave propagation across each individual module and spherical wave propagation across different modules. Furthermore, the authors of [260] studied the complete near-field modeling and performance analysis of the modular array design and showed that it exhibits a more significant near-field effect that is more suitable for NFC. Additionally, to address the issue of grating lobes for the modular array, the authors of [308] conceived a user grouping and scheduling method, where different groups of users are not scheduled in the same resource blocks if they are located in each other's grating lobe. Another geometry used to enlarge the near-field region is the uniform circular array (UCA) [309], as shown in Fig. 19(c). For linear and planar arrays, the near-field region is non-uniform in all directions. For instance, the ULA exhibits an ellipsoidal near-field region that is largest for $\theta = \pi/2$, and gradually diminishes to zero as $\theta \rightarrow 0$ or π [123]. This phenomenon is due to the fact that the linear antenna arrangement leads to different *effective apertures* in different directions. However, for a UCA, its rotationally symmetric

geometry results in the same effective aperture in all directions [309]. Therefore, a user has the potential to benefit from the near-field beamforming even if $\theta \rightarrow 0$ or π , and the near-field region is enlarged.

- *Control Techniques*: In NFC systems, achieving a large array aperture necessitates the use of a substantial number of antenna elements. However, this presents a challenge for fully digital control due to hardware limitations and power constraints [310]. A prevalent solution to this issue is to reduce the number of RF chains through hybrid digital and analog control, as illustrated in Fig. 20. To clarify, the digital control takes place at a baseband unit (BBU), which then transmits signals to the antenna elements through a limited number of RF chains and an analog control network. Fig. 20(a) depicts the conventional hybrid control architecture, where a fixed number of active RF chains is employed, and phase shifters (PSs) are used for analog control [310], [311]. However, this conventional hybrid control architecture may not be suitable for NFC for two primary reasons.

First, as discussed in previous sections, near-field MIMO channels exhibit distance-dependent DoFs. Specifically, the DoFs gradually decrease as the distance between the transmitter and receiver increases, resulting in a reduced number of supported data streams. To address this distance-dependent behaviour in NFC, the authors of [312] proposed a dynamic-RF-based hybrid control architecture shown in Fig. 20(b). In this architecture, each RF chain can be configured as active or inactive via a switch based on the distance between the transmitter and receiver. Theoretically, to achieve optimal performance, in this architecture the number of active RF chains should be at least twice the number of data streams, streams, i.e., DoFs [313], [314]. As a more energy-efficient solution, a novel double-PS-based hybrid control architecture was developed in [315], in which each RF chain and antenna element are connected by two PSs. Despite the doubled number of PSs, this architecture only requires the same number of active RF chains as the number of data streams, improving energy efficiency since PSs consume significantly less energy than RF chains.

Second, the near-field effect is stronger in high-frequency bands, where greater bandwidth resources are available. In wideband systems, an ELAA may encounter the spatial-wideband effect due to non-negligible propagation delays across the antenna array and the frequency-dependent wavenumber [316]. However, it is important to note that PSs provide the same phase shift for signals at different frequencies. Consequently, relying solely on PSs within the analog control network gives rise to an inherent problem in NFC, known as near-field beam splitting. This issue manifests itself as a misalignment between the beams at most frequencies and the user's location [114]. To address this challenge and enable effective wideband control, alternative solutions have been explored. One such solution is the utilization of true-time delays (TTDs), which have long been considered as a possible alternative for PSs for wideband beamforming [317]. In contrast to PSs, TTDs are capable of compensating for the propagation delay difference across the antenna array and facilitating a frequency-dependent phase shift. Substi-

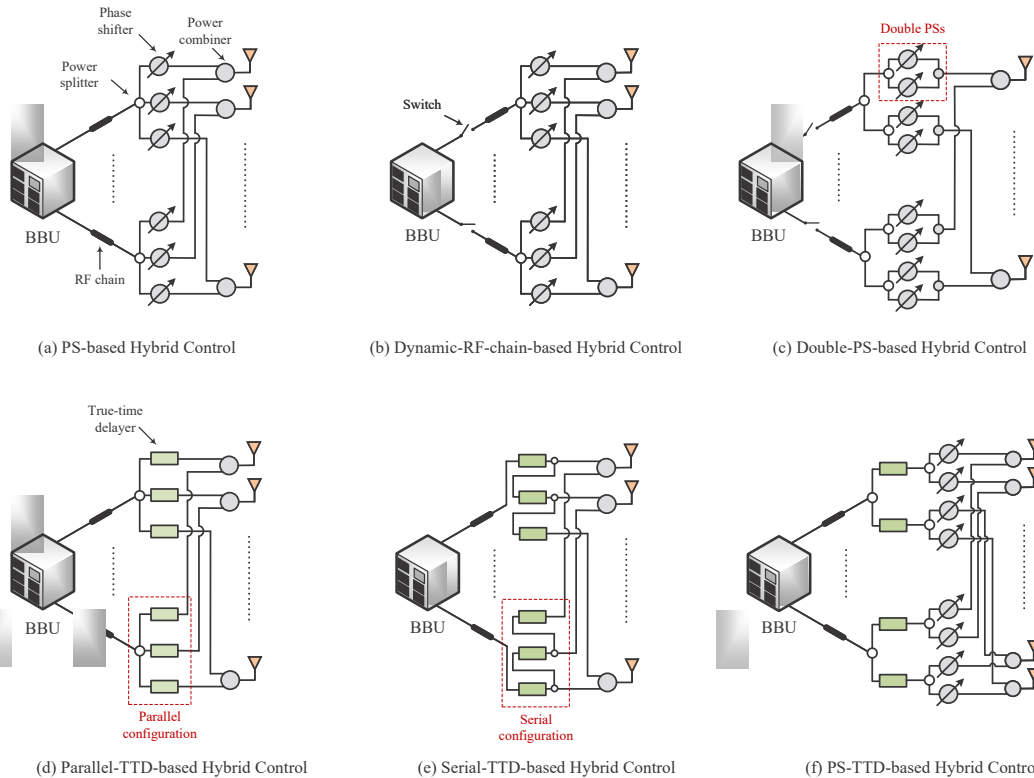


Fig. 20: Illustration of hybrid digital and analog control techniques for NFC.

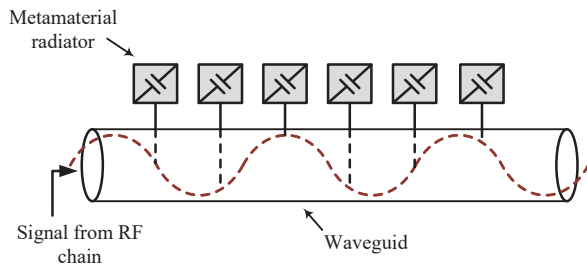


Fig. 21: Waveguide-based control for DMA.

tuting all PSs with TTDs results in the parallel-TTD-based hybrid control architectures in Fig. 20(d) [114], [317]–[319]. Nonetheless, TTDs are usually subject to a maximum delay constraint, which can pose a challenge in scenarios where extensive delay compensation is needed, particularly with extremely large antenna arrays. To address this limitation, a novel serial configuration, as exemplified in Fig. 20(e), has recently emerged as a solution for short-range TTDs [320], [321]. Compared to the conventional parallel configuration, the serial configuration can effectively bypass the maximum delay limit by accumulating delays across multiple TTDs. It is important to note that implementing TTDs presents significant challenges compared to PSs primarily due to the requirement for variable TTD blocks within a constrained chip area [317]. Additionally, TTDs tend to consume more power compared to PSs, making their widespread use in practical applications less desirable. The excessive use of TTDs can be avoided by adopting a PS-TTD-based hybrid control architecture [106], [322]–[324],

as shown in Fig. 20(f). In this architecture, although only a limited number of TTDs are inserted between the RF chains and PSs, a nearly optimal communication performance can be achieved.

Additionally, with the development of EM metamaterials [325], some new forms of antennas have emerged, which requires distinct control techniques compared to conventional antennas. DMA arrays [35] are a new type of metamaterial-based array that exploits a large number of sub-wavelength-sized metamaterial radiators that are densely arranged to realize an approximately continuous radiating surface. Compared to conventional antenna arrays, DMA arrays can achieve superior beamforming gain and spatial resolution. DMA arrays are controlled with the aid of a signal propagating along a waveguide [326], as illustrated in Fig. 21. The metamaterial radiators are excited by the waveguide signal and emit the signal after amplitude, phase, and polarization adjustment. However, arbitrary control of the metamaterial radiators is difficult to realize. According to the analysis in [326], there are three possible control mechanisms: binary control, amplitude-only control, and Lorentzian-constrained phase control. Binary control is the easiest control mechanism and simply toggles each radiator between ON and OFF states. Amplitude-only control can be realized by adjusting the damping factor of the near-resonance metamaterial radiator or the oscillator strength. Phase control is more complex than amplitude control because the amplitude will necessarily vary with the phase according to the inherent Lorentzian resonance.

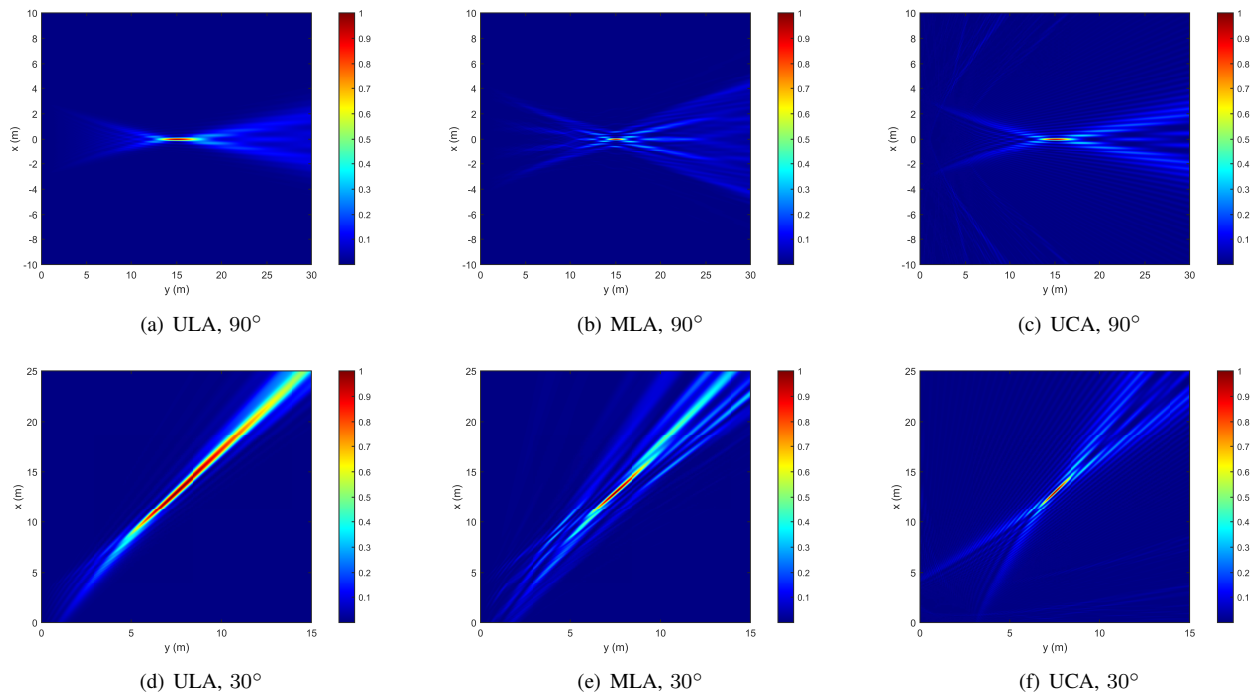


Fig. 22: The beamfocusing performance of different array geometries at 15 m and directions 90° or 30° with 3 GHz carrier frequency and 128 antennas. The ULA antenna spacing is set to $\lambda/2$. The MLA antennas are divided into 4 modules separated by 10λ , and $\lambda/2$ spacing within each module. The UCA has the same aperture as the ULA.

TABLE XV: Contributions on Near-Field Beamforming Design

Category	Ref.	Design Method	System Bandwidth	Control Technique	Characteristics
Analytical	[327]	Beamfocusing	Narrowband	—	Primer on beamfocusing by MRT
	[328]	Beamfocusing	Narrowband	—	Finite-resolution beamfocusing for ULA, UCA, and UPA
	[117]	Beamfocusing	Narrowband	—	NOMA with imperfect beamfocusing
	[329]	Beamfocusing	Narrowband	—	Controlable beamfocusing via carrier frequency offset
	[106]	Beamfocusing	Wideband	PS-TTD-based	Piecewise-far-field model for designing TTD coefficients
	[324]	Beamfocusing	Wideband	PS-TTD-based	Piecewise-near-field model for designing TTD coefficients
	[330]	Beamfocusing	Wideband	PS-based	Approximately frequency-flat beamforming gain
	[331]	Bessel beam	Narrowband	—	Bessel beam for near-field beamsteering
	[332]	Bessel beam	Wideband	—	Bessel beam for mitigating beam split
Optimization based	[333]	WMMSE, BCD	Narrowband	DMA-based	Beamforming under Lorentzian phase-shift constraint
	[334]	SCA, ADMM	Narrowband	DMA-based	Beamforming under various DAM constraints
	[312]	Water-filling, greedy search	Narrowband	Dynamic-RF-based	Distance-aware beamforming for near-field MIMO
	[335]	WMMSE, BCD	Narrowband	PS-based	Distance-domain security by ULA
	[336]	Rayleigh quotient, gradient descent	Narrowband	PS-based	Distance-domain security by modular array
	[337]	WMMSE, MM	Wideband	DMA-based	Wideband beamforming design for DMA
	[338]	Signal model-based learning	Wideband	PS-TTD-based	CSI-free single-user wideband beamforming with parallel TTDs
	[324]	PDD	Wideband	PS-TTD-based	Multi-user wideband beamforming with parallel TTDs
	[321]	PDD	Wideband	PS-TTD-based	Multi-user wideband beamforming with serial TTDs

[†] WMMSE: weighted minimum mean square error; BCD: block coordinate descent; SCA: successive convex approximation; ADMM: alternating direction method of multipliers; MM: majorization-minimization; PDD: Penalty Dual Decomposition.

2) *Beamforming Design*: Various near-field beamforming strategies have been explored, employing various antenna geometries and control techniques. In general, these existing designs can be categorized into two main groups: analytical beamforming design and optimization-based beamforming design. Specifically, analytical beamforming design primarily seeks closed-form solutions by capitalizing on the distinctive signal characteristics within the near-field region, while optimization-based beamforming design focuses on attaining optimal or near-optimal solutions under different hardware constraints in various application scenarios. In the following, we review research works on these two approaches.

- *Analytical Beamforming Design*: In [327], it was demon-

strated that near-field beamforming can control not only the beamwidth in the angular domain, as in far-field scenarios, but also the beamwidth in range. This unique characteristic opens up a new paradigm, known as *beamfocusing*, leveraging the ability to precisely focus the beam on a specific location. In Fig. 22, the beamfocusing performance of different array geometries is depicted. Expanding on this concept, the authors of [328] conducted a detailed analysis of the finite resolution of beamfocusing. This analysis is based on the 3 dB depth of focus, providing insights into the achievable beamfocusing region for different antenna geometries. Beamfocusing resolution was also studied in [117], with particular attention to users near the Rayleigh distance and for a case study

involving NOMA, where the near-field beam was reused to serve multiple users. As a further advance, [329] introduced an analytical beamfocusing model that offers valuable insights into the factors that influence focusing performance, including carrier frequency, array dimension, and user range. Based on this model, a pair of approaches was devised to achieve flexible beamfocusing through the manipulation of the carrier frequency offset. Wideband beamfocusing was first studied in [106], where the PS-TTD-based hybrid control architecture was harnessed to tackle the spatial-wideband effect. In particular, a piecewise-far-field model was proposed for designing the coefficients of the PSs and TTDs, ensuring that beams at all frequencies could be precisely focused at the desired location. Based on a similar idea, a piecewise-near-field model was conceived in [324], offering a more precise and accurate approach to wideband beamfocusing design, particularly in scenarios where the number of TTDs is limited. In a separate investigation, [330] explored wideband beamforming within the context of a PS-based hybrid control architecture applied to a circular planar array. This work introduced an innovative wideband beamforming approach named “InFocus” that capitalizes on a spatial frequency-modulated continuous waveform and achieves an almost uniformly flat beamforming gain across the entire frequency band of interest.

Apart from beamfocusing, the spherical-wave propagation in the near-field region also presents intriguing possibilities for more sophisticated beamforming design. For instance, a near-field beamforming approach based on Bessel beams was proposed in [331]. In contrast to beamfocusing, the Bessel beams facilitate “beamsteering” in the near-field region. However, a true Bessel beam requires infinite power. To address this issue, the authors devised a more practical quasi-Bessel beam approach that achieves beamsteering for a finite band of ranges in the near-field region. Furthermore, the authors of [332] investigated the performance of Bessel beams in wideband systems, demonstrating that such beams exhibit greater resilience to the spatial-wideband effect when compared to beamfocusing.

- *Optimization-Based Beamforming Design:* In [333], the authors studied optimized near-field beamfocusing employing different control architectures. In addition to the conventional full-digital and PS-based hybrid control architectures, the authors explored beamfocusing with a DMA array that can realize Lorentzian-constrained phase control. As a further advance, [334] compared the performance of amplitude-controlled and phase-controlled DMA arrays for near-field beamfocusing, and proposed optimized solutions for both single- and multi-user scenarios. Shifting the focus to near-field MIMO systems with dynamic DoFs, [312] presented a distance-aware beamforming optimization framework in which the number of active RF chains is adaptively adjusted based on the estimated DoFs of the near-field MIMO channel to maximize spectral efficiency. The study of secure near-field beamforming design was explored in [335] and [336], with a specific emphasis on ULAs and modular linear arrays, respectively. To optimize secrecy rates achieved by PS-based hybrid control architectures, the authors of [335] introduced a two-stage optimization algorithm, while the authors of [336]

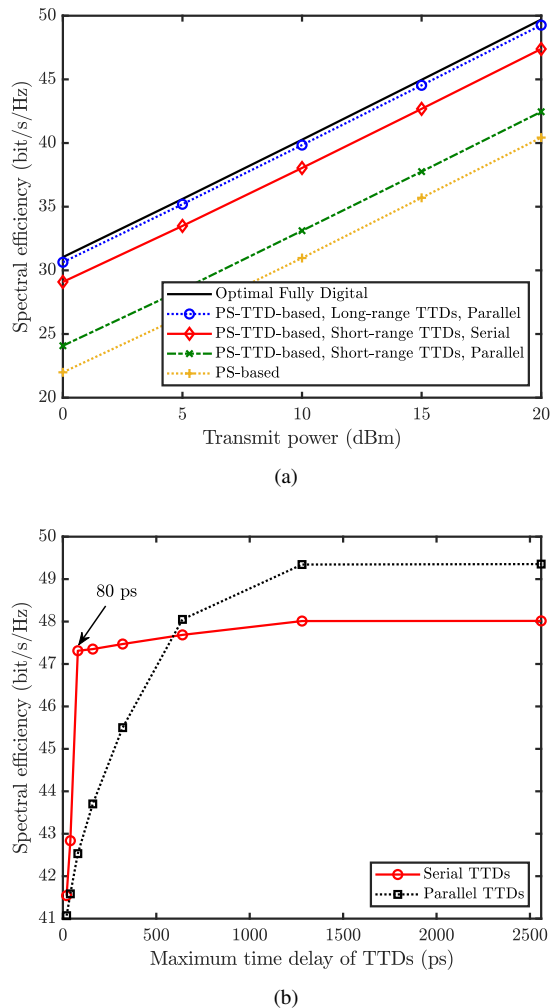


Fig. 23: The performance of different control architectures in near-field wideband system. (a) Spectral efficiency versus transmit power, where the maximum time delay of long-range TTDs is 1500 picosecond (ps) and that of short-range TTDs is 80 (ps); (b) Spectral efficiency versus the maximum time delay of TTDs, where the transmit power is 20 dBm.

proposed a non-constrained optimum-approaching algorithm. The collective findings of these studies underscore the potential of near-field beamfocusing to enhance physical layer security in the range domain.

There are also some works exploring near-field wideband beamforming optimization subject to the spatial-wideband effect [321], [324], [337], [338]. Specifically, near-field wideband beamforming optimization for DMA arrays was studied in [337], where both amplitude-only control and the Lorentzian-constrained phase shift control were considered. The authors of [338] concentrated on a single-user wideband system with PS-TTD-based hybrid control, and introduced a deep-learning-based method to optimize near-field wideband beamforming without CSI. For the case of a multiuser system, [324] proposed a fully digital approximation and a heuristic two-stage approach for the design of the PSs and TTDs. Finally, the authors of [321] showed that a serial configuration of the TTDs can substantially reduce the maximum TTD delay

requirements compared with the parallel case.

C. Low-Complexity Near-Field Beam Training

In general, CSI is necessary for beamforming design. While there have been various methods proposed for channel estimation in NFC, the resultant pilot overhead can still be a limiting factor, especially in applications with stringent latency constraints. Beam training provides a promising solution to address this issue [310], [339]. Specifically, beam training involves an iterative exchange of information between the transmitter and receiver. The primary objective is to select the optimal beam with the highest received power from a pre-designed codebook. Beam training can achieve rapid beamforming design without the need for CSI, and also facilitates the rapid acquisition of partial CSI of the strongest signal path connecting the transmitter and the receiver. This partial CSI can then be harnessed to conduct more advanced beamforming designs. Although beam training has been extensively investigated in FFC, this prior work cannot be directly applied to NFC because of the additional range dimension in the near-field channels. Consequently, various tailored beam training protocols and codebooks have been designed for NFC.

1) *Polar-Domain Beam Training*: In FFC, beam training involves searching for the best beam in an angular-domain codebook [340]. However, a codebook based only on angle is not suitable for near-field beam training due to the additional dimension introduced by the near-field channels. To address this challenge, a polar-domain codebook was crafted in [111] comprising non-overlapping beams that cover the entire near-field region. A straightforward approach to identifying the optimal beams is to perform an exhaustive search within this polar-domain codebook, but this method may incur an impractical training overhead. A solution to this issue was proposed in [341], which introduced a hierarchical polar-domain codebook based on analyzing the near-field features. This codebook features multiple layers of codewords, or beams, with the upper layers serving to reduce the search overhead, and the lower layers to ensure high beamforming gains. As a further advance, optimization-based designs of hierarchical polar-domain codebooks were conceived in [342], where Gerchberg-Saxton-based and alternating-optimization-based algorithms were proposed for fully digital and PS-based hybrid control architectures, respectively. In [343], a polar-domain codebook was designed for holographic MIMO systems, which was in turn tailored to develop a multi-user beam training scheme. Additionally, the authors of [344] compared the performance of ULAs and UCAs in terms of polar-domain beam training. Their findings revealed a significant advantage for UCAs, as they can substantially reduce the codebook size, consequently mitigating beam-training complexity. Reducing near-field beam training complexity is also the goal of the deep-learning-based training method developed in [345], which leverages a neural network to determine the optimal codeword within a polar-domain codebook based on the power received from a set of wide far-field beams. The authors of [346] projected the polar-domain beams into the slope-intercept domain and introduced a novel spatial-chirp-based hierarchical beam training algorithm that can reduce

the training overhead by over 99% compared to conventional methods. In [114], the spatial-wideband effect was exploited to reduce the training complexity. In particular, a near-field beam training method referred to as the “near-field rainbow” was proposed based on the controllable beam split effect, which enables multiple beams focused on different locations at the same time but at different frequencies.

2) *Hybrid-Domain Beam Training*: Polar-domain beam training typically involves a two-dimensional search, which, in turn, results in a substantial number of search steps. To mitigate this issue, several works have explored the incorporation of other domains to reduce the required complexity. In [115], a two-stage near-field beam training approach was introduced. In the first stage, the coarse angle of the optimal beam is approximated in the angular domain, relying on conventional far-field beam training. Subsequently, in the second phase, polar-domain near-field beam training is conducted within a narrow range centered around the coarse angle. Building on this concept, [347] integrated hierarchical beam training into the aforementioned two-stage near-field beam training process. Hierarchical far-field and near-field codebooks were designed for the respective phases, resulting in a significant reduction in the number of search steps. 3D near-field beam training for a UPA was studied in [348], also employing a two-stage beam training method. Initially, 2D angular-domain far-field beam training is conducted, followed by 1D range-domain near-field beam training using an iterative Lloyd-Max algorithm. In contrast, the authors of [349] proposed a distinctive approach that prioritizes range information in the first stage. They designed a codebook containing omnidirectional beams in this stage, facilitating range estimation based on received power. Subsequently, in the second stage, the optimal beam angle is determined via an angular-domain search. An alternative two-stage near-field beam training algorithm was conceived that takes into consideration the concept of VR of the antenna array [350]. Based on the fact that different sub-arrays often have different VRs in the near-field, the authors of [350] proposed to first identify the VR of the optimal beam, followed by a search for the optimal beam within the identified VR. Then, the codebook for each stage was designed by exploiting contrastive learning.

D. Discussions and Outlook

In this section, we have undertaken a comprehensive review of pivotal signal processing techniques relevant to NFC, encompassing channel estimation, beamforming design, and low-complexity beam training. It is evident that the near-field effect holds the potential to enable distance-aware communication with a large number of DoFs. Moreover, substantial research works in NFC underscore the essential consideration of the near-field effect, particularly when exploiting ELAAs and high-frequency bands, to avert significant performance degradation. The effective realization of NFC demands intricate channel estimation, antenna design, and beamforming algorithms. Consequently, the development of low-complexity algorithms assumes a pivotal role in this context, where machine learning emerges as a powerful tool.

To fulfill the required performance targets of future wireless networks, several open research problems from the signal processing perspective remain.

- **Channel Estimation and Beamforming of CAP Arrays:** Compared to SPD cases, CAP arrays demonstrate significantly enhanced array gain and spatial resolution, owing to their continuous radiating surface. Nonetheless, such arrays present difficulties in channel estimation and beamforming design. Channel estimation methods developed for SPD arrays cannot be directly applied to CAP arrays due to the Green's function-based channel model. Additionally, beamforming with CAP arrays differs from SPD arrays as it relies on controlling the distribution of source currents rather than discrete element coefficients. Therefore, the channel estimation and beamforming design of CAP arrays for NFC remains an open research challenge.
- **Collimation Beamforming Design for NFC:** Due to the non-linear phase of near-field channels, it is easy to realize beamfocusing. However, beamfocusing is not always preferred due to its limited coverage. In some scenarios, collimation beamforming becomes necessary to cover multiple users with a single beam, particularly when the number of RF chains at the BS is constrained. Bessel beams are a good candidate to realize collimation beamforming [331], [332], although a true Bessel beam requires infinite power. As a result, only quasi-Bessel beams can be realized in practice, which can achieve collimation beamforming but only for a finite set of ranges. Therefore, more research efforts are required to address this challenge.

VI. INCORPORATING 6G WIRELESS TECHNOLOGIES IN THE NEAR FIELD

Having revealed the fundamental communication performance improvements by exploiting near-field characteristics, we discuss below the incorporation of near-field models in other promising 6G wireless technologies. Specifically, we will highlight research opportunities and challenges associated with the design of ISAC, RIS, WPT/SWIPT, NOMA, and PLS systems in near-field scenarios.

A. Near-Field ISAC

Apart from high-capacity communications, next-generation wireless networks are also envisioned to enable high-precision sensing, which motivates recent interest in ISAC [351]. In contrast to traditional localization and channel estimation techniques in wireless communication systems, wireless sensing relies on passively reflected echoes from objects illuminated by wireless signals instead of pilot signals transmitted by objects themselves. Many communication waveforms have been proven to be suitable for wireless sensing, such as OFDM [352], orthogonal time frequency space (OTFS) [353], and delay alignment modulation (DAM) [354] waveforms, which enables the seamless integration of sensing functions into existing wireless networks.

From a parameter estimation perspective, target sensing involves the estimation of angle, range, and velocity. In conventional far-field sensing, increasing the size of the antenna array only benefits angle estimation, while the resolution of range and velocity mainly relies on the signal bandwidth and the sensing duration [355]. Nevertheless, the spherical-wave propagation in the near field provides an alternative way to use a large antenna array for range and velocity estimation. A near-field channel can still effectively provide range information even with a very limited bandwidth, which opens new opportunities for distance estimation in narrowband systems [356]–[358]. In particular, [356] derived closed-form Cramér-Rao bounds (CRBs) for range estimation in both mono-static and bi-static sensing configurations using ULAs. Range estimation performance was further analyzed in MLAs [357], demonstrating the benefits of dividing the array into multiple widely-spaced subarrays. Joint waveform designs for near-field ISAC were studied in [358], where the CRBs for near-field sensing were minimized while guaranteeing minimum communication requirements.

Estimation of the velocity of an object generally depends on the estimation of the Doppler frequency of the radar echos. In conventional far-field systems, the Doppler frequency is only affected by the object's radial velocity (the velocity along the LoS direction) due to the plane-wave propagation [354], [359]–[361]. The lack of transverse velocity information (the velocity perpendicular to the LoS direction) makes it challenging to obtain the full motion status of the object. Interferometric radar is a method to facilitate transverse velocity estimation in the far field using the measurement of phase changes [362]–[364]. However, this technique conventionally relies on just two antennas, making it difficult to extend to ELAA cases for achieving high spatial resolution. Its compatibility with communication systems is also unclear. When it comes to near-field sensing systems, the Doppler frequencies of the echos involve both radial and transverse velocities because of the spherical-wave propagation [365]–[367]. The potential for joint estimation of radial and transverse velocities using Doppler frequencies in the near-field was first studied in [366]. This work also designed a predictive beamforming framework based on near-field velocity sensing. As a further advance, [367] investigated the estimation of both horizontal and pitch transverse velocities in a 3D ISAC system.

B. RIS-aided NFC

An RIS consists of a large number of low-cost reconfigurable elements, and their ability to intelligently modify the propagation environment makes them a promising technology for 6G. Deploying RISs in wireless networks can beneficially adjust the wireless channels between transmitters and receivers, thus improving the communication quality and coverage. For RIS-aided wireless communications, the impact of near-field propagation is significant since RISs usually have a large aperture to achieve sufficient beamforming gain, and one of the most common applications of RISs is to overcome the signal blockages in mmWave/THz communications. The large RIS aperture and high operating frequencies further

enlarge the near-field region of the RIS-aided communication link. It is also worth noting that the unique near-field channel propagation characteristics bring new opportunities for employing RISs. Recalling the fact that RISs are generally deployed to create a LoS-dominated channel with the transmitters/receivers, the corresponding spatial multiplexing gain would be limited in the far-field case due to the low-rank LoS MIMO channel. However, with a higher-rank near-field LoS MIMO channel, this drawback can be overcome and more efficient RIS-aided near-field multi-user/MIMO communications can be facilitated. Motivated by this, the investigation of RIS-aided NFC has attracted growing interest from the perspectives of performance analysis, beamforming design, and channel estimation [368].

1) *Performance Analysis of RIS-aided NFC*: The authors of [261] derived lower- and upper-bounds for the received SNR of an RIS-aided point-to-point communication system under the near-field NUSW channel model, considering element-wise variations in the RIS reflection amplitude and the impact of the projected aperture. This study revealed that, unlike the conventional far-field plane-wave model, SNR for a near-field NUSW channel cannot increase without bound as the number of RIS elements grows. In [369], the ergodic capacity of an RIS-aided communication system with outdated CSI in both the near-field and far-field regimes was studied, considering both centralized large-scale and distributed small-scale RIS deployment strategies. This study showed that due to the impact of near-field propagation, the achieved ergodic capacity is capped when the number of RIS elements grows large. In contrast to a conventional RIS comprising discrete patch elements, the authors of [77] proposed a near-field channel model based on Green's function method for spatially-continuous RISs and characterized the near-field end-to-end channel gain, DoFs, and power scaling law for an RIS-aided single-user communication system.

2) *Beamforming Design of RIS-aided NFC*: As the employment of large apertures leads to a massive number of RIS elements, a challenging problem in beamforming design for RIS-aided NFC is how to tackle the high computational complexity. To address this issue, [370] proposed an element-wise passive beamforming approach for maximizing the weighted sum rate (WSR) of a STAR-RIS-aided near-field multi-user MIMO communication system. Numerical results showed that compared to the conventional far-field channel model, the beamfocusing capabilities and the enhanced MIMO channel in the near field can be exploited to achieve better multi-user interference mitigation and further WSR improvement. The authors of [371] studied an RIS-aided single-user MIMO communication system in which the user is moving between the near-field and far-field regions. To reduce the computational complexity, a two-timescale joint user tracking and active/passive beamforming approach was proposed, where the RIS passive beamforming is less frequently optimized than the user localization and active beamforming. In [372], an RIS with an adjustable delay at each element was employed to mitigate the beam squint effect in near-/far-field THz communications. A transmissive RIS-aided uplink wireless communication system was investigated in [373], where the

user-RIS channel and the RIS-receiving horn antenna are characterized by far-field and near-field channel models, respectively. An alternating optimization-based algorithm was proposed for maximizing the sum rate over the cascaded far-field and near-field communication link. The authors of [374] presented a multi-beam design for RIS-aided multi-user systems in the near-field region, and addressed the resulting beam gain error minimization problem using block coordinate descent and majorization-minimization. A novel joint active and passive beamforming optimization algorithm for RIS-aided near-field MIMO systems was proposed in [375]. In particular, the passive beamforming at the RIS was designed through beam training considering far-field, near-field, and hybrid-field channel models for the BS-RIS and RIS-user channels. In [376], an RIS was exploited to realize flexible wavefront control in the near-field, achieving suitable near-field beamforming for receivers with different array geometries. In particular, for receivers with a ULA, the wavefront is converted into a cylindrical shape by the RIS, while for a single-antenna receiver, the wavefront is converted into a spherical shape.

3) *Channel Estimation for RIS-aided NFC*: Due to the passive nature of RIS, channel estimation becomes more challenging for RIS-aided systems, particularly for the near-field case. To address this issue, [377] proposed a two-phase compressive sensing-based CSI estimation method that determines the angular-domain parameters of the BS and the users in the first phase, and the cascaded angular- and polar-domain parameters of the RIS in the second phase. The authors of [378] introduced a hybrid spherical- and plane-wave channel model for near-field channel estimation in RIS-aided systems. Building upon this model, a compressive sensing-based channel estimation algorithm was developed, involving a separate-side estimation method and a dictionary-shrinkage estimation method. In [379], wideband CSI estimation for RIS-aided NFC was investigated. Using a wideband polar-domain representation, a 2D compressive sensing problem was formulated, which was solved using a multi-frequency parallelizable subspace recovery framework. The authors of [380] proposed a joint localization and channel estimation method for angle/distance estimations in RIS-aided THz-NFC. A parametric estimation method was proposed in [381] for polar-domain frequency-dependent channel estimation in RIS-aided wideband THz-NFC. The authors of [382] studied the hybrid-field channel estimation problem for RIS-aided communications using a U-shaped neural network based on the dedicated multilayer perceptron architecture to estimate the high-dimensional cascaded mixed-near-field/far-field CSI.

C. Near-Field WPT/SWIPT

The development of smart cities requires numerous battery-powered IoT/wearable/sensor devices to be deployed and connected to wireless networks. Against this background, WPT is a key enabling technology for conveniently charging these devices and extending their lifetime. For conventional far-field-WPT, the charging beam can be only steered towards specific angles, thus leading to a waste of energy and potential

interference with other wireless networks. On the other hand, near-field-WPT can exploit beamfocusing capability to focus the energy on specific locations and thus improve energy efficiency. In existing work, the design of near-field-WPT systems has been studied for different antenna structures. For example, the authors of [383] developed an implementation of dynamic near-field-WPT using a 2-bit 12×12 programmable metasurface, which employs near-field beamfocusing to improve the charging efficiency even for moving energy receivers. In [384], beamforming design of a DMA-based multi-user near-field-WPT system system was studied in which the weighted sum-harvested energy was maximized by jointly optimizing the DMA coefficients and the baseband digital precoding. The authors of [385] further studied indoor near-field-WPT, devising a novel beam diversity scheme to reduce the fading margin for initially accessing the energy harvesting devices. Transmit antenna deployment for an indoor near-field-WPT system was investigated in [386] with the aim of maximizing the minimum harvested energy among a collection of indoor users. Other researchers have focused on near-field-SWIPT design, including [387] which showed that no dedicated energy beam is required for hybrid beamforming-based near-field-SWIPT, and [388] which studied joint beam scheduling and power allocation in a mixed near-field and far-field SWIPT system.

D. Near-Field NOMA

Despite NFC providing enhanced spatial DoFs, the requirement of massive connectivity will require additional techniques for enhancing multiple access given the explosive number of users and devices in 6G networks. NOMA is one such technology for providing flexible resource allocation in multi-user FFC and NFC. The new characteristics of NFC provide new design flexibility for facilitating near-field NOMA. By exploiting near-field beamfocusing, the signal energy can be focused on users far from the BS. Unlike far-field-NOMA, where the effective channel gains of users in the same direction generally decay with distance, a higher effective channel gain can be achieved at users farther away from the array in near-field-NOMA. This implies that a ‘far-to-near’ channel-gain-based SIC order can be achieved in near-field-NOMA. Such an operation is beneficial for the case when the far user has a higher communication requirement than the near user. Inspired by this, the authors of [389] proposed two frameworks, namely single-location- and multiple-location-beamfocusing near-field-NOMA, and studied the corresponding resource allocation problem. Numerical results showed that the proposed near-field-NOMA schemes can achieve a higher spectral efficiency than conventional far-field-NOMA. The authors of [390] explored the employment of NOMA-based mixed near-field/far-field communications, where the spatial beam preconfigured for the legacy near-field user is exploited to serve an additional far-field user. The work in [117] revealed that NOMA can be employed to effectively improve the connectivity and system throughput in multi-user NFC when the near-field beamfocusing resolution is imperfect.

E. Near-Field PLS

Due to the broadcast nature of wireless communications, NFC design for secrecy is an important problem. For mmWave/THz communications, one critical issue in the far field is that guaranteeing secrecy is challenging if the eavesdropper lies in the same direction as the legitimate user, especially when the eavesdropper is closer to the BS. However, near-field beamfocusing can concentrate the energy of the confidential signal on the legitimate user’s location and thus greatly reduce the information leakage even to in-line eavesdroppers. Motivated by this, the study of secrecy in NFC systems was conducted in [335] and [336], with a specific emphasis on ULAs and modular linear arrays, respectively. To optimize secrecy rates achieved by PS-based hybrid beamforming architectures, [335] introduced a two-stage optimization algorithm, while [336] proposed an unconstrained optimum-approaching algorithm. The collective findings of these studies underscore the potential of near-field beamfocusing to enhance PLS in the range domain.

VII. CONCLUSIONS

This paper has provided a comprehensive survey of NFC, accentuating fundamental near-field operating principles, channel modeling, performance analysis, signal processing, and the integration of NFC with emerging technologies. i) In terms of fundamental principles, we delineated near-field properties from the viewpoint of both physics and communications, emphasizing their distinctiveness from FFC. ii) For channel modeling, we presented a comprehensive overview of current contributions tailored for both SPD and CAP antenna arrays that leverage the spatial non-stationarity of near-field channels. iii) Our survey covered current research on NFC performance analysis, encompassing DoFs/EDoFs, power scaling law, and transmission rate. iv) For signal processing, we delved into near-field channel estimation, beamforming design, and beam training, highlighting the influence of novel array architectures and corresponding designs. v) We also introduced the integration of NFC with other emerging technologies, including ISAC, RIS, WPT/SWIPT, NOMA, and PLS, outlining research opportunities and challenges in these areas.

Throughout this comprehensive review, we have pinpointed open problems and outlined future research directions within the realm of NFC. Despite the fact that the concept of NFC has been under discussion for four decades, its evolution, particularly under the new paradigms of multiple-antenna technology that embrace extremely large-scale aperture sizes, exceptionally high frequencies, and innovative antenna types, is still in its early stages. Given the present nascent state of NFC development, this review is expected to serve as a valuable asset, empowering researchers to explore the vast potential within this cutting-edge field.

REFERENCES

- [1] Qualcomm Technologies Inc., *The 5G Economy: How 5G Will Contribute to the Global Economy*. San Diego, CA, USA, 2019.
- [2] NTT Docomo, *White Paper: 5G Evolution and 6G*, 2022.
- [3] G. Wikström et al., *6G—Connecting a Cyber-Physical World*. Ericsson, 2022.

- [4] M. Cui, Z. Wu, Y. Lu, X. Wei, and L. Dai, "Near-field MIMO communications for 6G: Fundamentals, challenges, potentials, and future directions," *IEEE Commun. Mag.*, vol. 61, no. 1, pp. 40–46, Jan. 2023.
- [5] Y. Liu, Z. Wang, J. Xu, C. Ouyang, X. Mu, and R. Schober, "Near-field communications: A tutorial review," *IEEE Open J. Commun. Soc.*, vol. 4, pp. 1999–2049, 2023.
- [6] C. A. Balanis, *Antenna Theory: Analysis and Design*. Hoboken, NJ, USA: Wiley, 2016.
- [7] Y. Liu, J. Xu, Z. Wang, X. Mu, and L. Hanzo, "Near-field communications: What will be different?" *arXiv preprint arXiv:2303.04003*, 2023.
- [8] E. Dahlman, S. Parkvall, and J. Skold, *5G NR: The Next Generation Wireless Access Technology*. New York, NY, USA: Academic, 2020.
- [9] C. Huygens, *Traité de la Lumière*. Leiden, 1690.
- [10] T. Young, "The Bakerian lecture: Experiments and calculations relative to physical optics," *Philos. Trans. R. Soc. Lond.*, vol. 94, pp. 1–16, Nov. 1803.
- [11] J. von Fraunhofer, "Neue modifikation des lichten durch gegenseitige einwirkung und beugung der strahlen, und gesetze derselben," *Denkschriften der Königlichen Akademie der Wissenschaften zu München*, vol. 2, no. 8, pp. 3–76, 1824.
- [12] L. Rayleigh, "On pin-hole photography," *London, Edinburgh, Dublin Philos. Mag. J. Sci.*, vol. 31, no. 189, pp. 87–99, 1891.
- [13] C. Cutler, A. King, and W. Kock, "Microwave antenna measurements," *Proc. IRE*, vol. 35, no. 12, pp. 1462–1471, Dec. 1947.
- [14] C. Polk, "Optical Fresnel-zone gain of a rectangular aperture," *IRE Trans. Antennas Propag.*, vol. 4, no. 1, pp. 65–69, Jan. 1956.
- [15] C. A. Walton, "Portable radio frequency emitting identifier," May 1983, US Patent 4,384,288.
- [16] J. H. Winters, "Optimum combining in digital mobile radio with cochannel interference," *IEEE Trans. Veh. Technol.*, vol. 33, no. 3, pp. 144–155, Aug. 1984.
- [17] A. J. Paulraj and T. Kailath, "Increasing capacity in wireless broadcast systems using distributed transmission/directional reception (DTDR)," Sep. 1994, US Patent 5,345,599.
- [18] G. J. Foschini, "Layered space-time architecture for wireless communication in a fading environment when using multi-element antennas," *Bell Labs Tech. J.*, vol. 1, no. 2, pp. 41–59, Autumn 1996.
- [19] P. F. Driessen and G. J. Foschini, "On the capacity formula for multiple input-multiple output wireless channels: A geometric interpretation," *IEEE Trans. Commun.*, vol. 47, no. 3, pp. 173–176, Feb. 1999.
- [20] A. F. Molisch, M. Steinbauer, M. Toeltsch, E. Bonek, and R. S. Thoma, "Capacity of MIMO systems based on measured wireless channels," *IEEE J. Sel. Areas Commun.*, vol. 20, no. 3, pp. 561–569, Apr. 2002.
- [21] J.-S. Jiang and M. A. Ingram, "Path models and MIMO capacity for measured indoor channels at 5.8 GHz," in *Proc. IEEE 9th Int. Symp. Technol. Appl. Electromagn. (ANTEM)*, Jul. 2002, pp. 1–7.
- [22] —, "Distributed source model for short-range MIMO," in *Proc. IEEE 58th Veh. Technol. Conf. (VTC-Fall)*, Oct. 2003, pp. 357–362.
- [23] —, "Spherical-wave model for short-range MIMO," *IEEE Trans. Commun.*, vol. 53, no. 9, pp. 1534–1541, Sep. 2005.
- [24] T. L. Marzetta, "Noncooperative cellular wireless with unlimited numbers of base station antennas," *IEEE Trans. Wireless Commun.*, vol. 9, no. 11, pp. 3590–3600, Nov. 2010.
- [25] Z. Zhou, X. Gao, J. Fang, and Z. Chen, "Spherical wave channel and analysis for large linear array in LoS conditions," in *Proc. IEEE Globecom Workshops (GC Wkshps)*, Dec. 2015, pp. 1–6.
- [26] D. W. Prather, "5G moves into the light: Holographic massive MIMO," *IEEE ComSoc Technol. News*, Jun. 2023.
- [27] D. W. Prather, S. Shi, G. J. Schneider, P. Yao, C. Schuetz, J. Murakowski, J. C. Deroba, F. Wang, M. R. Konkol, and D. D. Ross, "Optically upconverted, spatially coherent phased-array-antenna feed networks for beam-space MIMO in 5G cellular communications," *IEEE Trans. Antennas Propag.*, vol. 65, no. 12, pp. 6432–6443, Dec. 2017.
- [28] S. Hu, F. Rusek, and O. Edfors, "The potential of using large antenna arrays on intelligent surfaces," in *Proc. IEEE 85th Veh. Technol. Conf. (VTC-Spring)*, Jun. 2017, pp. 1–6.
- [29] A. Amiri, M. Angjelichinoski, E. De Carvalho, and R. W. Heath, "Extremely large aperture massive MIMO: Low complexity receiver architectures," in *Proc. IEEE Globecom Workshops (GC Wkshps)*, Dec. 2018, pp. 1–6.
- [30] R. Deng, Y. Zhang, H. Zhang, B. Di, H. Zhang, and L. Song, "Reconfigurable holographic surface: A new paradigm to implement holographic radio," *IEEE Veh. Technol. Mag.*, vol. 18, no. 1, pp. 20–28, Mar. 2023.
- [31] C. Huang, S. Hu, G. C. Alexandropoulos, A. Zappone, C. Yuen, R. Zhang, M. D. Renzo, and M. Debbah, "Holographic MIMO surfaces for 6G wireless networks: Opportunities, challenges, and trends," *IEEE Wireless Commun.*, vol. 27, no. 5, pp. 118–125, Oct. 2020.
- [32] J. Gao, B. Deng, Y. Qin, H. Wang, and X. Li, "An efficient algorithm for MIMO cylindrical millimeter-wave holographic 3-D imaging," *IEEE Trans. Microw. Theory Techn.*, vol. 66, no. 11, pp. 5065–5074, Nov. 2018.
- [33] Y. Liu, X. Liu, X. Mu, T. Hou, J. Xu, M. Di Renzo, and N. Al-Dhahir, "Reconfigurable intelligent surfaces: Principles and opportunities," *IEEE Commun. Surv. Tut.*, vol. 23, no. 3, pp. 1546–1577, 3rd Quart., 2021.
- [34] J. Xu, Y. Liu, X. Mu, and O. A. Dobre, "STAR-RISs: Simultaneous transmitting and reflecting reconfigurable intelligent surfaces," *IEEE Commun. Lett.*, vol. 25, no. 9, pp. 3134–3138, May 2021.
- [35] N. Shlezinger, G. C. Alexandropoulos, M. F. Imani, Y. C. Eldar, and D. R. Smith, "Dynamic metasurface antennas for 6G extreme massive MIMO communications," *IEEE Wireless Commun.*, vol. 28, no. 2, pp. 106–113, Apr. 2021.
- [36] M. Boyarsky, T. Slesman, L. Pulido-Mancera, T. Fromenteze, A. Pedross-Engel, C. M. Watts, M. F. Imani, M. S. Reynolds, and D. R. Smith, "Synthetic aperture radar with dynamic metasurface antennas: A conceptual development," *J. Opt. Soc. Am. A*, vol. 34, no. 5, pp. A22–A36, May 2017.
- [37] K.-K. Wong, A. Shojaefard, K.-F. Tong, and Y. Zhang, "Fluid antenna systems," *IEEE Trans. Wireless Commun.*, vol. 20, no. 3, pp. 1950–1962, Mar. 2021.
- [38] E. Björnson, L. Sanguinetti, H. Wymeersch, J. Hoydis, and T. L. Marzetta, "Massive MIMO is a reality—What is next?: Five promising research directions for antenna arrays," *Digit. Signal Process.*, vol. 94, pp. 3–20, Nov. 2019.
- [39] K. Ying, Z. Gao, S. Chen, X. Gao, M. Matthaiou, R. Zhang, and R. Schober, "Reconfigurable massive MIMO: Harnessing the power of the electromagnetic domain for enhanced information transfer," *IEEE Wireless Commun.*, Early Access, 2023.
- [40] X. Gao, L. Dai, and A. M. Sayeed, "Low RF-complexity technologies to enable millimeter-wave MIMO with large antenna array for 5G wireless communications," *IEEE Commun. Mag.*, vol. 56, no. 4, pp. 211–217, Apr. 2018.
- [41] R. Deng, B. Di, H. Zhang, D. Niyato, Z. Han, H. V. Poor, and L. Song, "Reconfigurable holographic surfaces for future wireless communications," *IEEE Wireless Commun.*, vol. 28, no. 6, pp. 126–131, Dec. 2021.
- [42] R. Deng, Y. Zhang, H. Zhang, B. Di, H. Zhang, H. V. Poor, and L. Song, "Reconfigurable holographic surfaces for ultra-massive MIMO in 6G: Practical design, optimization and implementation," *IEEE J. Sel. Areas Commun.*, vol. 41, no. 8, pp. 2367–2379, Aug. 2023.
- [43] Z. Zhang and L. Dai, "Pattern-division multiplexing for multi-user continuous-aperture MIMO," *IEEE J. Sel. Areas Commun.*, vol. 41, no. 8, pp. 2350–2366, Aug. 2023.
- [44] M. Di Renzo, A. Zappone, M. Debbah, M. S. Alouini, C. Yuen, J. de Rosny, and S. Tretyakov, "Smart radio environments empowered by reconfigurable intelligent surfaces: How it works, state of research, and the road ahead," *IEEE J. Sel. Areas Commun.*, vol. 38, no. 11, pp. 2450–2525, Nov. 2020.
- [45] L. Zhu, W. Ma, and R. Zhang, "Movable antennas for wireless communication: Opportunities and challenges," *IEEE Commun. Mag.*, Early Access, 2023.
- [46] K.-K. Wong and K.-F. Tong, "Fluid antenna multiple access," *IEEE Trans. Wireless Commun.*, vol. 21, no. 7, pp. 4801–4815, Jul. 2022.
- [47] K.-K. Wong, K.-F. Tong, Y. Zhang, and Z. Zhongbin, "Fluid antenna system for 6G: When Bruce Lee inspires wireless communications," *Electron. Lett.*, vol. 56, no. 24, pp. 1288–1290, Nov. 2020.
- [48] H. Zhang, N. Shlezinger, F. Guidi, D. Dardari, and Y. C. Eldar, "6G wireless communications: From far-field beam steering to near-field beam focusing," *IEEE Commun. Mag.*, vol. 61, no. 4, pp. 72–77, Apr. 2023.
- [49] Z. Wang, X. Mu, and Y. Liu, "Terahertz near-field communications and sensing," *arXiv preprint arXiv:2306.09723*, 2023.
- [50] C. Ouyang, Y. Liu, X. Zhang, and L. Hanzo, "Near-field communications: A degree-of-freedom perspective," *arXiv preprint arXiv:2308.00362*, 2023.
- [51] H. Lu, Y. Zeng, C. You *et al.*, "A tutorial on near-field XL-MIMO communications towards 6G," *arXiv preprint arXiv:2310.11044*, 2023.
- [52] Z. Wang, J. Zhang, H. Du *et al.*, "A tutorial on extremely large-scale MIMO for 6G: Fundamentals, signal processing, and applications," *IEEE Commun. Surveys Tuts.*, Early Access, 2024.

- [53] Y. Han, S. Jin, M. Matthaiou, T. Q. Quek, and C.-K. Wen, "Towards extra large-scale MIMO: New channel properties and low-cost designs," *IEEE Internet Things J.*, vol. 10, no. 16, pp. 14 569–14 594, Aug. 2023.
- [54] T. Gong, I. Vinieratou, R. Ji *et al.*, "Holographic MIMO communications: Theoretical foundations, enabling technologies, and future directions," *IEEE Commun. Surveys Tuts.*, Early Access, 2023.
- [55] J. C. Maxwell, "A dynamical theory of the electromagnetic field," *Proc. Roy Soc. Lond.*, vol. 155, no. 1865, pp. 459–512, Jan. 1863.
- [56] A. Goldsmith, *Wireless Communications*. Cambridge, U.K.: Cambridge Univ. Press, 2005.
- [57] M. Pätzold, M. Patzold, and M. Paetzold, *Mobile Fading Channels*. Chichester, U.K.: Wiley, 2002.
- [58] H. S. Wang and N. Moayeri, "Finite-state Markov channel—A useful model for radio communication channels," *IEEE Trans. Veh. Technol.*, vol. 44, no. 1, pp. 163–171, Feb. 1995.
- [59] A. M. Chen and R. R. Rao, "On tractable wireless channel models," in *Proc. IEEE 9th Int. Symp. Pers. Indoor Mobile Radio Commun. (PIMRC)*, vol. 2, Sep. 1998, pp. 825–830.
- [60] V. Erceg, L. Greenstein, S. Tjandra, S. Parkoff, A. Gupta, B. Kulic, A. Julius, and R. Bianchi, "An empirically based path loss model for wireless channels in suburban environments," *IEEE J. Sel. Areas Commun.*, vol. 17, no. 7, pp. 1205–1211, Jul. 1999.
- [61] B. Sklar, "Rayleigh fading channels in mobile digital communication systems—Part I: Characterization," *IEEE Commun. Mag.*, vol. 35, no. 7, pp. 90–100, Jul. 1997.
- [62] S. O. Rice, "Reflection of electromagnetic waves from slightly rough surfaces," *Commun. Pure Appl. Math.*, vol. 4, no. 2-3, pp. 351–378, Aug. 1951.
- [63] M. Born and E. Wolf, *Principles of Optics: Electromagnetic Theory of Propagation, Interference and Diffraction of Light*, 6th ed. Oxford, U.K.: Pergamon, 1980.
- [64] J. Mathews and R. L. Walker, *Mathematical Methods of Physics*. W. A. Benjamin, Ed. Reading, MA, USA: Addison-Wesley, 1970.
- [65] R. Kouyoumjian and P. Pathak, "A uniform geometrical theory of diffraction for an edge in a perfectly conducting surface," *Proc. IEEE*, vol. 62, no. 11, pp. 1448–1461, Nov. 1974.
- [66] Q. N. Dinh and W.-S. Gan, "Green's function estimation in homogeneous and scattering medium for time reversal signal processing (TRSP) communication," in *Proc. 2nd Int. Conf. Digit. Telecommun. (ICDT)*, Jul. 2007, pp. 1–6.
- [67] F. H. Danufane, M. D. Renzo, J. de Rosny, and S. Tretyakov, "On the path-loss of reconfigurable intelligent surfaces: An approach based on Green's theorem applied to vector fields," *IEEE Trans. Commun.*, vol. 69, no. 8, pp. 5573–5592, Aug. 2021.
- [68] G. Kirchhoff, "Zur Theorie der Lichtstrahlen," *Annal. Phys.*, vol. 254, no. 4, pp. 663–695, Jan. 1882.
- [69] V. Pham-Xuan, I. Kavanagh, M. Condon, and C. Brennan, "On comparison of integral equation approaches for indoor wave propagation," in *Proc. 2014 IEEE-APS Topical Conf. Antennas Propag. Wireless Commun. (APWC)*, Aug. 2014, pp. 796–799.
- [70] S. Lin, E. Dohme, and Z. Peng, "A stochastic Green's function—Integral equation method for communication in diffuse multipath environments," in *Proc. IEEE Int. Conf. Electromagn. Adv. Appl. (ICEAA)*, Sep. 2018, pp. 567–570.
- [71] A. Kaye and D. George, "Transmission of multiplexed PAM signals over multiple channel and diversity systems," *IEEE Trans. Commun. Technol.*, vol. 18, no. 5, pp. 520–526, Oct. 1970.
- [72] J. Xu, Y. Liu, X. Mu, J. T. Zhou, L. Song, H. V. Poor, and L. Hanzo, "Simultaneously transmitting and reflecting intelligent omni-surfaces: Modeling and implementation," *IEEE Veh. Technol. Mag.*, vol. 17, no. 2, pp. 46–54, Jun. 2022.
- [73] F. Las-Heras, M. Pino, S. Loredó, Y. Alvarez, and T. Sarkar, "Evaluating near-field radiation patterns of commercial antennas," *IEEE Trans. Antennas and Propag.*, vol. 54, no. 8, pp. 2198–2207, Aug. 2006.
- [74] R. C. Maclaurin, *Light*. Cambridge, U.K.: Cambridge Univ. Press, 1909.
- [75] J. E. Greivenkamp, *Field Guide to Geometrical Optics*. Bellingham, WA, USA: SPIE Press, 2004.
- [76] J. D. Kraus and R. J. Marhefka, *Antennas: For All Applications*. New York, USA: McGraw-Hill, 2002.
- [77] J. Xu, X. Mu, and Y. Liu, "Exploiting STAR-RISs in near-field communications," *IEEE Trans. Wireless Commun.*, Early Access, 2023.
- [78] H. Lu and Y. Zeng, "How does performance scale with antenna number for extremely large-scale MIMO?" in *Proc. IEEE Int. Conf. Commun. (ICC)*, Jun. 2021, pp. 1–6.
- [79] J. Zhu, Z. Wan, L. Dai, M. Debbah, and H. V. Poor, "Electromagnetic information theory: Fundamentals, modeling, applications, and open problems," *IEEE Wireless Commun.*, Early Access, 2024.
- [80] M. D. Migliore, "On electromagnetics and information theory," *IEEE Trans. Antennas Propag.*, vol. 56, no. 10, pp. 3188–3200, Oct. 2008.
- [81] D. Tse and P. Viswanath, *Fundamentals of Wireless Communication*. Cambridge, U.K.: Cambridge Univ. Press, 2005.
- [82] T. Muharemovic, A. Sabharwal, and B. Aazhang, "Antenna packing in low-power systems: Communication limits and array design," *IEEE Trans. Inf. Theory*, vol. 54, no. 1, pp. 429–440, Jan. 2008.
- [83] S. Verdú, "Spectral efficiency in the wideband regime," *IEEE Trans. Inf. Theory*, vol. 48, no. 6, pp. 1319–1343, Jun. 2002.
- [84] D. A. B. Miller, "Communicating with waves between volumes: Evaluating orthogonal spatial channels and limits on coupling strengths," *Appl. Opt.*, vol. 39, no. 11, pp. 1681–1699, Apr. 2000.
- [85] Z. Xie, Y. Liu, J. Xu, X. Wu, and A. Nallanathan, "Performance analysis for near-field MIMO: Discrete and continuous aperture antennas," *IEEE Wireless Commun. Lett.*, vol. 12, no. 12, pp. 2258–2262, Dec. 2023.
- [86] V. Nurmela *et al.*, *METIS Channel Models*. Document ICT-317669/D1.4, METIS, New York, NY, USA, 2015.
- [87] A. Bourdoux *et al.*, "D1. 2 MaMi channel characteristics: Measurement results," *MMMOET*, Jun. 2015, Utrecht, The Netherlands, Tech. Rep. ICT-619086-D1.2.
- [88] J. Flordelis, X. Li, O. Edfors, and F. Tufvesson, "Massive MIMO extensions to the COST 2100 channel model: Modeling and validation," *IEEE Trans. Wireless Commun.*, vol. 19, no. 1, pp. 380–394, Jan. 2020.
- [89] C.-X. Wang, J. Bian, J. Sun, W. Zhang, and M. Zhang, "A survey of 5G channel measurements and models," *IEEE Commun. Surv. Tut.*, vol. 20, no. 4, pp. 3142–3168, 4th Quart. 2018.
- [90] C.-X. Wang, J. Huang, H. Wang, X. Gao, X. You, and Y. Hao, "6G wireless channel measurements and models: Trends and challenges," *IEEE Veh. Technol. Mag.*, vol. 15, no. 4, pp. 22–32, Dec. 2020.
- [91] J. Hoydis, C. Hoek, T. Wild, and S. ten Brink, "Channel measurements for large antenna arrays," in *Proc. IEEE Int. Symp. Wireless Commun. Syst. (ISWCS)*, Aug. 2012, pp. 811–815.
- [92] X. Gao, F. Tufvesson, O. Edfors, and F. Rusek, "Measured propagation characteristics for very-large MIMO at 2.6 GHz," in *Proc. 46th Asilomar Conf. Signals, Syst., Comput. (ASILOMAR)*, Nov. 2012, pp. 295–299.
- [93] A. O. Martinez, E. De Carvalho, and J. Ø. Nielsen, "Towards very large aperture massive MIMO: A measurement based study," in *Proc. IEEE Globecom Workshops (GC Wkshps)*, Dec. 2014, pp. 281–286.
- [94] X. Gao, O. Edfors, F. Rusek, and F. Tufvesson, "Massive MIMO performance evaluation based on measured propagation data," *IEEE Trans. Wireless Commun.*, vol. 14, no. 7, pp. 3899–3911, Jul. 2015.
- [95] X. Gao, O. Edfors, F. Tufvesson, and E. G. Larsson, "Massive MIMO in real propagation environments: Do all antennas contribute equally?" *IEEE Trans. Wireless Commun.*, vol. 63, no. 11, pp. 3917–3928, Nov. 2015.
- [96] E. De Carvalho, A. Ali, A. Amiri, M. Angjelichinoski, and R. W. Heath, "Non-stationarities in extra-large-scale massive MIMO," *IEEE Wireless Commun.*, vol. 27, no. 4, pp. 74–80, Aug. 2020.
- [97] Z. Dong and Y. Zeng, "Near-field spatial correlation for extremely large-scale array communications," *IEEE Commun. Lett.*, vol. 26, no. 7, pp. 1534–1538, Jul. 2022.
- [98] C. Wang, C. Li, Z. Zhong, L. Fan, W. Han, Q. Qin, and C.-X. Wang, "Characteristics of 5.3 GHz MIMO channels with an extremely large antenna array in urban macro scenarios," in *Proc. IEEE 95th Veh. Technol. Conf. (VTC-Spring)*, Jun. 2022, pp. 1–5.
- [99] R. Feng, C.-X. Wang, J. Huang, Y. Zheng, F. Lai, and W. Zhou, "Mutual coupling analysis of 6G ultra-massive MIMO channel measurements and models," in *Proc. IEEE Int. Conf. Commun. (ICC)*, May 2022, pp. 956–961.
- [100] A. Roederer, E. Farr, L. Foged, M. Francis, R. Hansen, R. Haupt, and K. Warmick, *IEEE Standard for Definitions of Terms for Antennas*. IEEE Standard 145-2013, 2014.
- [101] C. A. Balanis, *Advanced Engineering Electromagnetics*. Hoboken, NJ, USA: Wiley, 2012.
- [102] P. Bevelacqua, "Effective area (effective aperture)," 2019. [Online]. Available: <https://www.antenna-theory.com>
- [103] A. Yaghjian, "An overview of near-field antenna measurements," *IEEE Trans. Antennas Propag.*, vol. 34, no. 1, pp. 30–45, Jan. 1986.
- [104] F. Bøhagen, P. Orten, and G. E. Øien, "Design of optimal high-rank line-of-sight MIMO channels," *IEEE Trans. Wireless Commun.*, vol. 6, no. 4, pp. 1420–1425, Apr. 2007.

- [105] K. T. Selvan and R. Janaswamy, "Fraunhofer and Fresnel distances: Unified derivation for aperture antennas," *IEEE Antennas Propag. Mag.*, vol. 59, no. 4, pp. 12–15, Aug. 2017.
- [106] M. Cui and L. Dai, "Near-field wideband beamforming for extremely large antenna arrays," *arXiv preprint arXiv:2109.10054v3*, 2023.
- [107] F. Bøghagen, P. Orten, and G. E. Øien, "Modeling of line-of-sight 2×2 MIMO channels: Spherical versus plane waves," in *Proc. IEEE 17th Int. Symp. Pers. Indoor Mobile Radio Commun. (PIMRC)*, Sep. 2006, pp. 1–5.
- [108] —, "On spherical vs. plane wave modeling of line-of-sight MIMO channels," *IEEE Trans. Commun.*, vol. 57, no. 3, pp. 841–849, Mar. 2009.
- [109] L. Le Magoarou, A. Le Calvez, and S. Paquelet, "Massive MIMO channel estimation taking into account spherical waves," in *Proc. IEEE 20th Int. Wkshps. Signal Process. Adv. Wireless Commun. (SPAWC)*, Jul. 2019, pp. 1–5.
- [110] X. Wei and L. Dai, "Channel estimation for extremely large-scale massive MIMO: Far-field, near-field, or hybrid-field?" *IEEE Commun. Lett.*, vol. 26, no. 1, pp. 177–181, Jan. 2022.
- [111] M. Cui and L. Dai, "Channel estimation for extremely large-scale MIMO: Far-field or near-field?" *IEEE Trans. Commun.*, vol. 70, no. 4, pp. 2663–2677, Apr. 2022.
- [112] Y. Lu and L. Dai, "Near-field channel estimation in mixed LoS/NLoS environments for extremely large-scale MIMO systems," *IEEE Trans. Commun.*, vol. 71, no. 6, pp. 3694–3707, Jun. 2023.
- [113] X. Wei, L. Dai, Y. Zhao, G. Yu, and X. Duan, "Codebook design and beam training for extremely large-scale RIS: Far-field or near-field?" *China Commun.*, vol. 19, no. 6, pp. 193–204, Jun. 2022.
- [114] M. Cui, L. Dai, Z. Wang, S. Zhou, and N. Ge, "Near-field rainbow: Wideband beam training for XL-MIMO," *IEEE Trans. Wireless Commun.*, vol. 22, no. 6, pp. 3899–3912, Jun. 2023.
- [115] Y. Zhang, X. Wu, and C. You, "Fast near-field beam training for extremely large-scale array," *IEEE Wireless Commun. Lett.*, vol. 11, no. 12, pp. 2625–2629, Dec. 2022.
- [116] Z. Wu and L. Dai, "Multiple access for near-field communications: SDMA or LDMA?" *IEEE J. Sel. Areas Commun.*, vol. 40, no. 4, pp. 1317–1332, Apr. 2022.
- [117] Z. Ding, "Resolution of near-field beamforming and its impact on NOMA," *IEEE Wireless Commun. Lett.*, Early Access, 2023.
- [118] K. Nishimori, N. Honma, T. Seki, and K. Hiraga, "On the transmission method for short-range MIMO communication," *IEEE Trans. Veh. Technol.*, vol. 60, no. 3, pp. 1247–1251, Mar. 2011.
- [119] X. Pu, S. Shao, and Y. Tang, "Optimal 2×2 antenna placement for short-range communications," *IEEE Commun. Lett.*, vol. 17, no. 8, pp. 1560–1563, Aug. 2013.
- [120] X. Pu, S. Shao, K. Deng, and Y. Tang, "Analysis of the capacity statistics for 2×2 3D MIMO channels in short-range communications," *IEEE Commun. Lett.*, vol. 19, no. 2, pp. 219–222, Feb. 2014.
- [121] X. Pu, K. L. Law, S. Shao, and Y. Tang, "On the capacity for 3D LoS MIMO channels in short-range millimeter wave communications," in *Proc. 11th Int. Conf. Wireless Commun., Netw. Mobile Comput. (WiCOM)*, Sep. 2015, pp. 1–6.
- [122] X. Pu, Q. Chen, S. Shao, R. Chai, and Y. Tang, "Transmit design for short-range MIMO channels with the spherical-wave model," *IEEE Commun. Lett.*, vol. 21, no. 8, pp. 1875–1878, Apr. 2017.
- [123] H. Lu and Y. Zeng, "Communicating with extremely large-scale array/surface: Unified modeling and performance analysis," *IEEE Trans. Wireless Commun.*, vol. 21, no. 6, pp. 4039–4053, Jun. 2021.
- [124] C. Feng, H. Lu, Y. Zeng, T. Li, S. Jin, and R. Zhang, "Near-field modelling and performance analysis for extremely large-scale IRS communications," *IEEE Trans. Wireless Commun.*, Early Access, 2023.
- [125] K. Zhi, C. Pan, H. Ren, K. K. Chai, C.-X. Wang, R. Schober, and X. You, "Performance analysis and low-complexity design for XL-MIMO with near-field spatial non-stationarities," *IEEE J. Sel. Areas Commun.*, Early Access, 2024.
- [126] Y. Han, S. Jin, C.-K. Wen, and X. Ma, "Channel estimation for extremely large-scale massive MIMO systems," *IEEE Wireless Commun. Lett.*, vol. 9, no. 5, pp. 633–637, May 2020.
- [127] Y. Zhu, H. Guo, and V. K. Lau, "Bayesian channel estimation in multi-user massive MIMO with extremely large antenna array," *IEEE Trans. Signal Process.*, vol. 69, pp. 5463–5478, 2021.
- [128] D. Gabor, "Light and information," *Progress in Optics*, vol. 1, pp. 109–153, 1961.
- [129] R. F. Harrington, *Time-Harmonic Electromagnetic Fields*. New York, NY, USA: IEEE Press-Wiley, 2001.
- [130] J. D. Jackson, *Classical Electrodynamics*. Hoboken, NJ, USA: Wiley, 1999.
- [131] S. Hu, F. Rusek, and O. Edfors, "Cramér-Rao lower bounds for positioning with large intelligent surfaces," in *Proc. IEEE 86th Veh. Technol. Conf. (VTC-Fall)*, Sep. 2017, pp. 1–6.
- [132] —, "Beyond massive MIMO: The potential of data transmission with large intelligent surfaces," *IEEE Trans. Signal Process.*, vol. 66, no. 10, pp. 2746–2758, May 2018.
- [133] E. Björnson and L. Sanguinetti, "Power scaling laws and near-field behaviors of massive MIMO and intelligent reflecting surfaces," *IEEE Open J. Commun. Soc.*, vol. 1, pp. 1306–1324, 2020.
- [134] D. A. B. Miller, "Spatial channels for communicating with waves between volumes," *Opt. Lett.*, vol. 23, no. 21, pp. 1645–1647, Nov. 1998.
- [135] R. Piestun and D. A. B. Miller, "Degrees of freedom of an electromagnetic wave," in *Proc. 18th Congress of the Int. Commission for Opt.*, vol. 3749. SPIE, 1999, pp. 110–111.
- [136] R. Piestun and D. A. B. Miller, "Electromagnetic degrees of freedom of an optical system," *J. Opt. Soc. Amer. A, Opt. Image Sci.*, vol. 17, no. 5, pp. 892–902, May 2000.
- [137] Z. Wan, J. Zhu, Z. Zhang, L. Dai, and C.-B. Chae, "Mutual information for electromagnetic information theory based on random fields," *IEEE Trans. Commun.*, vol. 71, no. 4, pp. 1982–1996, Apr. 2023.
- [138] A. S. Y. Poon, R. W. Brodersen, and D. N. C. Tse, "Degrees of freedom in multiple-antenna channels: A signal space approach," *IEEE Trans. Inf. Theory*, vol. 51, no. 2, pp. 523–536, Feb. 2005.
- [139] D. Dardari, "Communicating with large intelligent surfaces: Fundamental limits and models," *IEEE J. Sel. Areas Commun.*, vol. 38, no. 11, pp. 2526–2537, Nov. 2020.
- [140] L. Wei, C. Huang, G. C. Alexandropoulos, Z. Yang, J. Yang, E. Wei, Z. Zhang, M. Debbah, and C. Yuen, "Tri-polarized holographic MIMO surfaces for near-field communications: Channel modeling and precoding design," *IEEE Trans. Wireless Commun.*, vol. 22, no. 12, pp. 8828–8842, Dec. 2023.
- [141] A. L. Imoize, A. E. Ibhaze, A. A. Atayero, and K. Kavitha, "Standard propagation channel models for MIMO communication systems," *Wirel. Commun. Mob. Comput.*, vol. 2021, pp. 1–36, 2021.
- [142] A. A. M. Saleh and R. Valenzuela, "A statistical model for indoor multipath propagation," *IEEE J. Sel. Areas Commun.*, vol. 5, no. 2, pp. 128–137, Feb. 1987.
- [143] Q. H. Spencer, B. D. Jeffs, M. A. Jensen, and A. L. Swindlehurst, "Modeling the statistical time and angle of arrival characteristics of an indoor multipath channel," *IEEE J. Sel. Areas Commun.*, vol. 18, no. 3, pp. 347–360, Mar. 2000.
- [144] C. Gustafson, K. Haneda, S. Wyne, and F. Tufvesson, "On mm-Wave multipath clustering and channel modeling," *IEEE Trans. Antennas Propag.*, vol. 62, no. 3, pp. 1445–1455, Mar. 2013.
- [145] A. L. Moustakas, H. U. Baranger, L. Balents, A. M. Sengupta, and S. H. Simon, "Communication through a diffusive medium: Coherence and capacity," *Science*, vol. 287, no. 5451, pp. 287–290, Jan. 2000.
- [146] S. Wu, C.-X. Wang, M. M. Alwakeel, X. You *et al.*, "A general 3-D non-stationary 5G wireless channel model," *IEEE Trans. Commun.*, vol. 66, no. 7, pp. 3065–3078, Jul. 2018.
- [147] A. M. Sayeed, "Deconstructing multiantenna fading channels," *IEEE Trans. Signal Process.*, vol. 50, no. 10, pp. 2563–2579, Oct. 2002.
- [148] R. R. Muller, "A random matrix model of communication via antenna arrays," *IEEE Trans. Inf. Theory*, vol. 48, no. 9, pp. 2495–2506, Sep. 2002.
- [149] A. G. Burr, "Capacity bounds and estimates for the finite scatterers MIMO wireless channel," *IEEE J. Sel. Areas Commun.*, vol. 21, no. 5, pp. 812–818, Jun. 2003.
- [150] H. Q. Ngo, E. G. Larsson, and T. L. Marzetta, "The multicell multiuser MIMO uplink with very large antenna arrays and a finite-dimensional channel," *IEEE Trans. Commun.*, vol. 61, no. 6, pp. 2350–2361, Jun. 2013.
- [151] E. Zhou, H. Jiang, and H. Qi, "4-D parameter estimation in bistatic MIMO radar for near-field target localization," in *Proc. IEEE Int. Wireless Symp. (IWS)*, Mar. 2015, pp. 1–4.
- [152] A. Abdi and M. Kaveh, "A space-time correlation model for multielement antenna systems in mobile fading channels," *IEEE J. Sel. Areas Commun.*, vol. 20, no. 3, pp. 550–560, Apr. 2002.
- [153] J. Gong, J. F. Hayes, and M. R. Soleymani, "The effect of antenna physics on fading correlation and the capacity of multielement antenna systems," *IEEE Trans. Veh. Technol.*, vol. 56, no. 4, pp. 1591–1599, Jul. 2007.
- [154] A. Abdi, J. A. Barger, and M. Kaveh, "A parametric model for the distribution of the angle of arrival and the associated correlation function and power spectrum at the mobile station," *IEEE Trans. Veh. Technol.*, vol. 51, no. 3, pp. 425–434, May 2002.

- [155] C. Oestges, V. Erceg, and A. J. Paulraj, "A physical scattering model for MIMO macrocellular broadband wireless channels," *IEEE J. Sel. Areas Commun.*, vol. 21, no. 5, pp. 721–729, Jun. 2003.
- [156] C. Oestges, B. Clerckx, D. Vanhoenacker-Janvier, and A. J. Paulraj, "Impact of fading correlations on MIMO communication systems in geometry-based statistical channel models," *IEEE Trans. Wireless Commun.*, vol. 4, no. 3, pp. 1112–1120, May 2005.
- [157] D.-S. Shiu, G. J. Foschini, M. J. Gans, and J. M. Kahn, "Fading correlation and its effect on the capacity of multielement antenna systems," *IEEE Trans. Commun.*, vol. 48, no. 3, pp. 502–513, Mar. 2000.
- [158] J.-P. Kermoal, L. Schumacher, K. I. Pedersen, P. E. Mogensen, and F. Frederiksen, "A stochastic MIMO radio channel model with experimental validation," *IEEE J. Sel. Areas Commun.*, vol. 20, no. 6, pp. 1211–1226, Aug. 2002.
- [159] A. M. Tulino, A. Lozano, and S. Verdú, "Impact of antenna correlation on the capacity of multi-antenna channels," *IEEE Trans. Inf. Theory*, vol. 51, no. 7, pp. 2491–2509, Jul. 2005.
- [160] —, "Capacity-achieving input covariance for single-user multi-antenna channels," *IEEE Trans. Inf. Theory*, vol. 5, no. 3, pp. 662–671, Mar. 2006.
- [161] A. Ali, E. De Carvalho, and R. W. Heath, "Linear receivers in non-stationary massive MIMO channels with visibility regions," *IEEE Wireless Commun. Lett.*, vol. 8, no. 3, pp. 885–888, Jun. 2019.
- [162] X. Li, S. Zhou, E. Björnson, and J. Wang, "Capacity analysis for spatially non-wide sense stationary uplink massive MIMO systems," *IEEE Trans. Wireless Commun.*, vol. 14, no. 12, pp. 7044–7056, Dec. 2015.
- [163] H. Özcelik, M. Herdin, W. Weichselberger, J. Wallace, and E. Bonek, "Deficiencies of 'Kronecker' MIMO radio channel model," *Electron. Lett.*, vol. 39, no. 16, p. 1, Aug. 2003.
- [164] E. Telatar, "Capacity of multi-antenna Gaussian channels," *Eur. Trans. Telecommun.*, vol. 10, no. 6, pp. 585–595, Nov. 1999.
- [165] W. Weichselberger, M. Herdin, H. Özcelik, and E. Bonek, "A stochastic MIMO channel model with joint correlation of both link ends," *IEEE Trans. Wireless Commun.*, vol. 5, no. 1, pp. 90–100, Jan. 2006.
- [166] W. Xu, S. A. Zekavat, and H. Tong, "A novel spatially correlated multiuser MIMO channel modeling: Impact of surface roughness," *IEEE Trans. Antennas Propag.*, vol. 57, no. 8, pp. 2429–2438, Aug. 2009.
- [167] V. C. Rodrigues, A. Amiri, T. Abrão, E. De Carvalho, and P. Popovski, "Low-complexity distributed XL-MIMO for multiuser detection," in *Proc. IEEE Int. Conf. Commun. Wkshps. (ICC Wkshps)*, Jun. 2020, pp. 1–6.
- [168] V. Croisfelt, T. Abrão, A. Amiri, E. De Carvalho, and P. Popovski, "Decentralized design of fast iterative receivers for massive MIMO with spatial non-stationarities," in *Proc. 55th Asilomar Conf. Signals, Syst., Comput. (ASILOMAR)*, Oct. 2021, pp. 1242–1249.
- [169] J. Zhang, J. Zhang, Y. Han, J. Wang, and S. Jin, "Average spectral efficiency for TDD-based non-stationary XL-MIMO with VR estimation," in *Proc. 14th Int. Conf. Wireless Commun. Signal Process. (WCSP)*, Nov. 2022, pp. 973–977.
- [170] V. Croisfelt, A. Amiri, T. Abrão, E. De Carvalho, and P. Popovski, "Accelerated randomized methods for receiver design in extra-large scale MIMO arrays," *IEEE Trans. Veh. Technol.*, vol. 70, no. 7, pp. 6788–6799, Jul. 2021.
- [171] X. Yang, F. Cao, M. Matthaiou, and S. Jin, "On the uplink transmission of extra-large scale massive MIMO systems," *IEEE Trans. Veh. Technol.*, vol. 69, no. 12, pp. 15 229–15 243, Dec. 2020.
- [172] M. R. McKay, *Random Matrix Theory Analysis of Multiple Antenna Communication Systems*. Ph.D. thesis, School Elect. Inf. Eng., Telecommun. Lab., Faculty Eng. Inf. Technol., Univ. Sydney, 2006.
- [173] O. S. Nishimura, J. C. Marinello, and T. Abrão, "A grant-based random access protocol in extra-large massive MIMO system," *IEEE Commun. Lett.*, vol. 24, no. 11, pp. 2478–2482, Nov. 2020.
- [174] A. Amiri, C. N. Manchón, and E. De Carvalho, "A message passing based receiver for extra-large scale MIMO," in *Proc. IEEE 8th Int. Workshop Comput. Adv. Multi-Sensor Adapt. Process. (CAMSAP)*, Dec. 2019, pp. 564–568.
- [175] —, "Uncoordinated and decentralized processing in extra-large MIMO arrays," *IEEE Wireless Commun. Lett.*, vol. 11, no. 1, pp. 81–85, Jan. 2022.
- [176] J. C. Marinello, T. Abrão, A. Amiri, E. De Carvalho, and P. Popovski, "Antenna selection for improving energy efficiency in XL-MIMO systems," *IEEE Trans. Veh. Technol.*, vol. 69, no. 11, pp. 13 305–13 318, Nov. 2020.
- [177] J. H. I. de Souza, A. Amiri, T. Abrão, E. De Carvalho, and P. Popovski, "Quasi-distributed antenna selection for spectral efficiency maximization in subarray switching XL-MIMO systems," *IEEE Trans. Veh. Technol.*, vol. 70, no. 7, pp. 6713–6725, Jul. 2021.
- [178] D. W. M. Guerra and T. Abrão, "Clustered double-scattering channel modeling for XL-MIMO with uniform arrays," *IEEE Access*, vol. 10, pp. 20 173–20 186, 2022.
- [179] H. Shin and J. H. Lee, "Capacity of multiple-antenna fading channels: Spatial fading correlation, double scattering, and keyhole," *IEEE Trans. Inf. Theory*, vol. 49, no. 10, pp. 2636–2647, Oct. 2003.
- [180] A. Amiri, S. Rezaie, C. N. Manchón, and E. De Carvalho, "Distributed receiver processing for extra-large MIMO arrays: A message passing approach," *IEEE Trans. Wireless Commun.*, vol. 21, no. 4, pp. 2654–2667, Apr. 2021.
- [181] D. Gesbert, H. Bolcskei, D. A. Gore, and A. J. Paulraj, "Outdoor MIMO wireless channels: Models and performance prediction," *IEEE Trans. Commun.*, vol. 50, no. 12, pp. 1926–1934, Dec. 2002.
- [182] T. Zwick, C. Fischer, and W. Wiesbeck, "A stochastic multipath channel model including path directions for indoor environments," *IEEE J. Sel. Areas Commun.*, vol. 20, no. 6, pp. 1178–1192, Aug. 2002.
- [183] R. Heddergott and P. Truffer, "Statistical characteristics of indoor radio propagation in NLOS scenarios," 2000, Tech. Rep. COST 259, Valencia, Spain, Tech. Rep. COST 259 TD(00) 024.
- [184] T. K. Sarkar, Z. Ji, K. Kim, A. Medouri, and M. Salazar-Palma, "A survey of various propagation models for mobile communication," *IEEE Antennas Propag. Mag.*, vol. 45, no. 3, pp. 51–82, Jun. 2003.
- [185] W. C. Chew, *Waves and Fields in Inhomogeneous Media*. Hoboken, NJ, USA: John Wiley & Sons, 1995.
- [186] H. Weyl, "Ausbreitung elektromagnetischer Wellen über einem ebenen Leiter," *J. Roy. Stat. Soc.*, vol. 365, no. 21, pp. 481–500, 1919.
- [187] D. S. Saxon, "Tensor scattering matrix for the electromagnetic field," *Phys. Rev.*, vol. 100, no. 6, p. 1771, Dec. 1955.
- [188] E. Gerjuoy and D. S. Saxon, "Variational principles for the acoustic field," *Phys. Rev.*, vol. 94, no. 6, p. 1445, Jun. 1954.
- [189] D. M. Kerns, "Plane-wave scattering-matrix theory of antennas and antenna-antenna interactions-formulation and applications," *J. Res. B Math. Sci. B*, vol. 80-B, no. 1, pp. 5–51, 1976.
- [190] M. Nieto-Vesperinas and E. Wolf, "Generalized stokes reciprocity relations for scattering from dielectric objects of arbitrary shape," *J. Opt. Soc. America A Opt. Image Sci. Vis.*, vol. 3, no. 12, pp. 2038–2046, 1986.
- [191] J. A. Stratton, *Electromagnetic Theory*. Hoboken, NJ, USA: Wiley, 2007, vol. 33.
- [192] A. Pizzo, L. Sanguinetti, and T. L. Marzetta, "Spatial characterization of electromagnetic random channels," *IEEE Open J. Commun. Soc.*, vol. 3, pp. 847–866, 2022.
- [193] I. S. Gradshteyn and I. M. Ryzhik, *Table of Integrals, Series, and Products*. New York, NY, USA: Academic, 2014.
- [194] A. Pizzo, T. L. Marzetta, and L. Sanguinetti, "Spatially-stationary model for holographic MIMO small-scale fading," *IEEE J. Sel. Areas Commun.*, vol. 38, no. 9, pp. 1964–1979, Sep. 2020.
- [195] A. Pizzo, L. Sanguinetti, and T. L. Marzetta, "Fourier plane-wave series expansion for holographic MIMO communications," *IEEE Trans. Wireless Commun.*, vol. 21, no. 9, pp. 6890–6905, Sep. 2022.
- [196] V. V. Veeravalli, Y. Liang, and A. M. Sayeed, "Correlated MIMO wireless channels: Capacity, optimal signaling, and asymptotics," *IEEE Trans. Inf. Theory*, vol. 51, no. 6, pp. 2058–2072, Jun. 2005.
- [197] T. L. Marzetta, "Spatially-stationary propagating random field model for massive MIMO small-scale fading," in *Proc. IEEE Int. Symp. Inf. Theory (ISIT)*, Jun. 2018, pp. 391–395.
- [198] A. Pizzo, T. Marzetta, and L. Sanguinetti, "Holographic MIMO communications under spatially-stationary scattering," in *Proc. 54th Asilomar Conf. Signals, Syst., Comput. (ASILOMAR)*, Nov. 2020, pp. 702–706.
- [199] X. Gao, B. Jiang, X. Li, A. B. Gershman, and M. R. McKay, "Statistical eigenmode transmission over jointly correlated MIMO channels," *IEEE Trans. Inf. Theory*, vol. 55, no. 8, pp. 3735–3750, Aug. 2009.
- [200] Y. Liu, M. Zhang, and T. Wang, "Effect of antenna pattern on the electromagnetic MIMO communication," in *Proc. IEEE 22nd Int. Conf. Commun. Technol. (ICCT)*, Nov. 2022, pp. 148–151.
- [201] T. Wang, W. Han, Z. Zhong, J. Pang, G. Zhou, S. Wang, and Q. Li, "Electromagnetic-compliant channel modeling and performance evaluation for holographic MIMO," in *Proc. IEEE Globecom Workshops (GC Wkshps)*, Dec. 2022, pp. 747–752.
- [202] Y. Zhang, J. Zhang, Y. Zhang, Y. Yao, and G. Liu, "Capacity analysis of holographic MIMO channels with practical constraints," *IEEE Wireless Commun. Lett.*, vol. 12, no. 6, pp. 1101–1105, Jun. 2023.

- [203] L. Wei, C. Huang, G. C. Alexandropoulos, E. Wei, Z. Zhang, M. Debbah, and C. Yuen, "Multi-user holographic MIMO surfaces: Channel modeling and spectral efficiency analysis," *IEEE J. Sel. Topics Signal Process.*, vol. 16, no. 5, pp. 1112–1124, Aug. 2022.
- [204] S. Bahanshal, Q.-U.-A. Nadeem, and M. J. Hossain, "Holographic MIMO: How many antennas do we need for energy efficient transmission?" in *Proc. IEEE Int. Conf. Commun. Workshops (ICC Wkshps)*, May 2023, pp. 1228–1233.
- [205] H. Lei, Z. Wang, H. Xiao, J. Zhang, and B. Ai, "Uplink performance of cell-free extremely large-scale MIMO systems," *arXiv preprint arXiv:2301.12086*, 2023.
- [206] Z. Liu, Z. Liu, X. Wang, J. Li, J. Zhang, and B. Ai, "Antenna selection of cell-free XL-MIMO systems with multi-agent reinforcement learning," in *Proc. Int. Conf. Ubiqu. Commun. (Ucom)*, Jul. 2023, pp. 379–383.
- [207] Z. Liu, Z. Liu, J. Zhang, H. Xiao, B. Ai, and D. W. K. Ng, "Uplink power control for extremely large-scale MIMO with multi-agent reinforcement learning and fuzzy logic," in *Proc. IEEE Conf. Comput. Commun. Workshops (INFOCOM WKSHPs)*, May 2023, pp. 1–6.
- [208] X. Zhang, S. Song, and K. B. Letaief, "Fundamental limits of holographic MIMO channels: Tackling non-separable transceiver correlation," *arXiv preprint arXiv:2304.00223*, 2023.
- [209] J. Zhang, C. Pan, F. Pei, G. Liu, and X. Cheng, "Three-dimensional fading channel models: A survey of elevation angle research," *IEEE Commun. Mag.*, vol. 52, no. 6, pp. 218–226, Jun. 2014.
- [210] Z. Hu, C. Chen, Y. Jin, L. Zhou, and Q. Wei, "Hybrid-field channel estimation for extremely large-scale massive MIMO system," *IEEE Commun. Lett.*, vol. 27, no. 1, pp. 303–307, Jan. 2023.
- [211] H. ElSawy, E. Hossain, and M. Haenggi, "Stochastic geometry for modeling, analysis, and design of multi-tier and cognitive cellular wireless networks: A survey," *IEEE Commun. Surveys Tuts.*, vol. 15, no. 3, pp. 996–1019, 3rd Quart., 2013.
- [212] R. W. Heath Jr and A. Lozano, *Foundations of MIMO Communication*. Cambridge, U.K.: Cambridge Univ. Press, 2018.
- [213] J. Xu and R. Janaswamy, "Electromagnetic degrees of freedom in 2-D scattering environments," *IEEE Trans. Antennas Propag.*, vol. 54, no. 12, pp. 3882–3894, Dec. 2006.
- [214] J. Xu, D. L. Goeckel, and R. Janaswamy, "The capacity of MIMO systems with increasing SNR by electromagnetic analysis," *IEEE Trans. Wireless Commun.*, vol. 8, no. 9, pp. 4752–4761, Sep. 2009.
- [215] P. Almers, F. Tufvesson, P. Karlsson, and A. F. Molisch, "The effect of horizontal array orientation on MIMO channel capacity," in *Proc. IEEE 57th Veh. Technol. Conf. (VTC-Spring)*, vol. 1, Apr. 2003, pp. 34–38.
- [216] D. McNamara, M. Beach, P. Fletcher, and P. Karlsson, "Temporal variation of multiple-input multiple-output (MIMO) channels in indoor environments," in *Proc. 7th Int. Conf. Antennas Propag. (ICAP)*, vol. 2, Apr. 2001, pp. 578–582.
- [217] M. A. Jensen and J. W. Wallace, "RF and algorithmic considerations for practical MIMO wireless implementation," in *Proc. IEEE Radio Wireless Conf. (RAWCON)*, Sep. 2004, pp. 147–150.
- [218] O. M. Bucci and G. Franceschetti, "On the degrees of freedom of scattered fields," *IEEE Trans. Antennas Propag.*, vol. 37, no. 7, pp. 918–926, Jul. 1989.
- [219] M. D. Migliore, "On the role of the number of degrees of freedom of the field in MIMO channels," *IEEE Trans. Antennas Propag.*, vol. 54, no. 2, pp. 620–628, Feb. 2006.
- [220] M. Franceschetti, M. D. Migliore, P. Minero, and F. Schettino, "The information carried by scattered waves: Near-field and nonasymptotic regimes," *IEEE Trans. Antennas Propag.*, vol. 63, no. 7, pp. 3144–3157, Jul. 2015.
- [221] S. S. Yuan, Z. He, X. Chen, C. Huang, and E. Wei, "Electromagnetic effective degree of freedom of an MIMO system in free space," *IEEE Antennas and Wireless Propag. Lett.*, vol. 21, no. 3, pp. 446–450, Mar. 2022.
- [222] M. O'Neil, L. Greengard, and A. Pataki, "On the efficient representation of the half-space impedance Green's function for the Helmholtz equation," *Wave Motion*, vol. 51, no. 1, pp. 1–13, Jan. 2014.
- [223] Y. Jiang and F. Gao, "Electromagnetic channel model for near field MIMO systems in the half space," *IEEE Commun. Lett.*, vol. 27, no. 2, pp. 706–710, Feb. 2022.
- [224] S. McKee, D. Wall, and S. Wilson, "An alternating direction implicit scheme for parabolic equations with mixed derivative and convective terms," *J. Comput. Phys.*, vol. 126, no. 1, pp. 64–76, Nov. 1996.
- [225] A. A. Zaporozhets and M. F. Levy, "Bistatic RCS calculations with the vector parabolic equation method," *IEEE Trans. Antennas Propag.*, vol. 47, no. 11, pp. 1688–1696, Nov. 1999.
- [226] Y. Shen, Z. He, E. Wei, S. S. Yuan, and X. Chen, "Electromagnetic effective-degree-of-freedom prediction with parabolic equation method," *IEEE Trans. Antennas Propag.*, vol. 71, no. 4, pp. 3752–3757, Apr. 2023.
- [227] G. Bartoli, A. Abrardo, N. Decarli, D. Dardari, and M. Di Renzo, "Spatial multiplexing in near field MIMO channels with reconfigurable intelligent surfaces," *IET Signal Process.*, vol. 17, no. 3, pp. 1–17, 2023.
- [228] X. Pu, S. Shao, K. Deng, and Y. Tang, "Effects of array orientations on degrees of freedom for 3D LoS channels in short-range communications," *IEEE Wireless Commun. Lett.*, vol. 4, no. 1, pp. 106–109, Feb. 2014.
- [229] D. Slepian, "Some asymptotic expansions for prolate spheroidal wave functions," *J. Math. Phys.*, vol. 44, no. 1-4, pp. 99–140, 1965.
- [230] J. C. Ruiz-Sicilia, M. Di Renzo, M. D. Migliore, M. Debbah, and H. V. Poor, "On the degrees of freedom and eigenfunctions of line-of-sight holographic MIMO communications," *arXiv preprint arXiv:2308.08009*, 2023.
- [231] A. Walthers, "Gabor's theorem and energy transfer through lenses," *J. Opt. Soc. America*, vol. 57, no. 5, pp. 639–644, 1967.
- [232] N. Decarli and D. Dardari, "Communication modes with large intelligent surfaces in the near field," *IEEE Access*, vol. 9, pp. 165 648–165 666, 2021.
- [233] H. Landau, "On Szegő's eigenvalue distribution theorem and non-Hermitian kernels," *J. d'Analyse Mathématique*, vol. 28, no. 1, pp. 335–357, 1975.
- [234] H. J. Landau and H. Widom, "Eigenvalue distribution of time and frequency limiting," *J. Math. Anal. Appl.*, vol. 77, no. 2, pp. 469–481, 1980.
- [235] M. Franceschetti, "On Landau's eigenvalue theorem and information cut-sets," *IEEE Trans. Inf. Theory*, vol. 61, no. 9, pp. 5042–5051, Sep. 2015.
- [236] A. Pizzo and A. Lozano, "On Landau's eigenvalue theorem for line-of-sight MIMO channels," *IEEE Wireless Commun. Lett.*, vol. 11, no. 12, pp. 2565–2569, Dec. 2022.
- [237] H. Do, N. Lee, and A. Lozano, "Parabolic wavefront model for line-of-sight MIMO channels," *IEEE Trans. Wireless Commun.*, vol. 22, no. 11, pp. 7620–7634, Nov. 2023.
- [238] —, "Line-of-sight MIMO via intelligent reflecting surface," *IEEE Trans. Wireless Commun.*, vol. 22, no. 6, pp. 4215–4231, Jun. 2023.
- [239] A. Pizzo, A. de Jesus Torres, L. Sanguinetti, and T. L. Marzetta, "Nyquist sampling and degrees of freedom of electromagnetic fields," *IEEE Trans. Signal Process.*, vol. 70, pp. 3935–3947, 2022.
- [240] L. Ding, E. G. Ström, and J. Zhang, "Degrees of freedom in 3D linear large-scale antenna array communications—a spatial bandwidth approach," *IEEE J. Sel. Areas Commun.*, vol. 40, no. 10, pp. 2805–2822, Oct. 2022.
- [241] X. Q. Zhang, R. W. Shao, H. Xu, J. W. Wu, and T. J. Cui, "Electromagnetic effective degree of freedom of MIMO system in nonfree space," in *Proc. Int. Appl. Comput. Electromagn. Soc. Symp. (ACES-China)*, Dec. 2022, pp. 1–3.
- [242] S. S. Yuan, Z. He, S. Sun, X. Chen, C. Huang, and W. E. Sha, "Electromagnetic effective-degree-of-freedom limit of a MIMO system in 2-D inhomogeneous environment," *Electronics*, vol. 11, no. 19, p. 3232, 2022.
- [243] S. S. Yuan and E. Wei, "Electromagnetic degree of freedom of a MIMO communication system," in *Proc. IEEE 5th Int. Conf. Electron. Inf. Commun. Technol. (ICEICT)*, Aug. 2022, pp. 667–669.
- [244] Y. Wang, X. Chen, X. Liu, J. Yi, J. Chen, A. Zhang, and A. A. Kishk, "Improvement of diversity and capacity of MIMO system using scatterer array," *IEEE Trans. Antennas Propag.*, vol. 70, no. 1, pp. 789–794, Jan. 2021.
- [245] S. S. Yuan, X. Chen, C. Huang, and E. Wei, "Effects of mutual coupling on degree of freedom and antenna efficiency in holographic MIMO communications," *IEEE Open J. Antennas Propag.*, vol. 4, pp. 237–244, 2023.
- [246] R. Ji, S. Chen, C. Huang, J. Yang, E. Wei, Z. Zhang, C. Yuen, and M. Debbah, "Extra DoF of near-field holographic MIMO communications leveraging evanescent waves," *IEEE Wireless Commun. Lett.*, vol. 12, no. 4, pp. 580–584, Apr. 2023.
- [247] A. Pizzo, T. L. Marzetta, and L. Sanguinetti, "Degrees of freedom of holographic MIMO channels," in *Proc. IEEE 21st Int. Workshop Signal Process. Adv. Wireless Commun. (SPAWC)*, May 2020, pp. 1–5.

- [248] E. Björnson and L. Sanguinetti, "Rayleigh fading modeling and channel hardening for reconfigurable intelligent surfaces," *IEEE Wireless Commun. Lett.*, vol. 10, no. 4, pp. 830–834, Apr. 2020.
- [249] S. Sun and H. Yan, "Small-scale spatial-temporal correlation and degrees of freedom for reconfigurable intelligent surfaces," *IEEE Wireless Commun. Lett.*, vol. 10, no. 12, pp. 2698–2702, Dec. 2021.
- [250] S. Sun and M. Tao, "Characteristics of channel eigenvalues and mutual coupling effects for holographic reconfigurable intelligent surfaces," *Sensors*, vol. 22, no. 14, p. 5297, 2022.
- [251] L. Hanlen and M. Fu, "Wireless communication systems with-spatial diversity: A volumetric model," *IEEE Trans. Wireless Commun.*, vol. 5, no. 1, pp. 133–142, Jan. 2006.
- [252] B. H. Fleury, "First-and second-order characterization of direction dispersion and space selectivity in the radio channel," *IEEE Trans. Inf. Theory*, vol. 46, no. 6, pp. 2027–2044, Sep. 2000.
- [253] A. Jones and L. Bayvel, *Electromagnetic Scattering and its Applications*. London, U.K.: Applied Science Publishers Ltd., 1981.
- [254] O. Bucci and G. Franceschetti, "On the spatial bandwidth of scattered fields," *IEEE Trans. Antennas Propag.*, vol. 35, no. 12, pp. 1445–1455, Dec. 1987.
- [255] H. Q. Ngo, E. G. Larsson, and T. L. Marzetta, "Energy and spectral efficiency of very large multiuser MIMO systems," *IEEE Trans. Commun.*, vol. 61, no. 4, pp. 1436–1449, Apr. 2013.
- [256] Q. Wu and R. Zhang, "Intelligent reflecting surface enhanced wireless network via joint active and passive beamforming," *IEEE Trans. Wireless Commun.*, vol. 18, no. 11, pp. 5394–5409, Nov. 2019.
- [257] E. Basar, M. Di Renzo, J. De Rosny, M. Debbah, M.-S. Alouini, and R. Zhang, "Wireless communications through reconfigurable intelligent surfaces," *IEEE Access*, vol. 7, pp. 116 753–116 773, 2019.
- [258] E. Björnson and L. Sanguinetti, "Demystifying the power scaling law of intelligent reflecting surfaces and metasurfaces," in *Proc. IEEE 8th Int. Workshop Comput. Adv. Multi-Sensor Adapt. Process. (CAMSAP)*, Dec. 2019, pp. 549–553.
- [259] B. Zheng and R. Zhang, "Simultaneous transmit diversity and passive beamforming with large-scale intelligent reflecting surface," *IEEE Trans. Wireless Commun.*, vol. 22, no. 2, pp. 920–933, Feb. 2023.
- [260] X. Li, H. Lu, Y. Zeng, S. Jin, and R. Zhang, "Near-field modeling and performance analysis of modular extremely large-scale array communications," *IEEE Commun. Lett.*, vol. 26, no. 7, pp. 1529–1533, Jul. 2022.
- [261] C. Feng, H. Lu, Y. Zeng, S. Jin, and R. Zhang, "Wireless communication with extremely large-scale intelligent reflecting surface," in *Proc. IEEE/CIC Int. Conf. Commun. China (ICCC Wkshps)*, Jul. 2021, pp. 165–170.
- [262] S. Zeng, H. Zhang, B. Di, H. Qin, X. Su, and L. Song, "Reconfigurable refractive surfaces: An energy-efficient way to holographic MIMO," *IEEE Commun. Lett.*, vol. 26, no. 10, pp. 2490–2494, Oct. 2022.
- [263] R. Deng, B. Di, H. Zhang, and L. Song, "HDMA: Holographic-pattern division multiple access," *IEEE J. Sel. Areas Commun.*, vol. 40, no. 4, pp. 1317–1332, Apr. 2022.
- [264] Q. Zhang, S. Jin, K.-K. Wong, H. Zhu, and M. Matthaiou, "Power scaling of uplink massive MIMO systems with arbitrary-rank channel means," *IEEE J. Sel. Topics Signal Process.*, vol. 8, no. 5, pp. 966–981, Oct. 2014.
- [265] H. Do, N. Lee, and A. Lozano, "Reconfigurable ULAs for line-of-sight MIMO transmission," *IEEE Trans. Wireless Commun.*, vol. 20, no. 5, pp. 2933–2947, May 2021.
- [266] A. de Jesus Torres, L. Sanguinetti, and E. Björnson, "Near-and far-field communications with large intelligent surfaces," in *Proc. 54th Asilomar Conf. Signals, Syst., Comput. (ASILOMAR)*, Nov. 2020, pp. 564–568.
- [267] H. Lu and Y. Zeng, "Near-field modeling and performance analysis for multi-user extremely large-scale MIMO communication," *IEEE Commun. Lett.*, vol. 26, no. 2, pp. 277–281, Feb. 2021.
- [268] T. Gong, L. Wei, C. Huang, Z. Yang, J. He, M. Debbah, and C. Yuen, "Holographic MIMO communications with arbitrary surface placements: Near-field LoS channel model and capacity limit," *IEEE J. Sel. Areas Commun.*, Early Access, 2024.
- [269] F. Rusek and A. Prlja, "Optimal channel shortening for MIMO and ISI channels," *IEEE Trans. Wireless Commun.*, vol. 11, no. 2, pp. 810–818, Feb. 2011.
- [270] S. Hu, X. Gao, and F. Rusek, "Linear precoder design for MIMO-ISI broadcasting channels under channel shortening detection," *IEEE Signal Process. Lett.*, vol. 23, no. 9, pp. 1207–1211, Sep. 2016.
- [271] J. Mercer, "Functions of positive and negative type, and their connection the theory of integral equations," *Philos. Trans. Roy. Soc. London A, Containing Papers Math. Phys. Character*, vol. 209, no. 441-458, pp. 415–446, Jan. 1909.
- [272] B. Simon, *Trace Ideals and Their Applications*. Providence, RI, USA: American Mathematical Society, 2005, no. 120.
- [273] Z. Wan, J. Zhu, and L. Dai, "Can continuous aperture MIMO obtain more mutual information than discrete MIMO?" *IEEE Commun. Lett.*, vol. 27, no. 12, pp. 3185–3189, Dec. 2023.
- [274] L. Sanguinetti, A. A. D'Amico, and M. Debbah, "Wavenumber-division multiplexing in line-of-sight holographic MIMO communications," *IEEE Trans. Wireless Commun.*, vol. 22, no. 4, pp. 2186–2201, Apr. 2023.
- [275] A. A. D'Amico, L. Sanguinetti, and M. Debbah, "Performance analysis of WDM in LoS communications with arbitrary orientation and position," *IEEE Wireless Commun. Lett.*, vol. 11, no. 9, pp. 1880–1884, Sep. 2022.
- [276] X. Yang, X. Li, S. Zhang, and S. Jin, "On the ergodic capacity of mmWave systems under finite-dimensional channels," *IEEE Trans. Wireless Commun.*, vol. 18, no. 11, pp. 5440–5453, Nov. 2019.
- [277] B. Xu, Z. Wang, H. Xiao, J. Zhang, B. Ai, and D. W. Kwan Ng, "Low-complexity precoding for extremely large-scale MIMO over non-stationary channels," in *Proc. IEEE Int. Conf. Commun. (ICC)*, May 2023, pp. 6516–6522.
- [278] K. Mullen, "A note on the ratio of two independent random variables," *Amer. Statist.*, vol. 21, no. 3, pp. 30–31, Jun. 1967.
- [279] A. Grant, "Rayleigh fading multi-antenna channels," *EURASIP J. Appl. Signal Process.*, vol. 2002, pp. 316–329, Mar. 2002.
- [280] E. T. Browne, *Introduction to the Theory of Determinants and Matrices*. Chapel Hill, NC, USA: Univ. North Carolina Press, 1958.
- [281] R. Couillet, M. Debbah, and J. W. Silverstein, "A deterministic equivalent for the analysis of correlated MIMO multiple access channels," *IEEE Trans. Inf. Theory*, vol. 57, no. 6, pp. 3493–3514, Jun. 2011.
- [282] J.-J. Van De Beek, O. Edfors, M. Sandell, S. K. Wilson, and P. O. Borjesson, "On channel estimation in OFDM systems," in *Proc. IEEE 45th Veh. Technol. Conf. Countdown Wireless 21st Century*, vol. 2, IEEE, Jul. 1995, pp. 815–819.
- [283] W. U. Bajwa, J. Haupt, A. M. Sayeed, and R. Nowak, "Compressed channel sensing: A new approach to estimating sparse multipath channels," *Proc. IEEE*, vol. 98, no. 6, pp. 1058–1076, Jun. 2010.
- [284] A. Alkhateeb, O. El Ayach, G. Leus, and R. W. Heath, "Channel estimation and hybrid precoding for millimeter wave cellular systems," *IEEE J. Sel. Topics Signal Process.*, vol. 8, no. 5, pp. 831–846, Oct. 2014.
- [285] J. Lee, G.-T. Gil, and Y. H. Lee, "Channel estimation via orthogonal matching pursuit for hybrid MIMO systems in millimeter wave communications," *IEEE Trans. Commun.*, vol. 64, no. 6, pp. 2370–2386, Jun. 2016.
- [286] Z. Guo, X. Wang, and W. Heng, "Millimeter-wave channel estimation based on 2-D beamspace MUSIC method," *IEEE Trans. Wireless Commun.*, vol. 16, no. 8, pp. 5384–5394, Aug. 2017.
- [287] A. Liao, Z. Gao, Y. Wu, H. Wang, and M.-S. Alouini, "2D unitary ESPRIT based super-resolution channel estimation for millimeter-wave massive MIMO with hybrid precoding," *IEEE Access*, vol. 5, pp. 24 747–24 757, Nov. 2017.
- [288] R. Shafin, L. Liu, Y. Li, A. Wang, and J. Zhang, "Angle and delay estimation for 3-D massive MIMO/FD-MIMO systems based on parametric channel modeling," *IEEE Trans. Wireless Commun.*, vol. 16, no. 8, pp. 5370–5383, Aug. 2017.
- [289] X. Guo, Y. Chen, and Y. Wang, "Compressed channel estimation for near-field XL-MIMO using triple parametric decomposition," *IEEE Trans. Veh. Technol.*, vol. 72, no. 11, pp. 15 040–15 045, Nov. 2023.
- [290] X. Zhang, H. Zhang, and Y. C. Eldar, "Near-field sparse channel representation and estimation in 6G wireless communications," *IEEE Trans. Commun.*, Early Access, 2023.
- [291] J. Cao, J. Du, M. Han, J. Liu, X. Li, and D. B. da Costa, "Efficient sparse Bayesian channel estimation for near-field ultra-scale massive MIMO systems," *IEEE Wireless Commun. Lett.*, vol. 12, no. 12, pp. 2133–2137, Dec. 2023.
- [292] M. Cui and L. Dai, "Near-field wideband channel estimation for extremely large-scale MIMO," *Sci. China. Inf. Sci.*, vol. 66, no. 7, p. 172303, Jun. 2023.
- [293] A. M. Elbir, W. Shi, A. K. Papazafeiropoulos, P. Kourtessis, and S. Chatzinos, "Near-field Terahertz communications: Model-based and model-free channel estimation," *IEEE Access*, vol. 11, pp. 36 409–36 420, Apr. 2023.
- [294] W. Yang, M. Li, and Q. Liu, "A practical channel estimation strategy for XL-MIMO communication systems," *IEEE Commun. Lett.*, vol. 27, no. 6, pp. 1580–1583, Jun. 2023.

- [295] S. Tarboush, A. Ali, and T. Y. Al-Naffouri, "Cross-field channel estimation for ultra massive-MIMO THz systems," *arXiv preprint arXiv:2305.13757*, 2023.
- [296] K. Seo, G.-T. Gil, G. Kwon, S. Hong, and H. Park, "Cumulant matrix-based channel estimation for near-field massive MIMO systems," in *Proc. 12th Int. Conf. Inf. Commun. Technol. Converg.*, Oct. 2021, pp. 1603–1608.
- [297] M. Ghermezcheshmeh and N. Zlatanov, "Parametric channel estimation for LoS dominated holographic massive MIMO systems," *IEEE Access*, vol. 11, pp. 44 711–44 724, May 2023.
- [298] X. Zhu, Y. Liu, and C.-X. Wang, "Sub-array based millimeter wave massive MIMO channel estimation," *IEEE Wireless Commun. Lett.*, vol. 12, no. 9, pp. 1608–1612, Sep. 2023.
- [299] H. Lei, J. Zhang, H. Xiao, X. Zhang, B. Ai, and D. W. K. Ng, "Channel estimation for XL-MIMO systems with polar-domain multi-scale residual dense network," *IEEE Trans. Veh. Technol.*, Early Access, 2023.
- [300] X. Zhang, Z. Wang, H. Zhang, and L. Yang, "Near-field channel estimation for extremely large-scale array communications: A model-based deep learning approach," *IEEE Commun. Lett.*, vol. 27, no. 4, pp. 1155–1159, Apr. 2023.
- [301] Y. Chen, L. Yan, and C. Han, "Hybrid spherical-and planar-wave modeling and DCNN-powered estimation of Terahertz ultra-massive MIMO channels," *IEEE Trans. Commun.*, vol. 69, no. 10, pp. 7063–7076, Oct. 2021.
- [302] W. Yu, Y. Shen, H. He, X. Yu, S. Song, J. Zhang, and K. B. Letaief, "An adaptive and robust deep learning framework for THz ultra-massive MIMO channel estimation," *IEEE J. Sel. Topics Signal Process.*, vol. 17, no. 4, pp. 761–776, Jul. 2023.
- [303] A. L. Swindlehurst, G. Zhou, R. Liu, C. Pan, and M. Li, "Channel estimation with reconfigurable intelligent surfaces—A general framework," *Proc. IEEE*, vol. 110, no. 9, pp. 1312–1338, Sep. 2022.
- [304] H. L. Van Trees, *Optimum Array Processing: Part IV of Detection, Estimation, and Modulation theory*. John Wiley & Sons, 2002.
- [305] R. J. Mailloux, *Phased Array Antenna Handbook*. Artech house, 2017.
- [306] X. Song, W. Rave, N. Babu, S. Majhi, and G. Fettweis, "Two-level spatial multiplexing using hybrid beamforming for millimeter-wave backhaul," *IEEE Trans. Wireless Commun.*, vol. 17, no. 7, pp. 4830–4844, Jul. 2018.
- [307] L. Yan, Y. Chen, C. Han, and J. Yuan, "Joint inter-path and intra-path multiplexing for Terahertz widely-spaced multi-subarray hybrid beamforming systems," *IEEE Trans. Commun.*, vol. 70, no. 2, pp. 1391–1406, Feb. 2021.
- [308] X. Li, Z. Dong, Y. Zeng, S. Jin, and R. Zhang, "Multi-user modular XL-MIMO communications: Near-field and beam focusing pattern and user grouping," *arXiv preprint arXiv:2308.11289*, 2023.
- [309] Z. Wu, M. Cui, and L. Dai, "Enabling more users to benefit from near-field communications: From linear to circular array," *IEEE Trans. Wireless Commun.*, Early Access, 2023.
- [310] R. W. Heath, N. Gonzalez-Prelcic, S. Rangan, W. Roh, and A. M. Sayeed, "An overview of signal processing techniques for millimeter wave MIMO systems," *IEEE J. Sel. Topics Signal Process.*, vol. 10, no. 3, pp. 436–453, Apr. 2016.
- [311] E. Björnson, Y. C. Eldar, E. G. Larsson, A. Lozano, and H. V. Poor, "Twenty-five years of signal processing advances for multiantenna communications: From theory to mainstream technology," *IEEE Signal Process. Mag.*, vol. 40, no. 4, pp. 107–117, Jun. 2023.
- [312] Z. Wu, M. Cui, Z. Zhang, and L. Dai, "Distance-aware precoding for near-field capacity improvement in XL-MIMO," in *Proc. IEEE 95th Veh. Technol. Conf. (VTC-Spring)*, Jun. 2022, pp. 1–5.
- [313] X. Zhang, A. F. Molisch, and S.-Y. Kung, "Variable-phase-shift-based rf-baseband codesign for MIMO antenna selection," *IEEE Trans. Signal Process.*, vol. 53, no. 11, pp. 4091–4103, Nov. 2005.
- [314] F. Sohrabi and W. Yu, "Hybrid digital and analog beamforming design for large-scale antenna arrays," *IEEE J. Sel. Topics Signal Process.*, vol. 10, no. 3, pp. 501–513, Apr. 2016.
- [315] T. E. Bogale, L. B. Le, A. Haghigat, and L. Vandendorpe, "On the number of RF chains and phase shifters, and scheduling design with hybrid analog–digital beamforming," *IEEE Trans. Wireless Commun.*, vol. 15, no. 5, pp. 3311–3326, May 2016.
- [316] B. Wang, F. Gao, S. Jin, H. Lin, and G. Y. Li, "Spatial-and frequency-wideband effects in millimeter-wave massive MIMO systems," *IEEE Trans. Signal Process.*, vol. 66, no. 13, pp. 3393–3406, Jul. 2018.
- [317] H. Hashemi, T.-S. Chu, and J. Roderick, "Integrated true-time-delay-based ultra-wideband array processing," *IEEE Commun. Mag.*, vol. 46, no. 9, pp. 162–172, Sep. 2008.
- [318] M. Longbrake, "True time-delay beamsteering for radar," in *Proc. IEEE Nat. Aerosp. Electron. Conf. (NAECON)*, Jul. 2012, pp. 246–249.
- [319] R. Rotman, M. Tur, and L. Yaron, "True time delay in phased arrays," *Proc. IEEE*, vol. 104, no. 3, pp. 504–518, Mar. 2016.
- [320] B. Zhai, Y. Zhu, A. Tang, and X. Wang, "THzPrism: Frequency-based beam spreading for Terahertz communication systems," *IEEE Wireless Commun. Lett.*, vol. 9, no. 6, pp. 897–900, Jun. 2020.
- [321] Z. Wang, X. Mu, Y. Liu, and R. Schober, "TTD configurations for near-field beamforming: Parallel, serial, or hybrid?" *arXiv preprint arXiv:2309.06861*, 2023.
- [322] F. Gao, B. Wang, C. Xing, J. An, and G. Y. Li, "Wideband beamforming for hybrid massive MIMO Terahertz communications," *IEEE J. Sel. Areas Commun.*, vol. 39, no. 6, pp. 1725–1740, Jun. 2021.
- [323] L. Dai, J. Tan, Z. Chen, and H. V. Poor, "Delay-phase precoding for wideband thz massive MIMO," *IEEE Trans. Wireless Commun.*, vol. 21, no. 9, pp. 7271–7286, Sep. 2022.
- [324] Z. Wang, X. Mu, and Y. Liu, "Beamfocusing optimization for near-field wideband multi-user communications," *arXiv preprint arXiv:2306.16861*, 2023.
- [325] T. J. Cui, M. Q. Qi, X. Wan, J. Zhao, and Q. Cheng, "Coding metamaterials, digital metamaterials and programmable metamaterials," *Light Sci. Appl.*, vol. 3, no. 10, pp. e218–e218, Oct. 2014.
- [326] D. R. Smith, O. Yurduseven, L. P. Mancera, P. Bowen, and N. B. Kundtz, "Analysis of a waveguide-fed metasurface antenna," *Phys. Rev. Appl.*, vol. 8, no. 5, p. 054048, Nov. 2017.
- [327] E. Björnson, Ö. T. Demir, and L. Sanguinetti, "A primer on near-field beamforming for arrays and reconfigurable intelligent surfaces," in *Proc. 55th Asilomar Conf. Signals, Syst., Comput.*, Oct. 2021, pp. 105–112.
- [328] A. Kosasih and E. Björnson, "Finite beam depth analysis for large arrays," *arXiv preprint arXiv:2306.12367*, 2023.
- [329] L. Li, H. Li, Z. Chen, W. Chen, and S. Li, "An analytical range-angle dependent beam focusing model for Terahertz linear antenna array," *IEEE Wireless Commun. Lett.*, vol. 11, no. 9, pp. 1870–1874, Sep. 2022.
- [330] N. J. Myers and R. W. Heath, "Infocus: A spatial coding technique to mitigate misfocus in near-field LoS beamforming," *IEEE Trans. Wireless Commun.*, vol. 21, no. 4, pp. 2193–2209, Apr. 2022.
- [331] A. Singh, A. J. Alqaraghuli, and J. M. Jornet, "Wavefront engineering at Terahertz frequencies through intelligent reflecting surfaces," in *Proc. IEEE 23rd Int. Workshop Signal Process. Adv. Wireless Commun. (SPAWC)*, Jul. 2022, pp. 1–5.
- [332] A. Singh, V. Petrov, and J. M. Jornet, "Utilization of Bessel beams in wideband sub Terahertz communication systems to mitigate beamsplit effects in the near-field," in *Proc. IEEE Int. Conf. Acoust., Speech Signal Process. (ICASSP)*, Jun. 2023, pp. 1–5.
- [333] H. Zhang, N. Shlezinger, F. Guidi, D. Dardari, M. F. Imani, and Y. C. Eldar, "Beam focusing for near-field multiuser MIMO communications," *IEEE Trans. Wireless Commun.*, vol. 21, no. 9, pp. 7476–7490, Sep. 2022.
- [334] Y. Li, S. Gong, H. Liu, C. Xing, N. Zhao, and X. Wang, "Near-field beamforming optimization for holographic XL-MIMO multiuser systems," *IEEE Trans. Commun.*, Early Access, 2023.
- [335] Z. Zhang, Y. Liu, Z. Wang, X. Mu, and J. Chen, "Physical layer security in near-field communications," *arXiv preprint arXiv:2302.04189*, 2023.
- [336] W. Gao, X. Lu, C. Han, and Z. Chen, "On multiple-antenna techniques for physical-layer range security in the Terahertz band," *arXiv preprint arXiv:2201.06253*, 2022.
- [337] J. Xu, L. You, G. C. Alexandropoulos, X. Yi, W. Wang, and X. Gao, "Near-field wideband extremely large-scale MIMO transmission with holographic metasurface antennas," *arXiv preprint arXiv:2205.02533*, 2022.
- [338] Y. Zhang and A. Alkhateeb, "Deep learning of near field beam focusing in Terahertz wideband massive MIMO systems," *IEEE Wireless Commun. Lett.*, vol. 12, no. 3, pp. 535–539, Mar. 2023.
- [339] B. Ning, Z. Tian, W. Mei, Z. Chen, C. Han, S. Li, J. Yuan, and R. Zhang, "Beamforming technologies for ultra-massive MIMO in Terahertz communications," *IEEE Open J. Commun. Soc.*, vol. 4, pp. 614–658, Feb. 2023.
- [340] Z. Xiao, T. He, P. Xia, and X.-G. Xia, "Hierarchical codebook design for beamforming training in millimeter-wave communication," *IEEE Trans. Wireless Commun.*, vol. 15, no. 5, pp. 3380–3392, May 2016.
- [341] J. Chen, F. Gao, M. Jian, and W. Yuan, "Hierarchical codebook design for near-field mmwave MIMO communications systems," *IEEE Wireless Commun. Lett.*, vol. 12, no. 11, pp. 1926–1930, Nov. 2023.

- [342] Y. Lu, Z. Zhang, and L. Dai, "Hierarchical beam training for extremely large-scale MIMO: From far-field to near-field," *IEEE Trans. Commun.*, Early Access, 2023.
- [343] Y. Zhang, B. Di, H. Zhang, and L. Song, "Near-far field beamforming for holographic multiple-input multiple-output," *J. Commun. Inf. Netw.*, vol. 8, no. 2, pp. 99–110, Jun. 2023.
- [344] Y. Xie, B. Ning, L. Li, and Z. Chen, "Near-field beam training in THz communications: The merits of uniform circular array," *IEEE Wireless Commun. Lett.*, vol. 12, no. 4, pp. 575–579, Apr. 2023.
- [345] W. Liu, H. Ren, C. Pan, and J. Wang, "Deep learning based beam training for extremely large-scale massive MIMO in near-field domain," *IEEE Commun. Lett.*, vol. 27, no. 1, pp. 170–174, Jan. 2023.
- [346] X. Shi, J. Wang, Z. Sun, and J. Song, "Spatial-chirp codebook-based hierarchical beam training for extremely large-scale massive MIMO," *IEEE Trans. Wireless Commun.*, Early Access, 2023.
- [347] C. Wu, C. You, Y. Liu, L. Chen, and S. Shi, "Two-stage hierarchical beam training for near-field communications," *IEEE Trans. Veh. Technol.*, Early Access, 2023.
- [348] S. Hu, H. Wang, and M. C. Ilter, "Design of near-field beamforming for large intelligent surfaces," *IEEE Trans. Wireless Commun.*, Early Access, 2023.
- [349] T. Wang, J. Lv, H. Tong, and C. Yin, "Near-field beam training of intelligent reflecting surface: A novel two-layer codebook," *arXiv preprint arXiv:2303.06962*, 2023.
- [350] X. Zhang, H. Zhang, C. Li, Y. Huang, and L. Yang, "Environment-specific beam training for extremely large-scale MIMO systems via contrastive learning," *IEEE Commun. Lett.*, vol. 27, no. 10, pp. 2638–2642, Oct. 2023.
- [351] F. Liu, Y. Cui, C. Masouros, J. Xu, T. X. Han, Y. C. Eldar, and S. Buzzi, "Integrated sensing and communications: Toward dual-functional wireless networks for 6G and beyond," *IEEE J. Sel. Areas Commun.*, vol. 40, no. 6, pp. 1728–1767, Jun. 2022.
- [352] C. Sturm and W. Wiesbeck, "Waveform design and signal processing aspects for fusion of wireless communications and radar sensing," *Proc. IEEE*, vol. 99, no. 7, pp. 1236–1259, Jul. 2011.
- [353] W. Yuan, Z. Wei, S. Li, J. Yuan, and D. W. K. Ng, "Integrated sensing and communication-assisted orthogonal time frequency space transmission for vehicular networks," *IEEE J. Sel. Topics Signal Process.*, vol. 15, no. 6, pp. 1515–1528, Nov. 2021.
- [354] Z. Xiao and Y. Zeng, "Integrated sensing and communication with delay alignment modulation: Performance analysis and beamforming optimization," *IEEE Trans. Wireless Commun.*, vol. 22, no. 12, pp. 8904–8918, Dec. 2023.
- [355] J. A. Zhang, F. Liu, C. Masouros, R. W. Heath, Z. Feng, L. Zheng, and A. Petropulu, "An overview of signal processing techniques for joint communication and radar sensing," *IEEE J. Sel. Topics Signal Process.*, vol. 15, no. 6, pp. 1295–1315, Nov. 2021.
- [356] H. Wang, Z. Xiao, and Y. Zeng, "Cramér-Rao bounds for near-field sensing with extremely large-scale MIMO," *arXiv preprint arXiv:2303.05736*, 2023.
- [357] S. Yang, X. Chen, Y. Xiu, W. Lyu, Z. Zhang, and C. Yuen, "Performance bounds for near-field localization with widely-spaced multi-subarray mmWave/THz MIMO," *arXiv preprint arXiv:2309.05944*, 2023.
- [358] Z. Wang, X. Mu, and Y. Liu, "Near-field integrated sensing and communications," *IEEE Commun. Lett.*, vol. 27, no. 8, pp. 2048–2052, Aug. 2023.
- [359] F. Liu, W. Yuan, C. Masouros, and J. Yuan, "Radar-assisted predictive beamforming for vehicular links: Communication served by sensing," *IEEE Trans. Wireless Commun.*, vol. 19, no. 11, pp. 7704–7719, Nov. 2020.
- [360] S. Sun and Y. D. Zhang, "4D automotive radar sensing for autonomous vehicles: A sparsity-oriented approach," *IEEE J. Sel. Topics Signal Process.*, vol. 15, no. 4, pp. 879–891, Jun. 2021.
- [361] X. Chen, Z. Feng, Z. Wei, X. Yuan, P. Zhang, J. A. Zhang, and H. Yang, "Multiple signal classification based joint communication and sensing system," *IEEE Trans. Wireless Commun.*, vol. 22, no. 10, pp. 6504–6517, Oct. 2023.
- [362] J. A. Nanzer, "On the resolution of the interferometric measurement of the angular velocity of moving objects," *IEEE Trans. Antennas Propag.*, vol. 60, no. 11, pp. 5356–5363, Nov. 2012.
- [363] J. A. Nanzer and M. D. Sharp, "On the estimation of angle rate in radar," *IEEE Trans. Antennas Propag.*, vol. 65, no. 3, pp. 1339–1348, Mar. 2017.
- [364] X. Wang, P. Wang, and V. C. Chen, "Simultaneous measurement of radial and transversal velocities using interferometric radar," *Trans. Aerosp. Electron. Syst.*, vol. 56, no. 4, pp. 3080–3098, Aug. 2020.
- [365] Z. Wang, X. Mu, and Y. Liu, "Rethinking integrated sensing and communication: When near field meets wideband," *arXiv preprint arXiv:2311.11416*, 2023.
- [366] —, "Near-field velocity sensing and predictive beamforming," *arXiv preprint arXiv:2311.09888*, 2023.
- [367] H. Luo, F. Gao, F. Liu, and S. Jin, "6D radar sensing and tracking in monostatic integrated sensing and communications system," *arXiv preprint arXiv:2312.16441*, 2023.
- [368] X. Mu, J. Xu, Y. Liu, and L. Hanzo, "RIS-aided near-field communications for 6G: Opportunities and challenges," *IEEE Veh. Technol. Mag.*, Early Access, 2024.
- [369] Y. Zhang, J. Zhang, M. Di Renzo, H. Xiao, and B. Ai, "Reconfigurable intelligent surfaces with outdated channel state information: Centralized vs. distributed deployments," *IEEE Trans. Commun.*, vol. 70, no. 4, pp. 2742–2756, Apr. 2022.
- [370] H. Li, Y. Liu, X. Mu, Y. Chen, Z. Pan, and Y. C. Eldar, "Near-field beamforming for STAR-RIS networks," *arXiv preprint arXiv:2306.14587*, 2023.
- [371] S. Palmucci, A. Guerra, A. Abrardo, and D. Dardari, "Two-timescale joint precoding design and RIS optimization for user tracking in near-field MIMO systems," *IEEE Trans. Signal Process.*, vol. 71, pp. 3067–3082, Aug. 2023.
- [372] W. Hao, X. You, F. Zhou, Z. Chu, G. Sun, and P. Xiao, "The far-/near-field beam squint and solutions for THz intelligent reflecting surface communications," *IEEE Trans. Veh. Technol.*, vol. 72, no. 8, pp. 10 107–10 118, Aug. 2023.
- [373] Z. Li, W. Chen, Q. Wu, X. Zhu, H. Qin, K. Wang, and J. Li, "Towards transmissive RIS transceiver enabled uplink communication systems: Design and optimization," *IEEE Internet Things J.*, Early Access, 2023.
- [374] D. Shen, L. Dai, X. Su, and S. Suo, "Multi-beam design for near-field extremely large-scale RIS-aided wireless communications," *IEEE Trans. Green Commun. Netw.*, vol. 7, no. 3, pp. 1542–1553, Sep. 2023.
- [375] S. Lv, Y. Liu, X. Xu, A. Nallanathan, and A. L. Swindlehurst, "RIS-aided near-field MIMO communications: Codebook and beam training design," *arXiv preprint arXiv:2310.00294*, 2023.
- [376] Y. Jiang, F. Gao, M. Jian, S. Zhang, and W. Zhang, "Reconfigurable intelligent surface for near field communications: Beamforming and sensing," *IEEE Trans. Wireless Commun.*, vol. 22, no. 5, pp. 3447–3459, May 2023.
- [377] S. Yang, W. Lyu, Z. Hu, Z. Zhang, and C. Yuen, "Channel estimation for near-field XL-RIS-aided mmwave hybrid beamforming architectures," *IEEE Trans. Veh. Technol.*, vol. 72, no. 8, pp. 11 029–11 034, Aug. 2023.
- [378] Y. Chen, R. Li, C. Han, S. Sun, and M. Tao, "Hybrid spherical-and planar-wave channel modeling and estimation for Terahertz integrated UM-MIMO and IRS systems," *IEEE Trans. Wireless Commun.*, vol. 22, no. 12, pp. 9746–9761, Dec. 2023.
- [379] S. Yang, C. Xie, W. Lyu, B. Ning, Z. Zhang, and C. Yuen, "Near-field channel estimation for extremely large-scale reconfigurable intelligent surface (XL-RIS)-aided wideband mmwave systems," *arXiv preprint arXiv:2304.00440*, 2023.
- [380] Y. Pan, C. Pan, S. Jin, and J. Wang, "RIS-aided near-field localization and channel estimation for the Terahertz system," *IEEE J. Sel. Topics Signal Process.*, vol. 17, no. 4, pp. 878–892, Jul. 2023.
- [381] J. Wu, S. Kim, and B. Shim, "Parametric sparse channel estimation for RIS-assisted terahertz systems," *IEEE Trans. Commun.*, vol. 71, no. 9, pp. 5503–5518, Sep. 2023.
- [382] J. Xiao, J. Wang, Z. Chen, and G. Huang, "U-MLP based hybrid-field channel estimation for XL-RIS assisted millimeter-wave MIMO systems," *IEEE Wireless Commun. Lett.*, vol. 12, no. 6, pp. 1042–1046, Jun. 2023.
- [383] J. Han, L. Li, X. Ma, X. Gao, Y. Mu, G. Liao, Z. J. Luo, and T. J. Cui, "Adaptively smart wireless power transfer using 2-bit programmable metasurface," *IEEE Trans. Ind. Electron.*, vol. 69, no. 8, pp. 8524–8534, Aug. 2022.
- [384] H. Zhang, N. Shlezinger, F. Guidi, D. Dardari, M. F. Imani, and Y. C. Eldar, "Near-field wireless power transfer with dynamic metasurface antennas," in *Proc. IEEE 23rd Int. Workshop Signal Process. Adv. Wireless Commun. (SPAWC)*, Jul. 2022, pp. 1–5.
- [385] B. J. B. Deuschmann, T. Wilding, E. G. Larsson, and K. Witrisal, "Location-based initial access for wireless power transfer with physically large arrays," in *Proc. IEEE Int. Conf. Commun. Workshops (ICC Wkshps)*, May 2022, pp. 127–132.
- [386] K. M. Mayer, L. Cottatellucci, and R. Schober, "Optimal transmit antenna deployment and power allocation for wireless power supply in an indoor space," *arXiv preprint arXiv:2307.02076*, 2023.

- [387] Z. Zhang, Y. Liu, Z. Wang, X. Mu, and J. Chen, "Simultaneous wireless information and power transfer in near-field communications," *arXiv preprint arXiv:2305.03775*, 2023.
- [388] Y. Zhang, C. You, W. Yuan, F. Liu, and R. Zhang, "Joint beam scheduling and power allocation for SWIPT in mixed near- and far-field channels," *arXiv preprint arXiv:2304.07945*, 2023.
- [389] J. Zuo, X. Mu, and Y. Liu, "Non-orthogonal multiple access for near-field communications," *arXiv preprint arXiv:2304.13185*, 2023.
- [390] Z. Ding, R. Schober, and H. V. Poor, "NOMA-based coexistence of near-field and far-field massive MIMO communications," *IEEE Wireless Commun. Lett.*, vol. 12, no. 8, pp. 1429–1433, Aug. 2023.